Oxidative Decomposition Pathways and Catalyst Protection Strategies in Olefin Metathesis

Stephanie Jean Ton

Thesis submitted to the University of Ottawa
in partial fulfillment of the requirements for the degree of
Master of Science

Center for Catalysis Research and Innovation
Department of Chemistry of Biomolecular Sciences
University of Ottawa

Table of Contents

List of Figures

List of Schemes

List of Tables

List of Charts

Abstract

Olefin metathesis is an outstandingly versatile methodology for the catalytic assembly of carbon-carbon bonds. Metathesis methodologies have been widely embraced since the advent of easily-handled ruthenium catalysts. However, industrial implementation has lagged. Problems of reliability and productivity arising from catalyst decomposition have impeded broad uptake of metathesis in process chemistry. Such challenges also hamper deployment of metathesis in forefront applications such as chemical biology. Better understanding of the mechanisms by which catalysts decompose can thus improve performance in demanding applications, as well as providing guidelines for informed process and catalyst design.

Oxygen is often viewed as a relatively innocuous contaminant in reactions promoted by these late transition metal catalysts. Indeed, multiple reports comment on the desirability and operational simplicity of metathesis in air. We suspected, however, that deleterious impacts of O_2 may be masked by the high catalyst loadings typically deployed in such reports. The first part of this thesis focuses on examining the robustness of leading metathesis catalysts toward oxygen. Systems examined include the classic, dominant N-heterocyclic carbene (NHC) derivatives, as well as recent breakthrough analogues containing cyclic alkyl amino carbene (CAAC) ligands. Both are shown to be decomposed by oxygen, but the CAAC catalysts are found to be not only more productive, but significantly more O_2-tolerant. This is important as it overturns the widespread belief that high catalyst activity is invariably a trade-off against higher sensitivity. Studies of the initial oxidation event for the second-generation Grubbs catalyst $RuCl_2(H_2IMes)(PCy_3)(=CHPh)$ suggest that [2+2] cycloaddition of O_2, as well as bimolecular decomposition of the four-coordinate species generated by PCy_3 oxidation, account for ca. 90% of the observed decomposition. A previously-proposed pathway involving attack of O_2 at the benzylidene ligand appears to be a minor contributor.

In Chapter 3 of this thesis, a new strategy for inhibiting catalyst decomposition is examined. Specifically, cationic metathesis catalysts were encapsulated within a supramolecular resorcinarene capsule, which self-assembles around the catalysts in water-saturated toluene. Encapsulation nearly doubles RCM yields relative to the parent, neutral catalyst in water-saturated

toluene. The increased catalyst productivity is enabled by site-isolation of the catalyst within the capsule, which prevents bimolecular decomposition, and by the hydrophobic nature of the capsule interior, which limits decomposition by water.

A final study focuses on attempts to identify a more robust catalyst via ligand redesign. Examined for this purpose are recently reported, electron-rich pyridinylide aminophosphines (PyAPs; these take the general form $R_2P–N=Ar$), which exhibit enhanced σ-donor properties relative to NHCs. Strategies for incorporation of PyAP ligands into Ru metathesis catalysts are developed, and the catalytic activity of these species is described. PyAP catalysts are found be significantly less active than the corresponding NHC catalysts, despite their higher donicity. Poor performance results from facile catalyst decomposition. Where the N=Ar group lacks substituents at the *ortho* sites, *o*-metalation enables decomposition of the precatalyst. More problematically, the nitrogen atom appears to participate in nucleophilic attack on the key, metathesis-enabling [Ru]=CHR functionality, limiting the potential use of this class of phosphine in metathesis. Criteria for the development of more robust second-generation phosphine catalysts are proposed.

List of Contributions

Publications

1. **Ton S.J.**, Fogg D. E., The Impact of Oxygen on Leading and Emerging Ru-Carbene Catalysts for Olefin Metathesis: An Unanticipated Correlation Between Robustness and Metathesis Activity. *ACS Catal*. **2019**, 9, 12, 11329-11334.

2. Jongkind L.J., Rahimi M.R., Poole D., **Ton S.J.**, Fogg D. E., Reek J.N.H. "Protection of Ruthenium Olefin Metathesis Catalysts by Encapsulation in a Self-Assembled Resorcinarene Capsule." *ChemCatChem,* 2020; Early View Article. https://chemistry-europe.onlinelibrary.wiley.com/doi/full/10.1002/cctc.202000111

3. **Ton, S.J.**, Rotterig, P., Löwe P., Dielmann F., Fogg, D. E, Pyridinylide Aminophosphine: Ligands Lessons in Ligation for Ruthenium Catalyzed Olefin Metathesis. (Manuscript in preparation).

Presentations (O=Oral, P=Poster; presenting author in bold)

P2. **Ton, S.J.**, Rotterig, P., Dielmann F., Fogg, D. E, Novel Ruthenium Metathesis Catalysts Containing Strongly Electron-Donating Phosphines. Inorganic Discussion Weekend, Oshawa Canada, **2019**.

O1. **Ton, S.J.** Fogg, D. E, The Impact of Oxygen on Olefin Metathesis: An Unanticipated Correlation Between Robustness and Reactivity. Ottawa-Carlton Chemistry Institute Day, Ottawa, Canada, **2019**.

P1. **Ton, S.J.**; Fogg, D. E, The Impact of Oxygen on Ruthenium-Catalyzed Olefin Metathesis. Canadian Chemistry Conference and Exhibition, Quebec, Canada, **2018**.

Acknowledgements

First and foremost, I would like to thank my supervisor Deryn Fogg for always having confidence in me. You have truly inspired my love of science, and I am very thankful for everything you have taught me, from the intricacies of organometallic catalysis to how to sabre a bottle of champagne. I have grown so much as a researcher and a person under your guidance.

To members of the Fogg lab, past and present: Thank you for your valuable discussions and friendship – you all have been very important to my development over these past few years. Daniel Nascimento, thank you for taking the time to mentor me and teaching me the ropes of Fogg lab. I'll treasure my glovebox certification from you always. Andrew White, thank you for always being there to discuss even my worst chemistry ideas with enthusiasm, and for being a source of positive thinking on the days when grad school seemed like a bad decision. To the "breaky squad", Craig, Alex and Daniel: I miss our weekly F&S trips and our board game nights that always got taken way too seriously. I am happy to have you all as my friends. Xinrui, Gwen, Steph, Mason, and all other members of the lab: thank you for your support. I'm glad that our time in the Fogg lab overlapped.

Professor Dielmann and all the members of the Dielmann group: thank you so much for inviting me to spend time in your lab and making my time in Munster so enjoyable. I learnt so much during my short stay and am very grateful for the opportunity.

Finally, to my family: Mom, Samantha and everyone else – thank you for your encouragement and understanding, and for always motivating me when I needed it most.

List of Compounds

Organic and Main Group Compounds

Compound	Structure	Compound	Structure
1	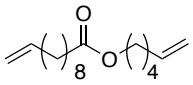	**1'**	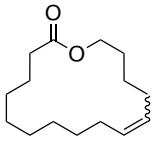
2	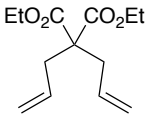	**2'**	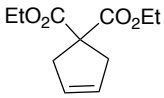
3	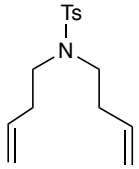	**3'**	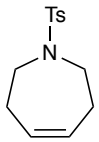
4	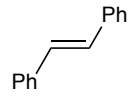	**5**	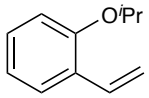
6	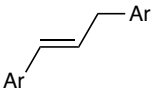	**6'**	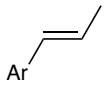
CAAC	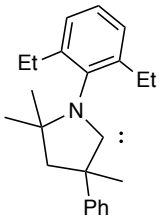	**H_2IMes**	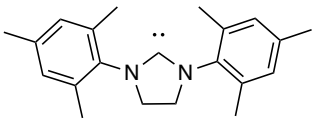
IMes	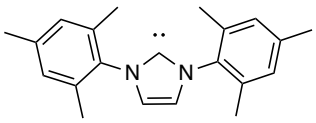	**P1**	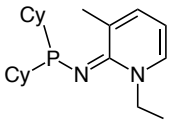
P2	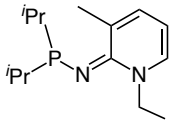	**P3**	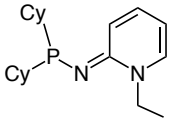
P4	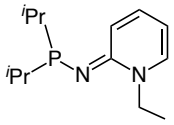	**P5**	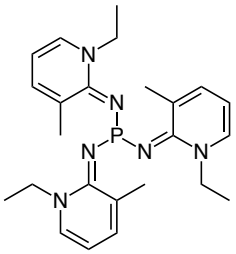

P6	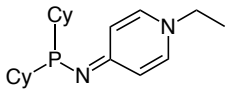	**P7**	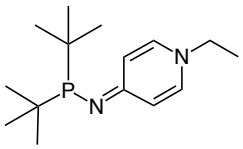

Transition Metal Complexes

Compound	Structure	Compound	Structure
GI	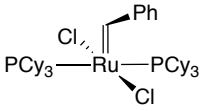	**GII**	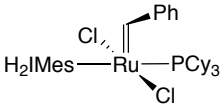
HI	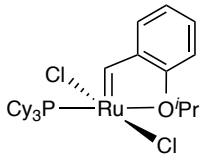	**HII**	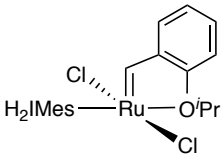
nG	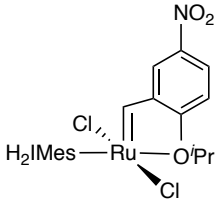	**nG[c]**	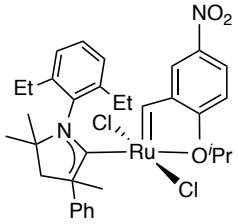
PII	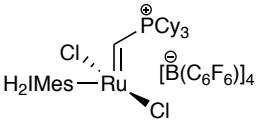	**GIIm**	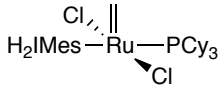
HII-OH	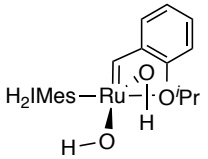	**HC**	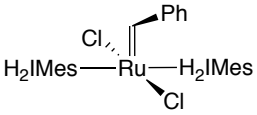
M2	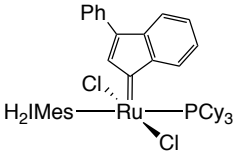	**Ru2[c]**	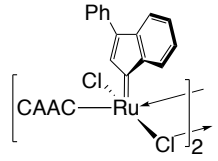
UC	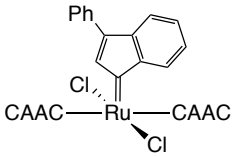	**AM**	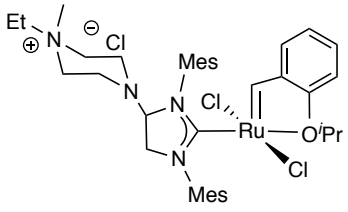

SC	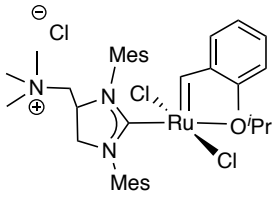	**SC'**	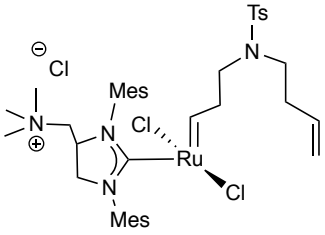
H-PPh$_3$	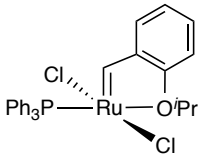	**nG-PCy$_3$**	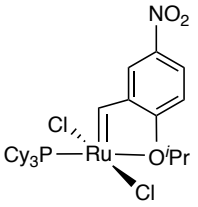
nG-P1	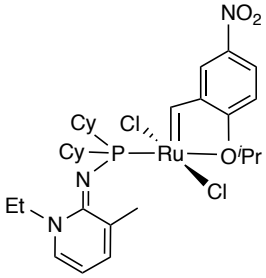	**nG-P2**	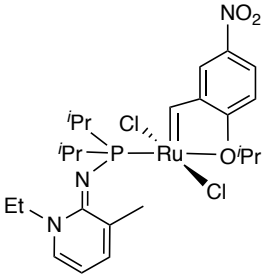
nG-P3	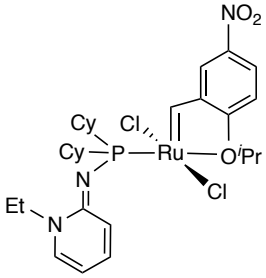	**nG-P5**	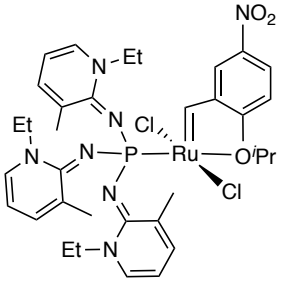
H-P1	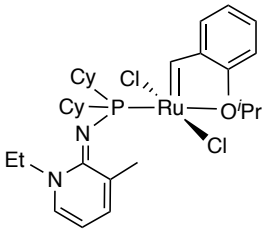	**H-P4**	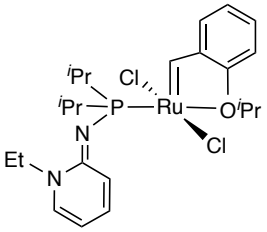
H-P5	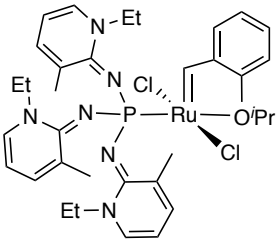	**Mo-1**	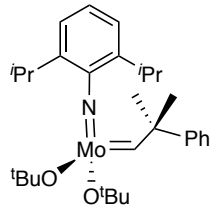

Ru-1	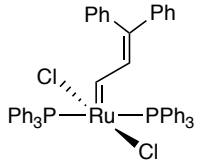	**Ru-2**	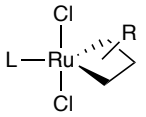
Ru-2*	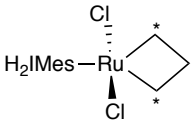	**Ru-3**	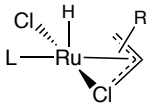
Ru-4	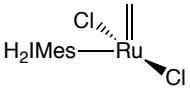	**Ru-5**	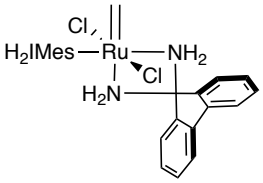
Ru-6	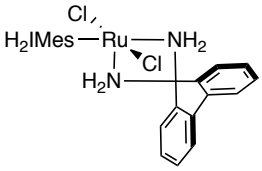	**Ru-7**	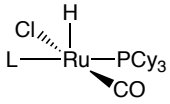
Ru-8	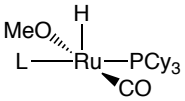	**Ru-9**	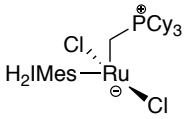
Ru-10	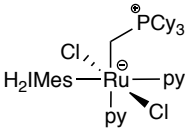	**Ru-11**	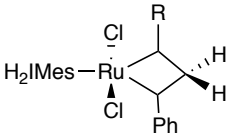
Ru-12	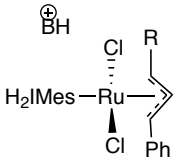	**Ru-13**	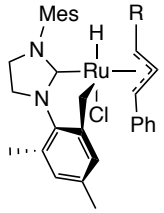
Ru-14	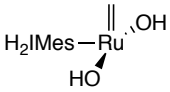	**Ru-15**	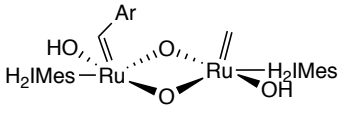
Ru-16	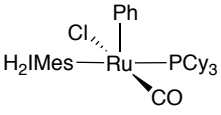	**Ru-17**	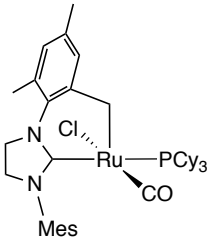
Ru-18	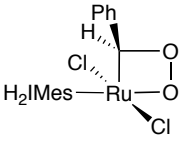	**Ru-19**	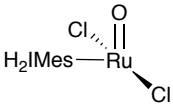

Ru-20	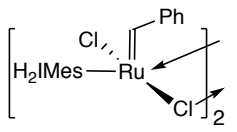	**Ru-21**	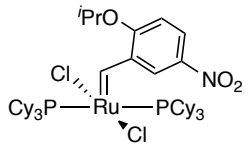
Ru-22	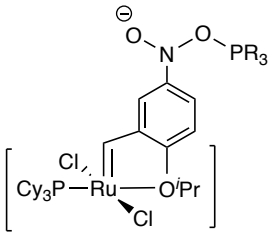	**Ru-23**	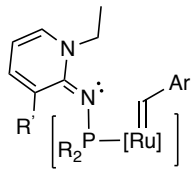
Ru-24	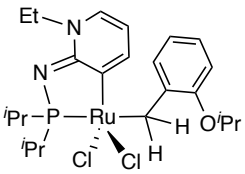	**Ru-25**	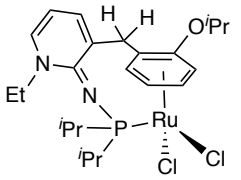
Ru-26	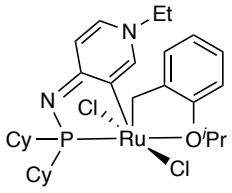	**Ru-27**	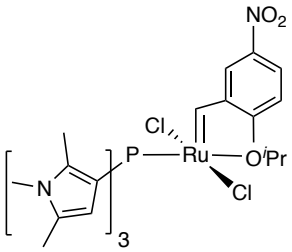
Ru-28	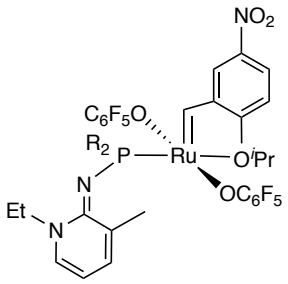		

List of Abbreviations

ADMET	Acyclic diene metathesis
BMC	Bimolecular coupling
CAAC	Cyclic alkyl amino carbene
CM	Cross-metathesis
DDM	Diethyl diallyl malonate
DMT	Dimethyl terephthalate
Dppb	1,4-Bis(diphenylphosphino)butane
Equiv	Equivalents
FID	Flame-ionization detector
GC	Gas chromatography
HPLC	High performance liquid chromatography
IAP	Imidazole-ylideamino phosphine
KTp	Potassium tris(1-pyrazolyl)borate
MCB	Metallacyclobutane
mRCM	Macrocyclic ring-closing metathesis
NHC	N-heterocyclic carbene
NMR	Nuclear magnetic resonance
ODA	*o*-Dianiline
PyAP	Pyridinylide aminophosphine
RCM	Ring-closing metathesis
ROMP	Ring-opening metathesis polymerization
RT	Room temperature
SHOP	Shell higher olefin process
SM	Self-metathesis
TEP	Tolman electronic parameter
THF	Tetrahydrofuran
TON	Turnover number

1 Introduction

1.1 Olefin Metathesis

Olefin metathesis is an exceptionally versatile tool for the catalytic formation of sp^2-sp^2 C-C bonds.[1-4] The first catalysts for this reaction, identified in the 1950s, were heterogeneous mixtures, commonly salts of titanium, molybdenum, tungsten, or rhenium.[5,6] Reactions were limited to unfunctionalized hydrocarbons by the poor functional-group tolerance of the organometallic intermediates. Nevertheless, the reaction found rapid use. A notable application was the production of detergent-range (C12 to C18) α-olefins via the Shell Higher Olefins Process (SHOP; Scheme 1.1).[7] This process was an early showcase example of the utility of olefin metathesis. The reaction has since found broad use in organic chemistry,[8,9] polymer science[10] and green chemistry.[11]

Scheme 1.1 Early Example of Metathesis: Linear α-Olefins via the SHOP Process.

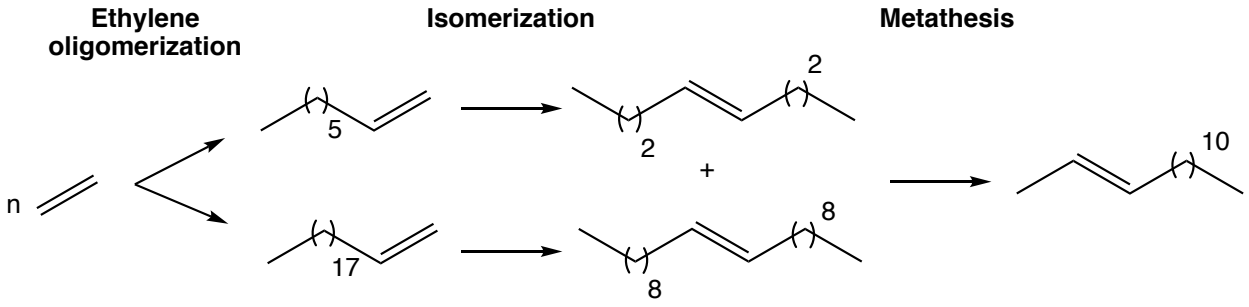

Olefin metathesis is also a showcase example of the importance of mechanistic understanding in catalysis. Only once Chauvin advanced the [2+2] cycloaddition mechanism for metathesis (see next) was the door opened to rational catalyst design.[12] However, even after the mechanism was accepted and molecularly well-defined homogeneous catalysts developed, the highly oxophilic nature of the dominant early-metal catalysts limited broad uptake.[13] A significant advance was thus the development of ruthenium catalysts, which are less air-sensitive and more functional-group tolerant than their predecessors.[14] This transformed olefin metathesis into a methodology that could be employed by the practicing organic chemist. In 2005, the Nobel Committee recognized the potential of olefin metathesis by awarding that year's Nobel Prize in chemistry to

Robert Grubbs, Richard Schrock, and Yves Chauvin.[2-4] Today, ruthenium-catalyzed olefin metathesis is widely employed for the formation of carbon-carbon bonds (albeit still primarily in "discovery" science),[15] and recent breakthroughs enable ppm-level catalyst loadings.[16,17]

1.2 Chauvin Mechanism

Olefin metathesis is now generally accepted as proceeding via the Chauvin mechanism: that is, [2+2] cycloaddition of an olefin and a metal-alkylidene complex, as shown in Scheme 1.2.[18] The resulting metallacyclobutane (MCB) intermediate can undergo cycloreversion to re-form the original olefin and metal-alkylidene complex (non-productive metathesis), or generate a new olefin and metal-alkylidene or methylidene complex (productive metathesis). The facile reversibility of these steps means that metathesis is normally under thermodynamic control.[1]

Scheme 1.2 Catalytic Cycle for Ruthenium-Catalyzed Olefin Metathesis of Terminal Olefins Showing Key Metallacyclobutane and Methylidene Intermediates.

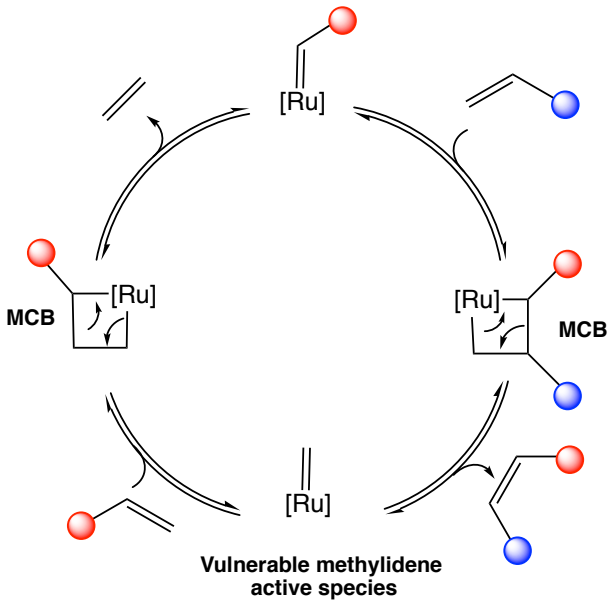

Olefin metathesis enables synthesis of a variety of olefin structures (Figure 1.1), via ring-closing metathesis (RCM), cross-metathesis (CM), ring-opening metathesis polymerization (ROMP), and acyclic diene metathesis polymerization (ADMET). Given thermoneutral nature of these reactions, a driving force is normally required to achieve high product yields.[19] Typical strategies include the

release of volatile products (often ethylene, which promotes forward reaction but does not confer selectivity: see below), the release of ring strain (ROMP), or the formation of a more stable olefin product.[15] An area that has seen exceptional interest is the RCM assembly of cyclic olefins that are challenging to access via traditional nucleophilic reaction paths, or that require harsh conditions.[20] Metathesis offers an atom-economical and mild approach to such structures, which are highly valued in the fine-chemical and pharmaceutical sectors.[9,21,22] Owing to its versatility, metathesis has also found use in the plastics industry, where ROMP offers access to polymers of controlled molecular weight.[23] Other emerging applications focus on the transformation of plant oils to building-block chemicals via cross-metathesis.[24-27]

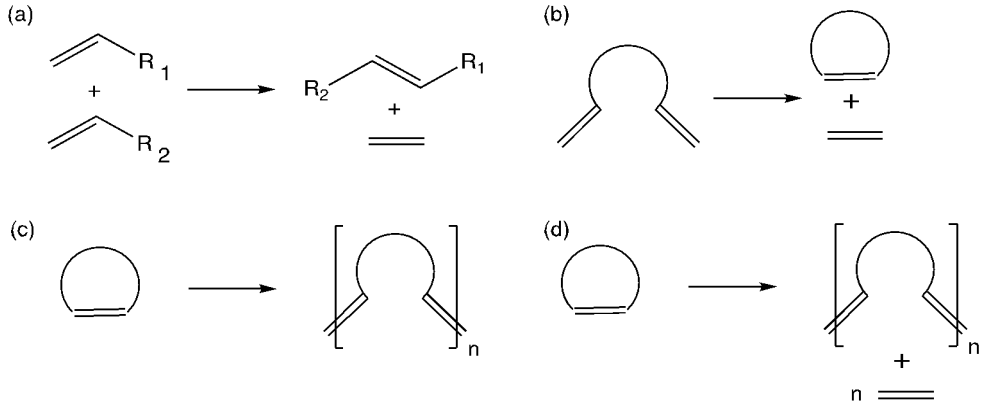

Figure 1.1 Selected leading metathesis manifolds. (a) Cross-metathesis, CM. (b) Ring-closing metathesis, RCM. (c) Ring-opening metathesis polymerization, ROMP. (d) Acyclic diene metathesis, ADMET.

The first well-defined ruthenium metathesis catalyst, $RuCl_2(PPh_3)_2(=CH\text{-}CH=CPh_2)$ (**Ru-1**; Chart 1.1), was reported by Fu and Grubbs in 1992.[28] Subsequent replacement of the arylphosphine ligands by the more electron-rich ligand PCy_3, and introduction of a benzylidene ligand, gave the more active first-generation Grubbs catalyst (**GI**).[14] The vast majority of ruthenium metathesis catalysts reported to date are of the general structure $RuX_2L_2(=CHR)$. **GI** was significant in the development of metathesis for practical use due to its ease of handling.[29] However, a drawback was its poor activity compared to Schrock-class catalysts such as **Mo-1**.[12]

Chart 1.1 Early Examples of Ru Metathesis Catalysts, and a Selected Mo Schrock Catalyst.

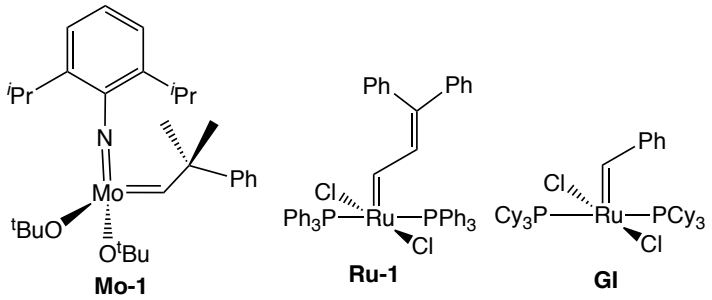

1.3 Ligand Modification

An important serendipitous discovery by the Hoveyda group in 1999 led to a more robust class of Ru metathesis catalysts.[30] In metathesis reactions with 2-isopropoxy styrene, formation of a stable five-membered chelate was observed, which was revealed by X-ray analysis to be the chelated ether complex $RuCl_2(PCy_3)(=CHPh\text{-}2\text{-}O^iPr)$ (**HI**; Chart 1.2). This is now known as the first-generation Hoveyda catalyst **HI.** Based on experiments measuring the rate of cyclooctene metathesis, Hoveyda and co-workers suggested that **HI** may initiate ca. 30x slower than **GI**, but propagate nearly 4x faster.[30,31]

An important contributor to the performance of **HI** relative to the Grubbs catalysts is now known to be elimination of decomposition pathways promoted by the powerfully nucleophilic PCy_3 ligand (see Section 1.4.2 below). Optimization of the Hoveyda catalyst by the Grela group was described in 2004. Incorporation of a nitro group *para* to the ether functionality gave the more active catalyst **nG**,[32] in which the electron-withdrawing nitro group weakens σ-donation from the ether ligand, accelerating initiation. In a reaction with 1-hexene, **nG** was found to initiate 4x faster than **HII**.[33]

A step-change in catalyst activity came from replacing a PCy_3 ligand on the first-generation Grubbs catalyst **GI** with a strongly donating N-heterocyclic carbene ligand (NHC; see Chart 1.2).[34] The NHCs are singlet carbenes stabilized by two adjacent nitrogen atoms, which form very stable bonds with transition metals.[35,36] Nolan has suggested that the improved metathesis reactivity of the second-generation Grubbs catalyst (**GII**) originates in increased back-donation to the olefin.[37]

Chart 1.2 Selected Ruthenium Metathesis Catalysts of the Grubbs and Hoveyda Classes, Showing Significant Developments in Ligand Design.

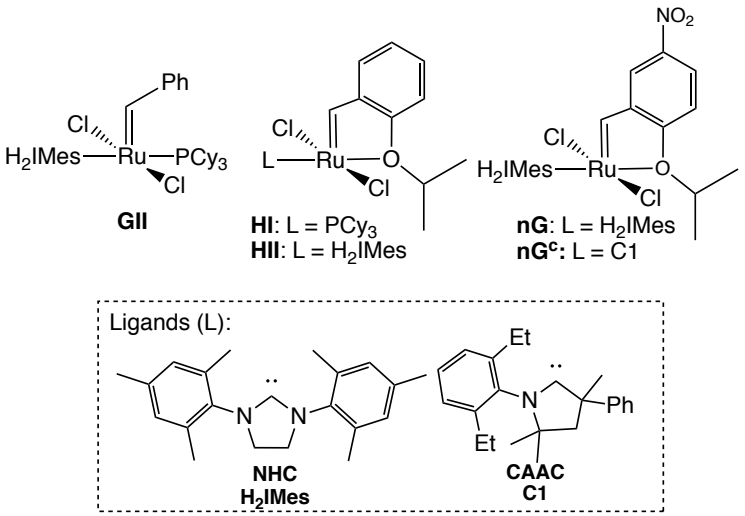

Many NHC ligands have been explored in metathesis. Steric tuning to increase selectivity for particular types of olefins has met with some success. NHCs with decreased steric bulk were claimed as a breakthrough in enabling metathesis of bulky tetrasubstituted olefins,[38,39] although these have seen little use beyond the original reports, probably owing to their rapid decomposition. NHCs with increased steric bulk and unsymmetrical NHC ligands have been suggested as key to site-selective metathesis or stereoselective metathesis.[40-42] Other studies focus on improving the solubility of metathesis catalysts in water via cationic substituents on the NHC,[43-45] an objective limited by the still unresolved challenge of catalyst decomposition by water.[27,46,47]

In 2007, Grubbs and Bertrand reported a new class of carbene ligands for metathesis catalysts, the cyclic alkyl amino carbenes (CAAC; see Chart 1.2 above).[48] In the CAAC ligands, the carbene site is flanked by an N-aryl group and a quaternary carbon. Removal of one electronegative nitrogen atom increases σ-donation relative to NHCs.[49] As well, however, CAACs are more π-accepting than NHCs, because loss of one π-donating nitrogen atom permits the carbene lone pair to accept more electron density from the metal center. Incorporation of these ligands into metathesis catalysts has resulted in the highest turnover number yet reported for the metathesis of internal olefins with ethylene (340,000) .[17] The high productivity of CAAC catalysts was recently shown to be due in large part to their resistance to decomposition,[50] a subject we turn to next.

1.4 Decomposition of Ruthenium Metathesis Catalysts

To improve catalyst performance, control over decomposition is essential. Facile catalyst decomposition necessitates use of higher catalyst loadings to obtain high conversions: this results in contamination by ruthenium products that must be removed. As well, these Ru species may catalyze non-metathesis reactions, resulting in undesired side products that limit yields and add to purification challenges.[51-54] The decomposition pathways intrinsic to Ru metathesis catalysts, as well as those induced by external agents, have been studied in mechanistic detail in recent years, to a great extent by the Fogg group.[53-68] Knowledge gained from such studies is critical to the rational design of both metathesis processes, and new catalysts with improved productivity.[9]

1.4.1 Intrinsic Decomposition Pathways

Intrinsic decomposition pathways include β-hydride elimination from the MCB intermediate **Ru-2** (Scheme 1.3a),[69] and bimolecular coupling of the methylidene **Ru-4** (Scheme 1.3b).[67] In the former pathway, a hydride is transferred from the β-position of the MCB to Ru, and the resulting allyl hydride intermediate **Ru-3** undergoes reductive elimination, releasing a propene and a coordinatively unsaturated ruthenium product that undergoes further decomposition.

Scheme 1.3 Intrinsic Decomposition Pathways for Ruthenium Metathesis Catalysts. (a) β-Hydride Elimination. (b) Bimolecular Coupling.

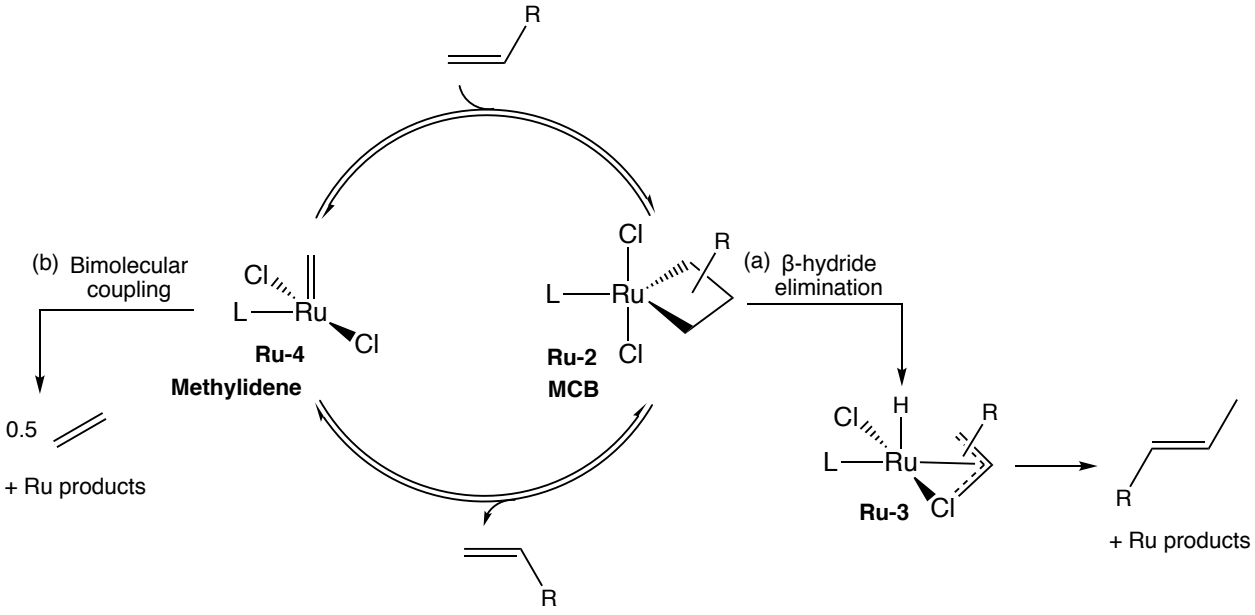

Compelling evidence for β-hydride elimination was reported by Piers and co-workers in studies of the four-coordinate phosphonium alkylidene complex **PII** (Scheme 1.4).[69-71] Treating a solution of **PII** with ^{13}C-labelled ethylene at –50 °C to generate the unsubstituted MCB (**Ru-2***), then warming to room temperature, resulted in complete decomposition of the MCB and liberation of ^{13}C-labelled propylene. Recently, the Fogg group reported that the high productivity of CAAC catalysts is due in large part to their *resistance* to β-hydride elimination.[50]

Scheme 1.4 Evidence for β-hydride Elimination from Ru-2.

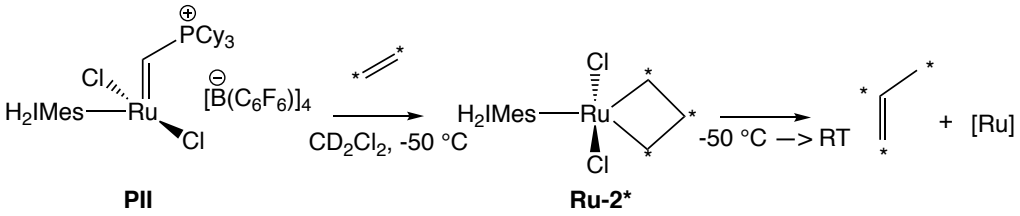

A second major decomposition pathway is bimolecular coupling (BMC) of the 14-electron, 4-coordinate species **Ru-4**. Schwab and Grubbs suggested BMC as a potential hazard for the PPh_3-stabilized catalysts.[14] Experimental evidence demonstrating that bimolecular coupling of [Ru]=CHCH=CMe_2 catalysts is facile even at room temperature was reported nearly 2 decades ago by Amoroso and Fogg, who isolated in high yields both the triene resulting from bimolecular coupling of [Ru]=CHCH=CPh_2, and the face-bridged diruthenium products.[55,56] Until recently, however, slow initiation was believed to render the second-generation systems resistant to this pathway, owing to a low concentration of **Ru-4** in solution.[72,73] The first experimental evidence demonstrating that BMC is in fact a major contributor to decomposition of second-generation Ru metathesis catalysts was reported by Bailey and Fogg in 2018.[67] Isolation of transiently-stabilized methylidene species **Ru-5** at –120 °C (Scheme 1.5), redissolving **Ru-5** with internal standard, and warming to room temperature, was shown to release ethylene via coupling of two methylidene ligands. Bimolecular coupling was additionally shown to occur for benzylidene ligands, although their bulk retarded coupling relative to the sterically accessible methylidene intermediate **Ru-4**.

Scheme 1.5 Bimolecular Coupling of Methylidene Species Ru-3.

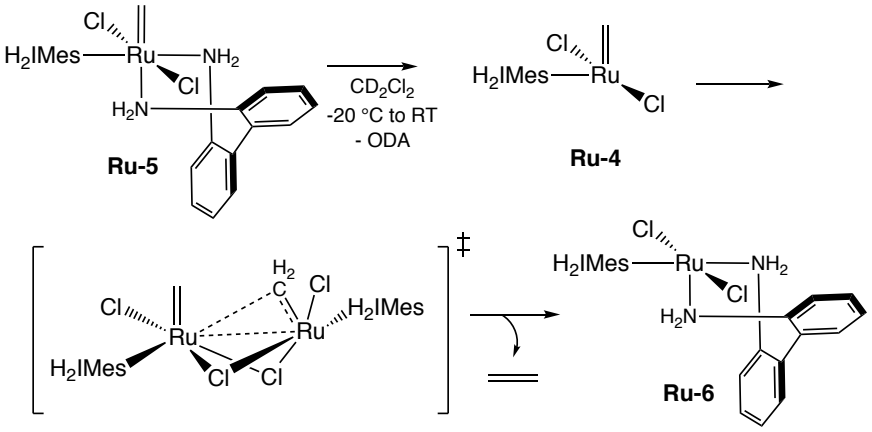

In recent work, Nascimento and Fogg demonstrated that CAAC-metathesis catalysts undergo BMC even more readily than their NHC analogues (Figure 1.2).[50] Complete loss of methylidene signals was seen in <5 min for a CAAC methylidene complex, vs. 3 h for the NHC analogue **Ru-4**. It may be noted that these NMR analyses are necessarily performed at Ru concentrations much higher than those customary in catalysis (20 mM), and this greatly accelerates decomposition. Importantly, however, the resistance of CAAC catalysts to decomposition by β-hydride elimination enables "real-world" metathesis at very low catalyst loadings, which limits the impact of BMC under catalytic conditions.

Ligand (L)	Time to complete loss of [Ru]=CH_2 signals	% ethylene generated
H_2IMes	3 h	81
CAAC	<5 min	75

Figure 1.2 Relative susceptibility of CAAC and H_2IMes methylidene complexes to bimolecular coupling.

1.4.2 Decomposition Induced by Exogenous Reagents

Catalyst decomposition by external reagents is a general concern for practitioners of metathesis whose interest lies in organic synthesis. The widespread description of Ru catalysts as functional-group tolerant presumes that few risks are posed by functionalities present on the substrate. The limitations of this assumption have become increasingly clear as metathesis moves into process chemistry in the pharmaceutical sector.[9,74,75] Polar functionalities may poison or decompose the catalyst, as may trace impurities (in one notable example, ppm levels of morpholine in technical-grade toluene),[76] or residues from previous steps in a synthetic process.[9,74,75] The risks arising from nucleophiles and Brønsted bases, water, and possibly oxygen have been highlighted.[9]

Heating **GII** with primary alcohols and base was found to generate hydride complex **Ru-7** (Scheme 1.6a).[58,77,78] Even at room temperature, methoxide ion reacts aggressively with the Ru catalysts, and formation of **Ru-8** was observed in the presence of excess methoxide (Scheme 1.6b).[58,78] Unwanted, competing C=C bond isomerization during metathesis is frequently attributed to these and other[57] well-defined hydride species. However, they appear improbable contributors based on their kinetic incompetence.[54] Ruthenium nanoparticles generated via catalyst decomposition[53] are a little-recognized, but potentially ubiquitous, contributor to such isomerization.

Scheme 1.6 Formation of Ruthenium Hydrides Ru-7 and Ru-8 by Decomposition of Metathesis Catalysts. (a) Decomposition by Primary Alcohols and Base. (b) Decomposition by Excess Methoxide.

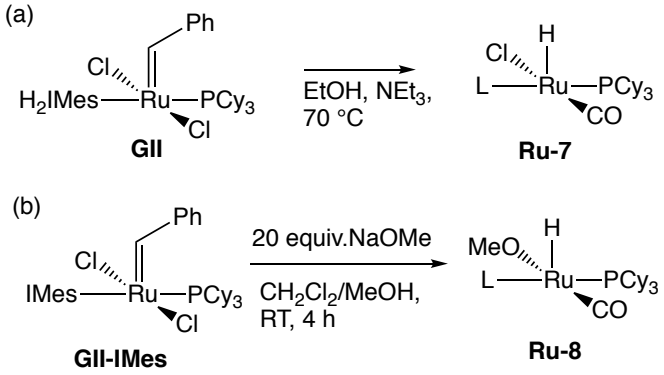

Nucleophiles have been shown to decompose ruthenium metathesis catalysts by abstracting the methylidene or alkylidene ligand.[61-64,79] This pathway is particularly problematic for Grubbs-class catalysts, where loss of the PCy_3 ligand – a potent nucleophile, as noted above – is necessary for entry into the catalytic cycle.[31] Once PCy_3 is liberated, it can attack at the methylidene ligand.[62] The process commonly culminates in loss of the methylidene ligand as the phosphonium salt $[MePCy_3]Cl$ (Scheme 1.7a).[57,61] It is greatly accelerated by donor ligands, which promote phosphine dissociation via an associative pathway.[64] Donor-accelerated decomposition was shown to be promoted by even very weak donors such as water and THF.

In the second-generation catalysts, William McClennan of this research group confirmed donor-accelerated decomposition by treating a H_2IMes-d_{22} isotopologue of $RuCl_2(H_2IMes)(PCy_3)(=CH_2)$ (**GIIm**) with pyridine (Scheme 1.7b). This effected immediate formation of a short-lived alkyl species **Ru-10**, which rapidly liberated $[MePCy_3]Cl$ by cyclometallation of the NHC at the mesityl *o*-methyl group. Smaller, more nucleophilic reagents such as primary amines not only accelerate methylidene abstraction by PCy_3, but can themselves abstract the methylidene ligand. Indeed, even small NHCs have been shown to participate in methylidene abstraction.[68]

Scheme 1.7 Decomposition of Grubbs Catalysts with Nucleophiles. (a) Attack by PCy_3 Lost from GIIm. (b) Donor-Accelerated Decomposition of GIIm on Treatment with Pyridine.

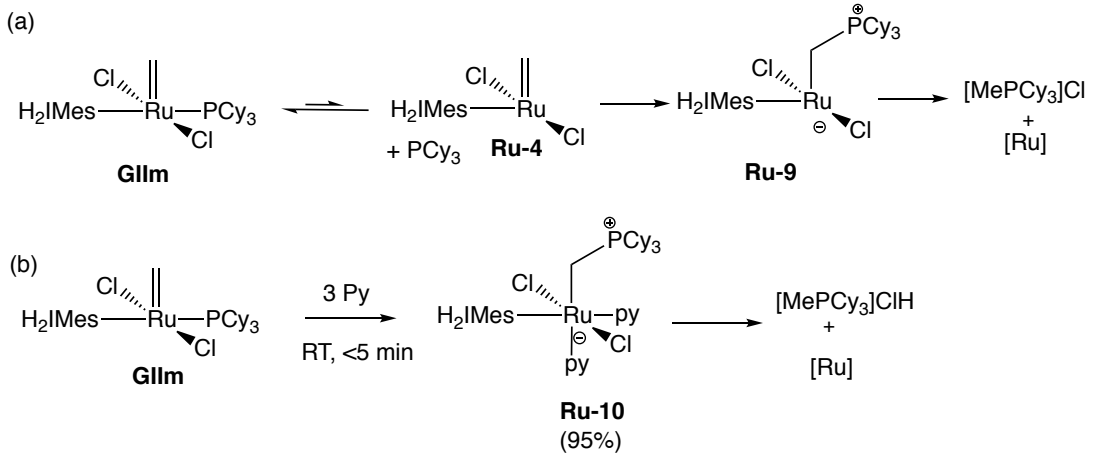

Brønsted bases give access to an alternative decomposition pathway. The negative impact of nitrogen compounds on metathesis yields has long been known,[80-82] but the nature of the problem remained unclear until studies by Benjamin Ireland and Gwen Bailey of the Fogg group.[27,63,83]

They showed that Brønsted bases can deprotonate the MCB intermediate (Scheme 1.8). The unexpected acidity of the MCB β-protons, probably coupled with their greater steric accessibility, greatly favours deprotonation at this site over the H_2IMes ligand. The latter had originally been presumed to be the initial site of deprotonation, on the basis of many crystallographic reports of Ru decomposition products with cyclometalated-NHC substituents. That Brønsted bases attack at the MCB intermediate instead was confirmed by labelling studies, supported by computational analysis.

Scheme 1.8 Decomposition of HII by Brønsted Base: MCB Deprotonation.

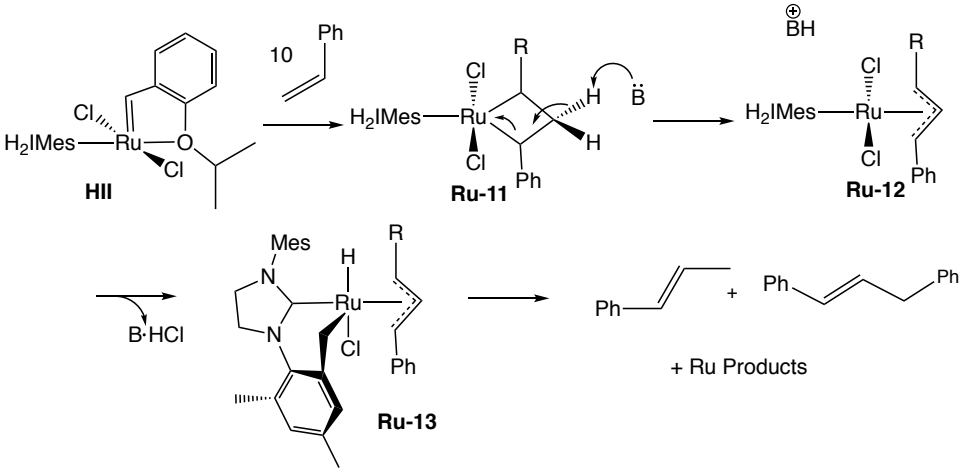

Finally, a recent study from Alexandre Goudreault of the Fogg group has shown that aqueous base also causes catalyst deactivation, a discovery that may prove critical to the application of olefin metathesis in chemical biology. From the observed cessation of metathesis activity, hydroxide ions present in solution were proposed to exchange with the chloride ligands of **HII**.[84] The deliberately-synthesized hydroxide complex **HII-OH** (Scheme 1.9) was shown to initiate slowly, and to decompose via a bimolecular mechanism in the first catalytic cycle. Importantly, the coordinatively unsaturated Ru products resulting from this decomposition were themselves shown to be capable of decomposing uninitiated **HII-OH**, amplifying the detrimental impact of hydroxide ion.

Scheme 1.9 Autocatalytic Decomposition of HII-OH on Treatment with Ethylene.

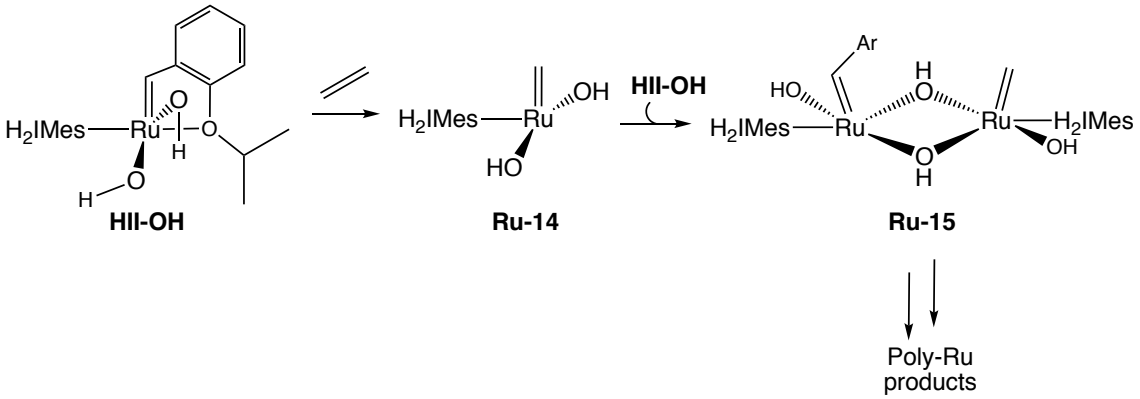

1.5 Scope of this Thesis

Because ruthenium metathesis catalysts are commonly viewed as robust and tolerant, performing metathesis in air has been proposed as a routinely viable synthetic approach.[46] However, no study has been carried out to evaluate the impact of oxygen on catalyst activity, and the mechanistic details of the reaction with oxygen are poorly understood. As is commonly the case, the few reports on catalyst decomposition are inferences based on crystallographically-identified products that serendipitously deposit from reaction mixtures, in undetermined yields. In the next Chapter, the impact of oxygen on metathesis yields is examined for high-performing NHC and CAAC catalysts, to determine the structural features that maximize O_2-tolerance. The mechanism by which oxygen decomposes the precatalysts is also explored.

Chapter 3 focuses on a new means of increasing catalyst productivity, by restricting access of contaminants to the catalyst. Encapsulation of metathesis catalysts in a self-assembled cage is described, and the impact on the lifetimes and productivity of the encapsulated catalysts is examined.

In an attempt to expand the structural diversity of metathesis catalysts, alternative stabilizing ligands were explored. Chapter 4 describes the synthesis and activity of catalysts containing pyridinylide aminophosphine (PyAP) ligands, which are more electron-rich than NHCs. Catalyst decomposition pathways that limit the activity of these catalysts are investigated. Finally, Chapter 5 highlights key findings and suggests future work.

1.6 References

(1) Grubbs, R. H.; Wenzel, A. G., *Handbook of Metathesis*. 2nd ed.; Wiley-VCH: Weinheim, 2015.

(2) Chauvin, Y., Olefin Metathesis: the Early Days (Nobel Lecture). *Angew. Chem., Int. Ed.* **2006**, *45*, 3741–3747.

(3) Schrock, R. R., Multiple Metal-Carbon Bonds for Catalytic Metathesis Reactions (Nobel Lecture). *Angew. Chem., Int. Ed.* **2006**, *45*, 3748–3759.

(4) Grubbs, R. H., Olefin-Metathesis Catalysts for the Preparation of Molecules and Materials (Nobel Lecture). *Angew. Chem., Int. Ed.* **2006**, *45*, 3760–3765.

(5) Eleuterio, H. S., Olefin Metathesis: Chance Favors Those Minds That are Best Prepared. *J. Mol. Catal.* **1991**, *65*, 55-61.

(6) Ivin, K. J.; Mol, J. C., *Olefin Metathesis and Metathesis Polymerization*. Academic Press: New York, 1997.

(7) Keim, W., Oligomerization of Ethylene to α-Olefins: Discovery and Development of the Shell Higher Olefin Process (SHOP). *Angew. Chem., Int. Ed.* **2013**, *52*, 12492–12496.

(8) Chatterjee, A. K.; Choi, T.-L.; Sanders, D. P.; Grubbs, R. H., A General Model for Selectivity in Olefin Cross Metathesis. *J. Am. Chem. Soc.* **2003**, *125*, 11360–11370.

(9) Higman, C. S.; Lummiss, J. A. M.; Fogg, D. E., Olefin Metathesis at the Dawn of Uptake in Pharmaceutical and Specialty Chemicals Manufacturing. *Angew. Chem., Int. Ed.* **2016**, *55*, 3552–3565.

(10) Sutthasupa1, S.; Shiotsuki, M.; Sanda, F., Recent Advances in Ring-Opening Metathesis Polymerization, and Application to Synthesis of Functional Materials. *Polymer J.* **2010**, *42*, 905–915.

(11) Mol, J. C., Applications of Olefin Metathesis in Oleochemistry: an Example of Green Chemistry. *Green Chem.* **2002**, *4*, 5–13.

(12) Schrock, R. R., High-Oxidation-State Molybdenum and Tungsten Alkylidyne Complexes. *Acc. Chem. Res.* **1986**, *19*, 342–348.

(13) Schrock, R. R., Recent Advances in High Oxidation State Mo and W Imido Alkylidene Chemistry. *Chem. Rev.* **2009**, *109*, 3211–3226.

(14) Schwab, P.; Grubbs, R. H.; Ziller, J. W., Synthesis and Applications of $RuCl_2(=CHR')(PR_3)_2$: The Influence of the Alkylidene Moiety on Metathesis Activity. *J. Am. Chem. Soc.* **1996**, *118*, 100–110.

(15) Grela, K., *Olefin Metathesis-Theory and Practice*. Wiley: Hoboken, NJ, 2014.

(16) Nascimento, D. L.; Gawin, A.; Gawin, R.; Guńka, P. A.; Zachara, J.; Skowerski, K.; Fogg, D. E., A Highly Reactive Ruthenium-Indenylidene Catalyst for Olefin Metathesis. *J. Am. Chem. Soc.* **2019**, *141*, 10626–10631.

(17) Marx, V. M.; Sullivan, A. H.; Melaimi, M.; Virgil, S. C.; Keitz, B. K.; Weinberger, D. S.; Bertrand, G.; Grubbs, R. H., Cyclic Alkyl Amino Carbene (CAAC) Ruthenium Complexes

as Remarkably Active Catalysts for Ethenolysis. *Angew. Chem., Int. Ed.* **2015**, *54*, 1919–1923.

(18) Hérisson, J. L.; Chauvin, Y., Catalysis of Olefin Transformations by Tungsten Complexes. II. Telomerization of Cyclic Olefins in the Presence of Acyclic Olefins. *Makromol. Chem.* **1971**, *141*, 161–176.

(19) Grubbs, R. H.; Carr, D. D.; Hoppin, C.; Burk, P. L., Consideration of the Mechanism of the Metal Catalyzed Olefin Metathesis Reaction. *J. Am. Chem. Soc.* **1976**, *98*, 3478–3483.

(20) White, D. E.; Stewart, I. C.; Grubbs, R. H.; Stoltz, B. M., The Catalytic Asymmetric Total Synthesis of Elatol. *J. Am. Chem. Soc.* **2008**, *130*, 810–811.

(21) Heinis, C., DRUG DISCOVERY Tools and rules for macrocycles. *Nat. Chem. Biol.* **2014**, *10*, 696-698

(22) Giordanetto, F.; Kihlberg, J., Macrocyclic Drugs and Clinical Candidates: What Can Medicinal Chemists Learn from Their Properties? *J. Med. Chem.* **2014**, *57*, 278-295.

(23) Mol, J. C., Industrial Applications of Olefin Metathesis. *J. Mol. Catal. A* **2004**, *213*, 39–45.

(24) Chikkali, S.; Mecking, S., Refining of Plant Oils to Chemicals by Olefin Metathesis. *Angew. Chem., Int. Ed.* **2012**, *51*, 5802−5808.

(25) Biermann, U.; Bornscheuer, U.; Meier, M. A. R.; Metzger, J. O.; Schafer, H. J., Oils and Fats as Renewable Raw Materials in Chemistry. *Angew. Chem., Int. Ed.* **2011**, *50*, 3854–3871.

(26) Lummiss, J. A. M.; Oliveira, K. C.; Pranckevicius, A.; Santos, A.; dos Santos, E. N.; Fogg, D. E., Chemical Plants: High-Value Molecules from Essential Oils. *J. Am. Chem. Soc.* **2012**, *134*, 18889–18891.

(27) Santos, A. G.; Bailey, G. A.; dos Santos, E. N.; Fogg, D. E., Overcoming Catalyst Decomposition in Acrylate Metathesis: Poly-phenol Resins as Enabling Agents for Phosphine-Stabilized Metathesis Catalysts. *ACS Catal.* **2017**, *7*, 3181−3189.

(28) Nguyen, S. T.; Johnson, L. K.; Grubbs, R. H.; Ziller, J. W., Ring-Opening Metathesis Polymerization (ROMP) of Norbornene by a Group VIII Carbene Complex in Protic Media. *J. Am. Chem. Soc.* **1992**, *114*, 3974–3975.

(29) Wolf, J.; Stuer, W.; Grunwald, C.; Werner, H.; Schwab, P.; Schulz, M., Ruthenium Trichloride, Tricyclohexylphosphine, 1-Alkynes, Magnesium, Hydrogen, and Water - Ingredients of an Efficient One-Pot Synthesis of Ruthenium Catalysts for Olefin Metathesis. *Angew. Chem., Int. Ed.* **1998**, *37*, 1124–1126.

(30) Kingsbury, J. S.; Harrity, J. P. A.; Bonitatebus, P. J.; Hoveyda, A. H., A Recyclable Ru-Based Metathesis Catalyst. *J. Am. Chem. Soc.* **1999**, *121*, 791–799.

(31) Sanford, M. S.; Love, J. A., Mechanism of Ruthenium-Catalyzed Olefin Metathesis Reactions. In *Handbook of Metathesis*, Grubbs, R. H., Ed. Wiley-VCH: Weinheim, Germany, 2003; Vol. 1, pp 112–131.

(32) Michrowska, A.; Bujok, R.; Harutyunyan, S.; Sashuk, V.; Dolgonos, G.; Grela, K., Nitro-Substituted Hoveyda-Grubbs Ruthenium Carbenes: Enhancement of Catalyst Activity through Electronic Activation. *J. Am. Chem. Soc.* **2004**, *126*, 9318–9325.

(33) Thiel, V.; Hendann, M.; Wannowius, K.-J.; Plenio, H., On the Mechanism of the Initiation Reaction in Grubbs-Hoveyda Complexes. *J. Am. Chem. Soc.* **2012**, *134*, 1104–1114.

(34) Scholl, M.; Ding, S.; Lee, C. W.; Grubbs, R. H., Synthesis and Activity of a New Generation of Ruthenium-Based Olefin Metathesis Catalysts Coordinated with 1,3-Dimesityl-4,5-dihydroimidazol-2-ylidene Ligands. *Org. Lett.* **1999**, *1*, 953–956.

(35) Herrmann, W. A.; Kocher, C., N-Heterocyclic Carbenes. *Angew. Chem., Int. Ed. Engl.* **1997**, *36*, 2163–2187.

(36) Jafarpour, L.; Nolan, S. P., Transition-Metal Systems Bearing a Nucleophilic Carbene Ancillary Ligand: from Thermochemistry to Catalysis. *Adv. Organomet. Chem.* **2001**, *46*, 181–222.

(37) McGuinness, D. S.; Cavell, K. J.; Skelton, B. W.; White, A. H., Zerovalent Palladium and Nickel Complexes of Heterocyclic Carbenes: Oxidative Addition of Organic Halides, Carbon−Carbon Coupling Processes, and the Heck Reaction. *Organometallics* **1999**, *18*, 1596–1605.

(38) Van Veldhuizen, J. J.; Campbell, J. E.; Giudici, R. E.; Hoveyda, A. H., A Readily Available Chiral Ag-Based N-Heterocyclic Carbene Complex for Use in Efficient and Highly Enantioselective Ru-Catalyzed Olefin Metathesis and Cu-Catalyzed Allylic Alkylation Reactions. *J. Am. Chem. Soc.* **2005**, *127*, 6877–6882.

(39) Stewart, I. C.; Douglas, C. J.; Grubbs, R. H., Increased Efficiency in Cross-Metathesis Reactions of Sterically Hindered Olefins. *Org. Lett.* **2008**, *10*, 441–444.

(40) Hoveyda, A. H.; Gillingham, D. G.; Van Veldhuizen, J. J.; Kataoka, O.; Garber, S. B.; Kingsbury, J. S.; Harrity, J. P. A., Ru Complexes Bearing Bidentate Carbenes: from Innocent Curiosity to Uniquely Effective Catalysts for Olefin Metathesis. *Org. Biomol. Chem.* **2004**, *2*, 8–23.

(41) Gillingham, D. G.; Kataoka, O.; Garber, S. B.; Hoveyda, A. H., Efficient Enantioselective Synthesis of Functionalized Tetrahydropyrans by Ru-Catalyzed Asymmetric Ring-Opening Metathesis/Cross-Metathesis (AROM/CM). *J. Am. Chem. Soc.* **2004**, *126*, 12288–12290.

(42) Vehlow, K.; Maechling, S.; Blechert, S., Ruthenium Metathesis Catalysts with Saturated Unsymmetrical N-Heterocyclic Carbene Ligands. *Organometallics* **2006**, *25*, 25–28.

(43) Hong, S. H.; Grubbs, R. H., Highly Active Water-Soluble Olefin Metathesis catalyst. *J. Am. Chem. Soc.* **2006**, *128*, 3508–3509.

(44) Hong, S. H.; Grubbs, R. H., Efficient Removal of Ruthenium Byproducts from Olefin Metathesis Products by Simple Aqueous Extraction. *Org. Lett.* **2007**, *9*, 1955–1957.

(45) Jordan, J. P.; Grubbs, R. H., Small-Molecule N-heterocyclic-Carbene-Containing Olefin-Metathesis Catalysts for Use in Water. *Angew. Chem., Int. Ed.* **2007**, *46*, 5152–5155.

(46) Guidone, S.; Songis, O.; Nahra, F.; Cazin, C. S. J., Conducting Olefin Metathesis Reactions in Air: Breaking the Paradigm. *ACS Catal.* **2015**, *5*, 2697–2701.

(47) Kim, M.; Eum, M. S.; Jin, M. Y.; Jun, K. W.; Lee, C. W.; Kuen, K. A.; Kim, C. H.; Chin, C. S., Reactions of Ruthenium Benzylidenes with H_2O to Give Benzaldehyde and (Aqua)ruthenium Complex. *J. Organomet. Chem.* **2004**, *689*, 3535–3540.

(48) Anderson, D. R.; Lavallo, V.; O'Leary, D. J.; Bertrand, G.; Grubbs, R. H., Synthesis and Reactivity of Olefin Metathesis Catalysts Bearing Cyclic (Alkyl)(Amino)Carbenes. *Angew. Chem., Int. Ed.* **2007**, *46*, 7262–7265.

(49) Soleilhavoup, M.; Bertrand, G., Cyclic (Alkyl)(Amino)Carbenes (CAACs): Stable Carbenes on the Rise. *Acc. Chem. Res.* **2015**, *48*, 256–266.

(50) Nascimento, D. L.; Fogg, D. E., Origin of the Breakthrough Productivity of Ruthenium-CAAC Catalysts in Olefin Metathesis (CAAC = Cyclic Alkyl Amino Carbene). *J. Am. Chem. Soc.* **2019**, *141*, 19236–19240.

(51) Alcaide, B.; Almendros, P.; Luna, A., Grubbs' Ruthenium-Carbenes Beyond the Metathesis Reaction: Less Conventional Non-Metathetic Utility. *Chem. Rev.* **2009**, *109*, 3817–3858.

(52) Larionov, E.; Li, H.; Mazet, C., Well-Defined Transition Metal Hydrides in Catalytic Isomerizations. *Chem. Commun.* **2014**, *50*, 9816–9826.

(53) Higman, C. S.; Lanterna, A. E.; Marin, M. L.; Scaiano, J. C.; Fogg, D. E., Catalyst Decomposition During Olefin Metathesis Yields Isomerization-Active Ru Nanoparticles. *ChemCatChem* **2016**, *8*, 2446–2449.

(54) Higman, C. S.; Plais, L.; Fogg, D. E., Isomerization During Olefin Metathesis: An Assessment of Potential Catalyst Culprits. *ChemCatChem* **2013**, *5*, 3548-3551.

(55) Amoroso, D.; Yap, G. P. A.; Fogg, D. E., Deactivation of Ruthenium Metathesis Catalysts via Facile Formation of Face-Bridged Dimers. *Organometallics* **2002**, *21*, 3335–3343.

(56) Amoroso, D.; Snelgrove, J. L.; Conrad, J. C.; Drouin, S. D.; Yap, G. P. A.; Fogg, D. E., An Attractive Route to Olefin Metathesis Catalysts: Facile Synthesis of a Ruthenium Alkylidene Complex Containing Labile Phosphane Donors. *Adv. Synth. Catal.* **2002**, *344*, 757–763.

(57) Hong, S. H.; Wenzel, A. G.; Salguero, T. T.; Day, M. W.; Grubbs, R. H., Decomposition of Ruthenium Olefin Metathesis Catalysts. *J. Am. Chem. Soc.* **2007**, *129*, 7961–7968.

(58) Beach, N. J.; Lummiss, J. A. M.; Bates, J. M.; Fogg, D. E., Reactions of Grubbs Catalysts with Excess Methoxide: Formation of Novel Methoxyhydride Complexes. *Organometallics* **2012**, *31*, 2349–2356.

(59) Lummiss, J. A. M.; Beach, N. J.; Smith, J. C.; Fogg, D. E., Targeting an Achilles Heel In Olefin Metathesis: A Strategy For High-Yield Synthesis of Second-Generation Grubbs Methylidene Catalysts. *Catal. Sci. Technol.* **2012**, *2*, 1630–1632.

(60) Lummiss, J. A. M.; Botti, A. G. G.; Fogg, D. E., Isotopic Probes for Ruthenium-Catalyzed Olefin Metathesis. *Catal. Sci. Technol.* **2014**, *4*, 4210–4218.

(61) Lummiss, J. A. M.; Ireland, B. J.; Sommers, J. M.; Fogg, D. E., Amine-Mediated Degradation in Olefin Metathesis Reactions that Employ the Second-Generation Grubbs Catalysts. *ChemCatChem* **2014**, *6*, 459–463.

(62) Lummiss, J. A. M.; McClennan, W. L.; McDonald, R.; Fogg, D. E., Donor-Induced Decomposition of the Grubbs Catalysts: An Intercepted Intermediate *Organometallics* **2014**, *33*, 6738–6741.

(63) Ireland, B. J.; Dobigny, B. T.; Fogg, D. E., Decomposition of a Phosphine-Free Metathesis Catalyst by Amines and Other Nitrogen Bases: Metallacyclobutane Deprotonation as a Major Deactivation Pathway. *ACS Catal.* **2015**, *5*, 4690−4698.

(64) McClennan, W. L.; Rufh, S. A.; Lummiss, J. A. M.; Fogg, D. E., A General Decomposition Pathway for Phosphine-Stabilized Metathesis Catalysts: Lewis Donors Accelerate Methylidene Abstraction. *J. Am. Chem. Soc.* **2016**, *138*, 14668−14677.

(65) Bailey, G. A.; Lummiss, J. A. M.; Foscato, M.; Occhipinti, G.; McDonald, R.; Jensen, V. R.; Fogg, D. E., Decomposition of Olefin Metathesis Catalysts by Brønsted Base: Metallacyclobutane Deprotonation as a Primary Deactivating Event. *J. Am. Chem. Soc.* **2017**, *139*, 16446–16449.

(66) Engel, J.; Smit, W.; Foscato, M.; Occhipinti, G.; Törnroos, K. W.; Jensen, V. R., Loss and Reformation of Ruthenium Alkylidene: Connecting Olefin Metathesis, Catalyst Deactivation, Regeneration, and Isomerization. *J. Am. Chem. Soc.* **2017**, *139*, 16609–16619.

(67) Bailey, G. A.; Foscato, M.; Higman, C. S.; Day, C. S.; Jensen, V. R.; Fogg, D. E., Bimolecular Coupling as a Vector for Decomposition of Fast-Initiating Olefin Metathesis Catalysts. *J. Am. Chem. Soc.* **2018**, *140*, 6931–6944.

(68) Rufh, S.; Goudreault, A. Y.; Foscato, M.; Jensen, V. R.; Fogg, D. E., Rapid Decomposition of Olefin Metathesis Catalysts by a Truncated N-Heterocyclic Carbene (NHC): Unprecedentedly Efficient Catalyst Quenching and NHC Vinylation. *ACS Catal.* **2018**, *8*, 11822−11826.

(69) Romero, P. E.; Piers, W. E., Direct Observation of a 14-Electron Ruthenacyclobutane Relevant to Olefin Metathesis. *J. Am. Chem. Soc.* **2005**, *127*, 5032–5033.

(70) Romero, P. E.; Piers, W. E.; McDonald, R., Rapidly Initiating Ruthenium Olefin-Metathesis Catalysts Angew. Chemie 2004 116, 6287-6291. *Angew. Chem., Int. Ed.* **2004**, *43*, 6161–6165.

(71) van der Eide, E. F.; Piers, W. E., Mechanistic Insights into the Ruthenium-Catalysed Diene Ring-Closing Metathesis Reaction. *Nature Chem.* **2010**, *2*, 571–576.

(72) Adlhart, C.; Chen, P., Comparing Intrinsic Reactivities of the First- and Second-Generation Ruthenium Metathesis Catalysts in the Gas Phase. *Helv. Chim. Acta* **2003**, *86*, 941–949.

(73) Romero, P. E.; Piers, W. E., Mechanistic Studies on 14-Electron Ruthenacyclobutanes: Degenerate Exchange with Free Ethylene. *J. Am. Chem. Soc.* **2007**, *129*, 1698–1704.

(74) Farina, V.; Horváth, A., Ring-Closing Metathesis in the Large-Scale Synthesis of Pharmaceuticals. In *Handbook of Metathesis*, Grubbs, R. H.; Wenzel, A. G., Eds. Wiley-VCH: Weinheim, 2015; Vol. 2, pp 633–658.

(75) Fandrick, K. R.; Savoie, J.; Jinhua, N. Y.; Song, J. J.; Senanayake, C. H., Challenges and Opportunities for Scaling the Ring-Closing Metathesis Reaction in the Pharmaceutical Industry. In *Olefin Metathesis – Theory and Practice*, Grela, K., Ed. Wiley: Hoboken, 2014; pp 349-366.

(76) Nicola, T.; Brenner, M.; Donsbach, K.; Kreye, P., First Scale-Up to Production Scale of a Ring Closing Metathesis Reaction Forming a 15-Membered Macrocycle as a Precursor of an Active Pharmaceutical Ingredient. *Org. Process Res. Dev.* **2005**, *9*, 513–515.

(77) Dinger, M. B.; Mol, J. C., Degradation of the Second-Generation Grubbs Metathesis Catalyst with Primary Alcohols and Oxygen. *Eur. J. Inorg. Chem.* **2003**, 2827–2833.

(78) Beach, N. J.; Camm, K. D.; Fogg, D. E., Hydrogenolysis versus Methanolysis of First- and Second-Generation Grubbs Catalysts: Rates, Speciation, and Implications for Tandem Catalysis. *Organometallics* **2010**, *29*, 5450–5455.

(79) Hansen, S. M.; Rominger, F.; Metz, M.; Hofmann, P., The First Grubbs-Type Metathesis Catalyst with Cis Stereochemistry: Synthesis of (h^2-dtbpm)$RuCl_2$(=CHCH=CMe_2) From a Novel, Coordinatively Unsaturated Dinuclear Ruthenium Dihydride. *Chem. – Eur. J.* **1999**, *5*, 557–566.

(80) Lafaye, K.; Bosset, C.; Nicolas, L.; Guérinot, A.; Cossy, J., Lewis Basicity Modulation of N-Heterocycles: A Key for Successful Cross-Metathesis. *Beilstein J. Org. Chem.* **2015**, *11*, 2223–2241.

(81) Yee, N. K.; Farina, V.; Houpis, I. N.; Haddad, N.; Frutos, R. P.; Gallou, F.; Wang, X.-J.; Wei, X.; Simpson, R. D.; Feng, X.; Fuchs, V.; Xu, Y.; Tan, J.; Zhang, L.; Xu, J.; Smith-Keenan, L. L.; Vitous, J.; Ridges, M. D.; Spinelli, E. M.; Johnson, M.; Donsbach, K.; Nicola, T.; Brenner, M.; Winter, E.; Kreye, P.; Samstag, W., Efficient Large-Scale Synthesis of BILN 2061, a Potent HCV Protease Inhibitor, by a Convergent Approach Based on Ring-Closing Metathesis. *J. Org. Chem.* **2006**, *71*, 7133–7145.

(82) Wang, H.; Goodman, S. N.; Dai, Q.; Stockdale, G. W.; Clark, W. M., Development of a Robust Ring-Closing Metathesis Reaction in the Synthesis of SB-462795, a Cathepsin K Inhibitor. *Org. Process Res. Dev.* **2008**, *12*, 226–234.

(83) Bailey, G. A. Fogg, D. E., Acrylate Metathesis via the Second-Generation Grubbs Catalyst: Unexpected Pathways Enabled by a PCy_3-Generated Enolate. *J. Am. Chem. Soc.* **2015**, *137*, 7318–7321.

(84) Goudreault, A. Y.; Walden, D. M.; Nascimento, D. L.; Botti, A. G.; Steinmann, S. N.; Michel, C.; Fogg, D. E., Hydroxide-Induced Degradation of Olefin Metathesis Catalysts: A Challenge for Metathesis in Alkaline Media. *ACS Catal.* **2020**, *10*, 3838−3843.

2 Impact of Oxygen on Ruthenium Catalysed Olefin Metathesis

2.1 Published Contribution

The Impact of Oxygen on Leading and Emerging Ru-Carbene Catalysts for Olefin Metathesis: An Unanticipated Correlation Between Robustness and Metathesis Activity S. J. Ton and D. E. Fogg.* ACS Catal. 2019, 11329-11334 (Communication). Copyright 2019 American Chemical Society. Reprinted with permission.

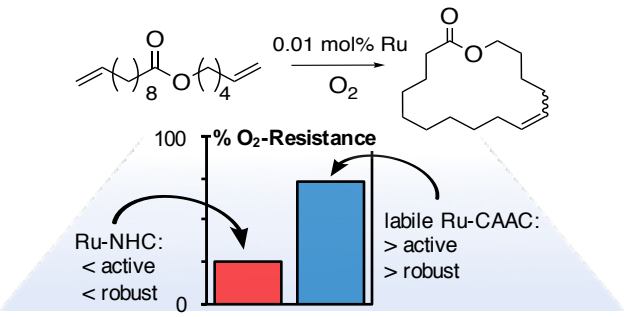

Abstract: The impact of O_2 on olefin metathesis promoted by Ru-NHC and Ru-CAAC catalysts is examined (NHC = N-heterocyclic carbene; CAAC = cyclic alkyl amino carbene). An atmosphere of 8% O_2 in Ar is found to decrease turnover numbers by ca. 15-95% in ring-closing metathesis, including macrocyclization reactions. All H_2IMes catalysts studied, irrespective of their ease of initiation, exhibit broadly similar O_2-sensitivity, within the middle of this range. Much greater disparities in performance emerge for the CAAC catalysts, which exhibit an unexpected correlation between reactivity and robustness. Fast-initiating CAAC catalysts show greatest resistance to O_2 of all systems studied. Mechanistic studies with the second-generation Grubbs catalyst $RuCl_2(H_2IMes)(PCy_3)(=CHPh)$ **GII**, which contains the useful PCy_3 and benzylidene reporter groups, suggest that [2+2] cycloaddition of O_2 dominates over the reported attack of O_2 at the benzylidene ligand. At catalyst concentrations compatible with NMR analysis (20 mM Ru), bimolecular coupling of **Ru-4** is also a significant contributor to decomposition.

Author Contributions: This manuscript was written by SJT and DEF. Experiments were conceived by SJT and DEF, and conducted by SJT.

2.2 Introduction

The transformative impact of olefin metathesis on organic synthesis[1,2] rests on the versatility of the reaction, its independence of activating groups, and Grubbs' pioneering discovery[3] of ruthenium catalysts that enable metathesis without rigorous exclusion of air. The latter was the breakthrough that put metathesis methodologies into the hands of the practicing organic chemist, and the Ru catalysts have hence been viewed as O_2-tolerant since their inception. This has important implications for applications in which catalyst productivity is critical, including pharmaceutical processes.[4]

Many Ru precatalysts, including most of those in Chart 2.1, are sufficiently oxygen-stable that they can be chromatographed in air.[5] Less clear is the stability of the active species. Tolerance is suggested by reports of aerobic metathesis.[6-10] These typically involve ring-closing metathesis (RCM) of readily-cyclized dienes, but several instances have been reported of the RCM assembly of challenging targets, such as tetrasubstituted olefins[7] and macrocyclic rings.[8]

Chart 2.1 N-Heterocyclic Carbene (NHC) and Cyclic Alkyl Amino Carbene (CAAC) Catalysts Discussed.

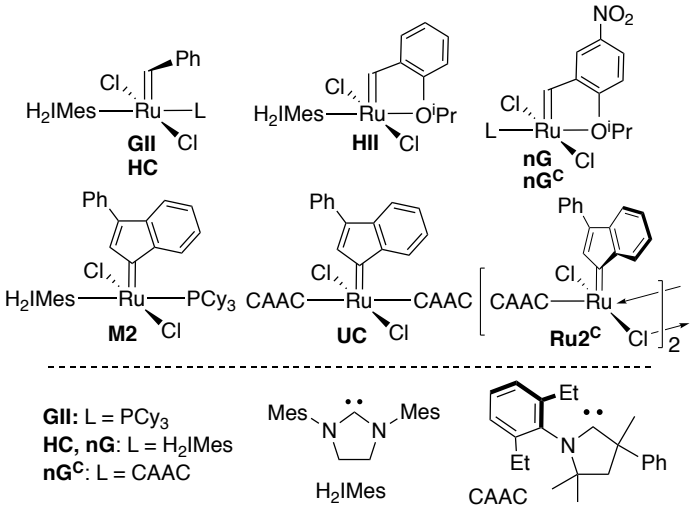

We queried, however, whether oxidative decomposition in these studies was potentially masked by "sacrificial" catalyst, i.e. relatively high catalyst loadings. Minimizing such loadings is desirable in target-directed synthesis, not merely for reasons of cost, but to simplify product

purification and protect isolated yields.[4,11] (A further consideration in process chemistry is the level of residual metals in active pharmaceutical ingredients).[4,12] However, at low catalyst loadings, the increased proportion of contaminants relative to catalyst presents more stringent challenges to productivity.[13,14] Here we examined leading NHC and emerging, highly productive CAAC catalysts (Chart 2.1), with three objectives. We sought, first, to determine which structural features confer greatest O_2-tolerance at synthetically optimal loadings; secondly, to assess the impact of the carbene ligand for reactions of widely varying difficulty; and finally, to gain insight into the reaction chemistry underlying catalyst decomposition.

2.3 Results and Discussion

We began by examining the impact of O_2 on macrocycle RCM (mRCM), with the rationale that challenging reactions should be most revealing. A core challenge in mRCM of conformationally unconstrained dienes such as **1** (Figure 2.1a) lies in the millimolar diene concentrations required. At optimal catalyst loadings,[13f,15] this translates into micromolar Ru concentrations, placing high demands on catalyst activity and longevity. Further, oligomerization of such dienes is kinetically favoured, even at high dilutions,[16] and the oligomers must be recycled into product via metathesis at internal, predominantly trans-olefinic sites.

To assess the impact of O_2, we compared mRCM yields under O_2 with those under N_2 (Figure 2.1a). An atmosphere of 8% O_2 in Ar was used as a proxy for air, in light of Cazin's important finding[7] that multiple constituents of air (O_2, CO_2, and particularly H_2O) have a negative impact on metathesis productivity.[a] We also drew on recent work on high-performing mRCM catalysts[13f] to identify a catalyst loading at which yields of **1'** would be high, but not quantitative, at ambient temperatures (0.01 mol% Ru).[b] Sub-quantitative yields in the control reaction are essential to ensure that decomposition is not masked by excessive catalyst.

---

[a] The finding that air is more detrimental than O_2 was replicated in the present work: see Appendix A, Table A5.

[b] This loading is 50x lower than that in the literature report of aerobic mRCM. See ref 8.

A negative impact of O_2 was evident for all catalysts studied. Least affected, as shown in Figure 2.1a, were the CAAC catalysts **Ru2^{C}** and **nG^{C}**. Even for the leading H_2IMes catalyst **nG** (the nitro-functionalized Grela catalyst),[17] mRCM yields dropped by ca. 60% under O_2 vs. N_2, as compared to ca. 25% for the top-performing CAAC catalyst **Ru2^{C}**. The breakthrough metathesis productivity of the CAAC catalysts[13f,15,18] thus appears to be reinforced by a higher commitment toward reaction with olefin, vs. oxygen.

An outlier in this trend is bis-CAAC complex **UC**,[19] for which mRCM yields drop from nearly 50% to ca. 5% in the presence of O_2. The negative impact of O_2 on metathesis by **UC** is clearly not due to the indenylidene ligand, as the indenylidene dimer **Ru2^{C}** was least affected of all catalysts studied. We speculate that O_2 binding to the sixth coordination site of the precatalyst **UC** may permit decomposition to compete with entry into the catalytic cycle. Factors favouring O_2 binding are the π-acidity of the CAAC ligands,[20,21] low ligand lability,[19] and the reduced steric pressure exerted by the rigid indenylidene unit (in contrast with the conformationally mobile benzylidene ligand present in **GII**[22] and, following dechelation, **nG** or **HII**). Crystallographic and reactivity studies confirm that **UC** and related bis-CAAC derivatives are much less sterically crowded than the corresponding carbene/PCy_3 catalysts.[13f,19]

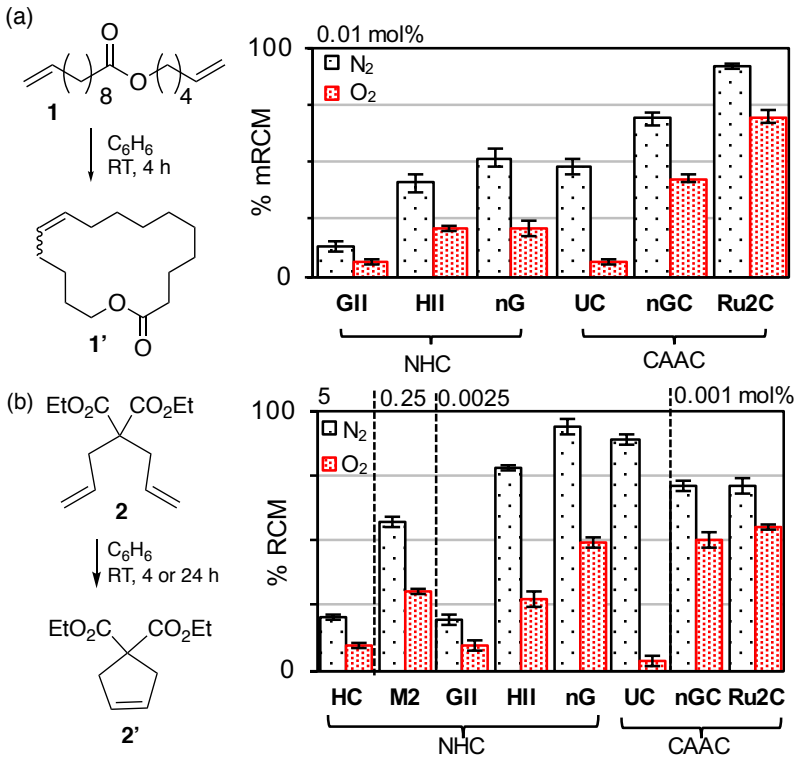

Figure 2.1 (a) Impact of O_2 on mRCM. (b) Impact of O_2 on RCM (reaction time 4 h, except for **HC**; 24 h). For numerical data and RCM yields at additional catalyst loadings, see Appendix A, Tables A-1 and A-2**.**

Having established that O_2 affects challenging metathesis reactions, we turned to its impact on RCM of diethyl diallyl malonate (**2**; Figure 2.1b), the classic substrate for aerobic metathesis. The ease with which **2** can be cyclized permits expansion of the range of catalysts to include slow-initiating **M2** and the Herrmann-class[23] bis-NHC catalyst **HC**. While the exceptionally facile RCM of **2** offers an aggressive test for the impact of O_2, it also greatly amplifies differences in catalyst activity. For RCM under N_2, loadings of 5 mol% and 0.25 mol%, respectively, were required to extract adequate activity from **HC** and **M2** at RT (Figure 2.1b). For the other catalysts examined, 0.05 mol% Ru (Figure 2.2b) was excessive for all but **GII**.[a] A 20-fold decrease (to 0.0025 mol% Ru) was more generally suitable, but remains too high for **Ru2**^{C} and **nG**^{C} (Figure 2.2a), for which 0.001 mol% Ru was required for sub-quantitative yields under N_2 (Figure 2.2c). The negative

[a] In light of these results, prior successes in the aerobic RCM of **2** at 0.1-5 mol% Ru are unsurprising. For a review, see ref 6.

impact of O_2 is again evident in all cases, at a level comparable to that in mRCM, despite the greater ease of the RCM reaction. Again, the highly labile[24] CAAC catalysts are most robust to O_2.

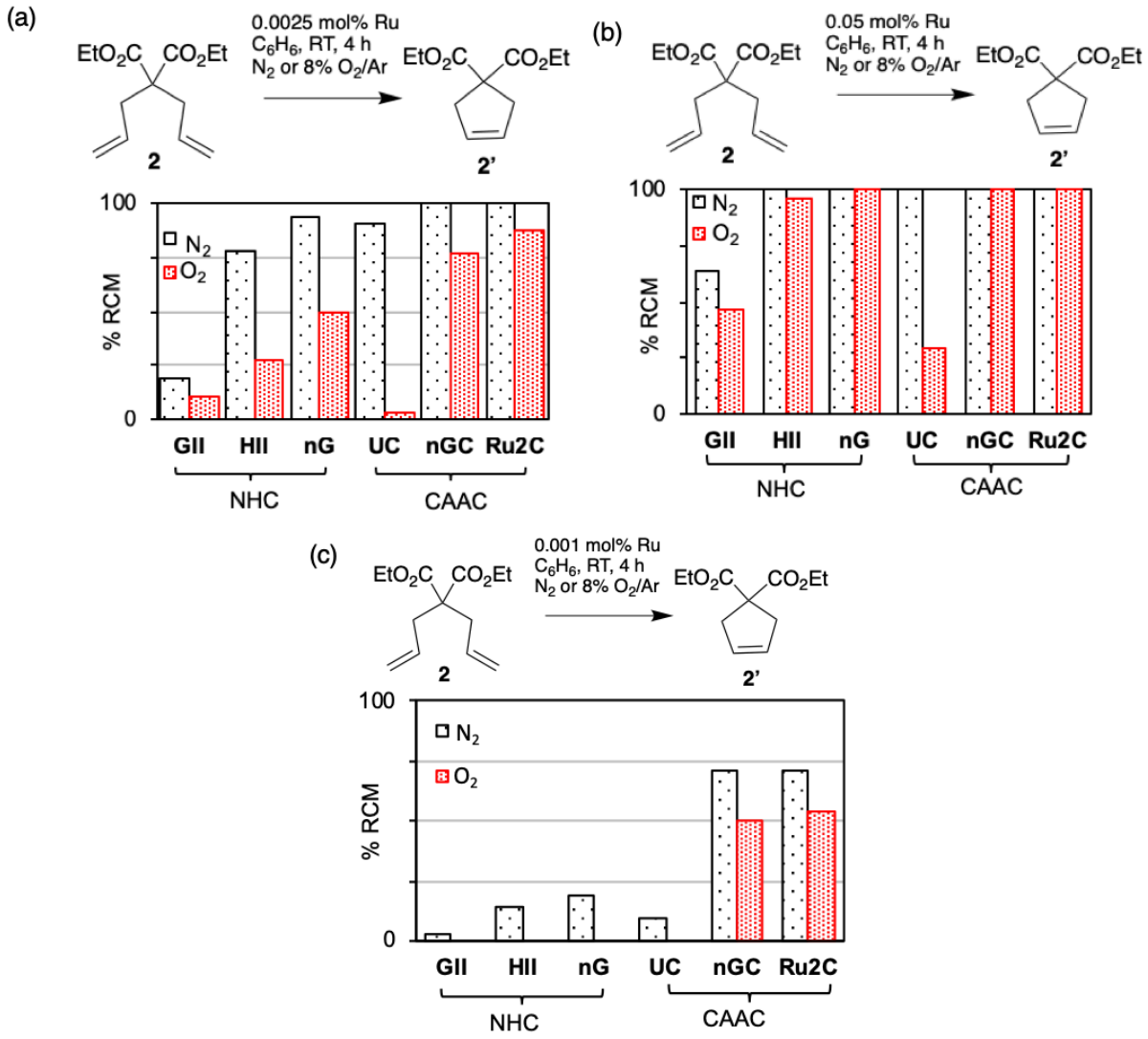

Figure 2.2 Attempts to assess the impact of O_2 on RCM of **2** (a) at 0.05 mol% Ru. Use of excessive catalyst results in 100% yield in the control experiments for all catalysts except **GII**, limiting the observable impact of O_2. (b) at 0.0025 mol% Ru catalyst loading is excessive for **Ru2**^{c} and **nG**^{C}**.** (c) at 0.001 mol% Ru. At this loading, the yields under N_2 are too low to accurately assess the impact of O_2 for **GII**, **HII**, **nG**, and **UC**, and the O_2 experiments are thus shown only for **Ru2**^{C} and **nG**^{C}. Note: catalysts **M2**, **HC** omitted. For numerical data, see Appendix A, Table A-3.

In the plots shown in Figure 2.1, the yields under O_2 are controlled by both O_2-sensitivity, and inherent metathesis activity. To isolate the impact of O_2, Figure 2.3 shows the resistance to O_2 for each catalyst, as a percentage of its RCM activity under N_2. Broadly similar performance is seen for *all* of the NHC catalysts, regardless of the ease with which they enter the catalytic cycle. Also notable is the fact that the most labile, most metathesis-active CAAC catalysts are also most O_2-tolerant, delivering the highest RCM yields in the presence of oxygen. This observation challenges the widely-held belief that, in general, poorer metathesis activity is offset by increased catalyst robustness.[25] Indeed, for **UC**, slow release of the active species appears to greatly increase sensitivity to oxygen.

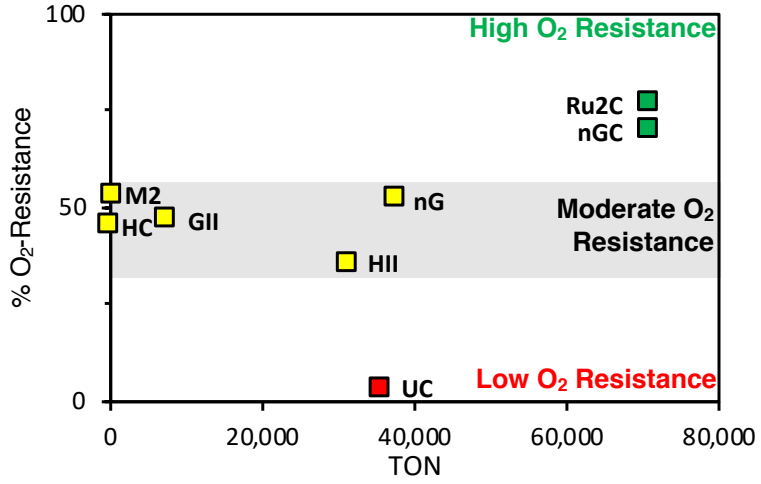

Figure 2.3 Assessing catalyst resistance to O_2 from performance in RCM of **2**. % O_2-resistance = 100 – [(Δ Yield / N_2 Yield) x 100]. For numerical data, see Appendix A, Table A-4.

The mechanism by which O_2 attacks the catalysts is of long-standing interest. In early work, Dinger and Mol noted that insight was hampered by difficulties in intercepting the Ru products, and resorted to solid-state reactions to limit decomposition.[26] Solid **GII** was completely consumed after 3 days under 50 atm O_2 at 60 °C, and phenyl complex **Ru-16** (Scheme 2.1a) was isolated as the sole identifiable Ru product in 29% yield.[26,27] Decomposition is retarded by added PCy_3 (Figure 2.4c), indicating that this pathway, as with those discussed below, proceed via four-coordinate **Ru-4**. Complex **Ru-16** was proposed to form by attack of O_2 at the benzylidene carbon, and deinsertion of CO from the putative [Ru]–C(O)Ph intermediate.[26] In concurrent work, Trnka and Grubbs (Scheme 2.1b) identified cyclometallated **Ru-17** from crystals that deposited on

inadvertent exposure of **GII** to air.[23b] These apparently distinct reactions may reflect two stages on the same pathway (see dashed arrow). NHC cyclometallation, with concomitant liberation of HX, is well established for Ru–X species[13b,28-34] (including Ru-alkyl intermediates formed during decomposition of **GII** and its resting-state methylidene derivative).[30]

A metathesis-like [2+2] cycloaddition of O_2 (Scheme 2.1c) has been invoked in group 6 chemistry, to account for formation of the aldehyde ^{t}BuCHO and Mo(O)(=NAr)(O^{t}Bu)$_2$ from the Schrock metathesis catalyst Mo(=NAr)(=CH^{t}Bu)(O^{t}Bu)$_2$.[35] This possibility has not, to our knowledge, been examined in the Ru systems. We set out to assess its relevance to the best-studied system, **GII**, which (like **UC**, but unlike **HII**: Appendix A, Figures A1-A5) is attacked by O_2 even in the absence of substrate. We regarded the benzylidene ligand in **GII** as a potentially important asset, which could offer mechanistic insight if it can be tracked in the organic products of decomposition.[36]

Scheme 2.1 Reported Ru Products Formed on Decomposition of GII by O_2. (a) At High O_2 Concentrations.[26] (b) At Low O_2 Concentrations.[23b] (c) Reported Cycloaddition of O_2 to a Group 6 Catalyst.[35]

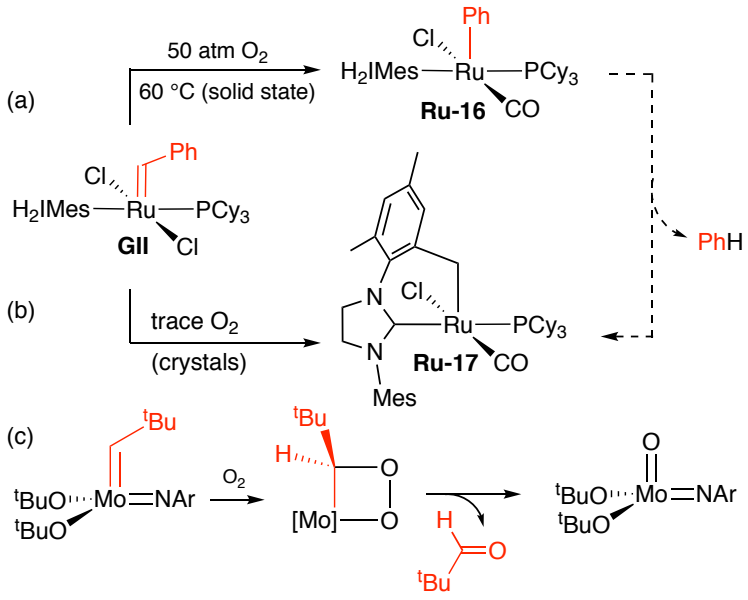

Accordingly, NMR experiments were carried out with ^{1}H and ^{31}P NMR integration standards present (the latter in a sealed capillary; see SI). The C_6D_6 solution was initially saturated with 8% O_2 in Ar, and replenished with the gas every 24 h. The proportion of **GII** decreased to ca. 25%

over the first 24 h, and to <5% after 48 h: no **GII** remained at 72 h (Figures 1.5, A1-A3). Quantitative $^{31}P\{^{1}H\}$ NMR analysis at full decomposition revealed minor amounts of the known Ru products **Ru-16** and **Ru-17** (7% and 4%, respectively; Scheme 2.2a). In comparison, benzaldehyde was present in 30% yield, consistent with [2+2] cycloaddition of O_2 to four-coordinate **Ru-4** (Scheme 2.2b).[37] We infer that O_2 engages in both cycloaddition[a] and attack at the benzylidene carbon, cycloaddition being dominant.

An additional, unexpected decomposition pathway is indicated by the observation of stilbene in significant amounts (55% based on starting **GII**; Figure 2.4a). Stilbene is a diagnostic marker for bimolecular coupling of **Ru-4** (Scheme 2.2c). Elimination of stilbene is normally slow for **GII**,[38] as the low lability of the PCy_3 ligand[24] limits the concentration of **Ru-4**. It occurs in minutes, however, on heating **GII** in the presence of the phosphine scavenger CuCl.[13f] In the present case, O_2 likewise sequesters PCy_3 (as the phosphine oxide: 58% detected by $^{31}P\{^{1}H\}$ NMR analysis), promoting bimolecular coupling (BMC) and elimination of stilbene. The proportion of stilbene is ca. twice that of benzaldehyde, indicating that **Ru-4** undergoes BMC faster than cycloaddition of O_2. It should be emphasized, however, that BMC is accelerated in these experiments by the relatively high Ru concentrations required for NMR analysis (ca. 20 mM Ru; cf. 0.5–0.05 mM under the metathesis conditions of Figure 2.1).

[a] Mechanistically distinct reactions might be expected for singlet and triplet oxygen in this pathway. The low concentration of singlet oxgen under standard reaction conditions puts it out of contention as a reagent in the present work, however.

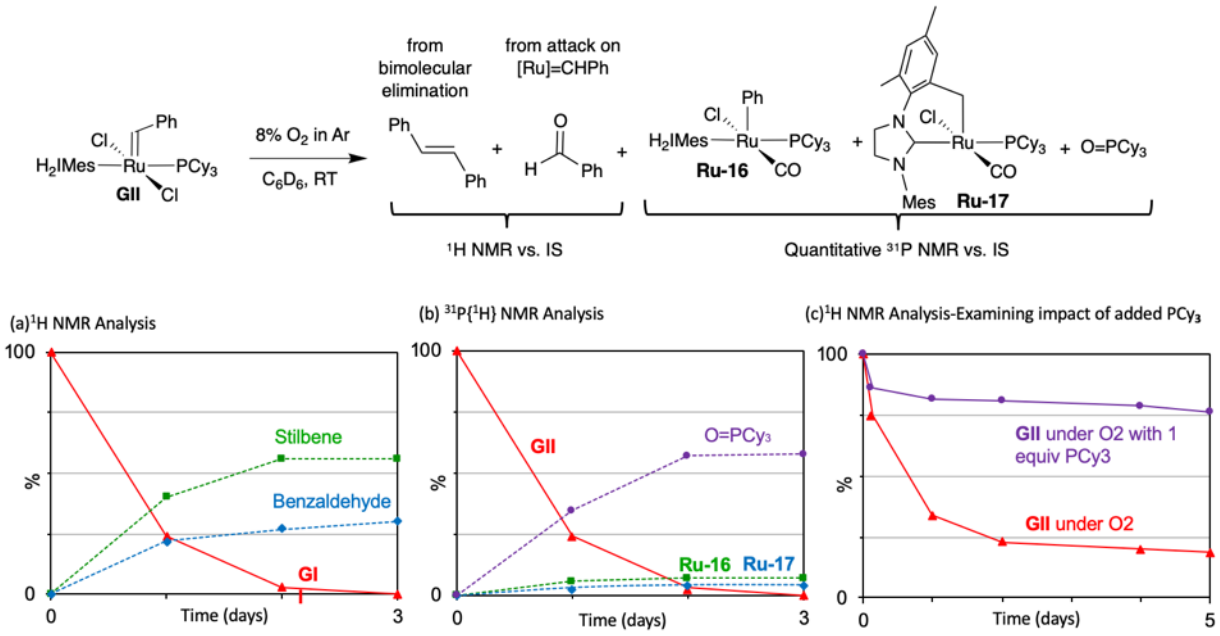

Figure 2.4 Rate profiles for decomposition of **GII** under O_2. (a) Loss of **GII** and formation of stilbene and benzaldehyde (^{1}H NMR analysis). O_2 atmosphere replenished every 24 h. (b) Parallel analysis by quantitative $^{31}P\{^1H\}$ NMR spectroscopy, showing loss of **GII** and formation of $O{=}PCy_3$, **Ru-16** and **Ru-17**. (c) Examining impact of added PCy_3 (^{1}H NMR analysis; O_2 atmosphere not replenished).

Scheme 2.2 Proposed Reactions of Ru-4 under O_2.[a] (a) O_2 Attack on Benzylidene.[26] (b) O_2 Cycloaddition. (c) Bimolecular Elimination of Stilbene.

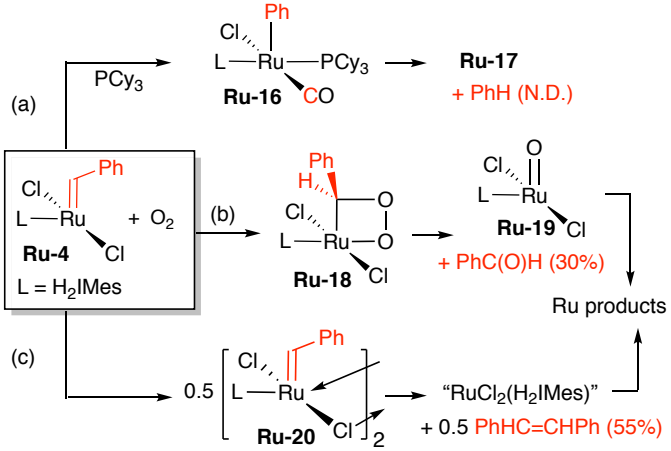

[a] N.D. = % not determined; yield of **Ru-16** + **Ru-17** = 11%. Conditions: 20 mM Ru; C_6D_6; RT (19 °C), 72 h.

2.4 Conclusions

The foregoing describes the impact of O_2 on metathesis via Ru-NHC and Ru-CAAC catalysts. A mechanistic study of an important model system, the Grubbs catalyst **GII**, revealed that oxidative decomposition occurs via 2+2 cycloaddition of O_2 and (as a minor pathway) attack at the benzylidene carbon. In addition, oxidation of the PCy_3 ligand promotes bimolecular elimination of the benzylidene ligand as stilbene: indeed, this is the fastest decomposition process at high (millimolar) catalyst concentrations. While broadly similar sensitivity was seen for all H_2IMes catalysts, an unexpected correlation between robustness and metathesis activity emerged for the CAAC catalysts. Of note, highly productive Ru-CAAC catalysts proved significantly more robust than their H_2IMes counterparts. Improved resistance to oxidative decomposition hence reinforces the breakthrough productivity established for Ru-CAAC catalysts in olefin metathesis. The origin of the remarkable robustness of these catalysts is under study, and will be reported in due course.

2.5 Experimental Details

2.5.1 General Procedures

Reactions with O_2 were carried out on a Schlenk line under 8% O_2 in Ar (Linde HIQ Certified 7.96%; contaminants <10 ppm). Control experiments were carried out on a Schlenk line under Ar, or (for greater convenience) in a glovebox under N_2. For validation of the latter experiments, see Section S2a. All reactions were carried out in HPLC grade C_6H_6, which was dried and degassed using a Glass Contour solvent purification system and stored under N_2 over 4 Å molecular sieves for at least 16 h prior to use. Karl-Fischer titration indicated 5 ppm water in C_6H_6 obtained from the drying column prior to storing over molecular sieves. The NMR solvent C_6D_6 (Cambridge Isotopes) was freeze-pump-thaw degassed[39] and stored under N_2 over 4 Å molecular sieves for at least 12 h prior to use. Potassium tris(1-pyrazolyl)borate (KTp; TCI), dimethyl terephthalate (DMT, Aldrich), anthracene (Aldrich) and 1,4-bis(diphenylphosphino)butane (dppb, Strem) were used as received. Metathesis catalysts **GII**,[40] **Ru2^C**,[41] **HII**,[42] **HC**[43] and **M2**[40] were prepared by literature methods, as were dienes **1**[44] and the RCM products **1'**[44] and **2'**[45] used for GC-FID calibration. The metathesis catalysts **nG**, **nG^C** and **UC** were generously provided by Apeiron

Synthesis. The RCM substrate diethyl diallylmalonate **2** (Aldrich, 98%), and dodecane (GC internal standard; Aldrich, anhydrous, 99%), both liquids, were freeze-pump-thaw degassed (≥3x, until no bubbles appear on thawing), and stored under N_2 in the glovebox over 4 Å molecular sieves.

Prior to carrying out metathesis experiments, catalyst purity was confirmed by NMR analysis, and substrate purity[a] by GC analysis. Analytes were quantified using an Agilent S7890A gas chromatograph (GC) equipped with an autosampler, flame ionization detector (FID) and HP-5 polysiloxane column (30 m length, 320 μm diameter). Calibration curves of peak areas versus concentration were established for dienes and RCM products in the relevant concentration regimes, using ca. 1:1 (w/w) of the analyte sample relative to the internal standard dodecane. In all cases, yields refer to the summed yields of the *E* and *Z* isomers for the RCM targets, as determined from the integrated peak areas versus internal standard. Reported values are averages of at least three trials (±3, except for two entries with a deviation of 4%).

NMR spectra were recorded on Avance 300 or Avance II 300 spectrometers at 23 ±2 °C. Chemical shifts are reported in ppm and referenced to the residual proton signals of the solvent (^{1}H NMR) or external 85% H_3PO_4 (^{31}P NMR). Details of quantitative ^{31}P{^{1}H} NMR analysis are given where relevant below (see Section 3).

[a] We did not, however, undertake multidimensional GC analysis at extreme high concentrations. Kadyrov and co-workers were able to observe a range of contaminants in commercial **2** by this approach using GC-GC-TOF MS even at purity levels of 99.99%. See: Lübbe, C.; Dumrath, A.; Neumann, H.; Schäffer, M.; Zimmermann, R.; Beller, M.; Kadyrov, R., How Important are Impurities in Catalysis? An Example from Ring-Closing Metathesis. *ChemCatChem* **2014**, *6*, 684–688

2.5.2 Catalyst Decomposition Experiments

Scheme 2.3 mRCM of Substrate 1, Showing Cyclized Product.

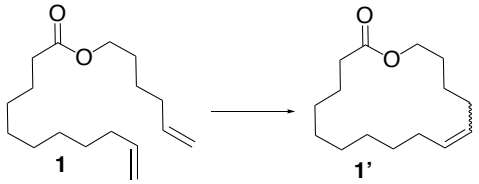

Control mRCM Experiments (Schlenk Line; Ar Atmosphere). A 25 mL Schlenk tube was charged with diene **1** (5.9 mg, 0.025 mmol), dodecane (4.3 mg, 5.7 μL, 0.025 mmol; internal standard, IS), and benzene (5.0 mL) in the glovebox, to give a final concentration of 5.0 mM. An aliquot was withdrawn for GC-FID analysis to establish the initial ratio of **1**:IS. The flask was then removed to the Schlenk line, where the solution was degassed by three freeze-pump-thaw cycles to remove N_2.[39] On the final cycle, the frozen solution was thawed under an atmosphere of Ar. The solution was stirred at RT for 30 min to permit thermal equilibration, after which catalyst (0.01 mol% Ru) was added via gas-tight syringe (e.g. **GII**: 21.2 μL of a 0.119 mM stock solution prepared in the glovebox; 10.1 mg in 1.010 mL benzene; diluted tenfold two times). The reaction was stirred at RT for 4 h. A sample was then removed, quenched[46] with KTp (10 mg/mL in THF), and analyzed by GC-FID to determine the conversion of diene **1** and yield of cyclic **1'**.

Control mRCM Experiments (Glovebox, in vials; N_2 Atmosphere). In the glovebox, a 20 mL vial was charged with all reagents as above. An aliquot was removed for GC-FID analysis to establish the initial ratio of **1**:IS, after which **GII** was added and the reaction was stirred for 4 h prior to analysis as above. Data from these experiments are in good agreement with those in Schlenk flasks (see Appendix A, Tables A-1, A-2).

mRCM O_2 Decomposition Experiments (Schlenk Line; 8% O_2 in Ar Atmosphere). A 25 ml Schlenk tube was charged with diene **1** (5.9 mg, 0.025 mmol), dodecane (4.3 mg, 5.7 μL, 0.025 mmol; internal standard, IS), and benzene (5.0 mL) in the glovebox. An aliquot was removed for GC-FID analysis to establish the initial ratio of **1**:IS. The flask was removed to the Schlenk line

and attached via a T-joint to a cylinder of 8% O_2 in Ar. The solution was freeze-pump-thaw degassed (3x) to remove N_2.[39] On the final cycle, the frozen solution was permitted to thaw under 8% O_2 in Ar. The solution was stirred open to the reagent gas at RT for 30 min to establish thermal equilibrium, after which catalyst was added, and the solution was conducted and analyzed as above.

mRCM Air-Induced Decomposition Experiments (Benchtop, in vials; Air Atmosphere). A 20 mL vial was charged with diene **1** (5.9 mg, 0.025 mmol) and dodecane (4.3 mg, 5.7 μL, 0.025 mmol; internal standard, IS) in the glovebox. The vial removed to the fumehood, where the solution was diluted with 5.0 mL benzene (HPLC grade C_6H_6 stirred in air overnight) to a final concentration of 5.0 mM. Reaction and analysis was then carried out as for the control experiment in vials above.

Scheme 2.4 RCM of Substrate 2, Showing Cyclized Product.

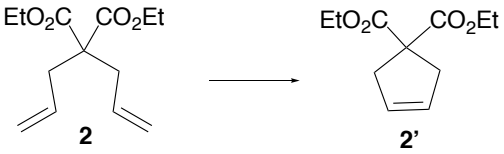

Control RCM Experiments (Schlenk line; Ar Atmosphere). A 10 ml Schlenk tube was charged with DDM **2** (96 mg, 97 μL, 0.40 mmol), dodecane (68 mg, 91 μL, 0.40 mmol; internal standard), and benzene (1.8 mL) in the glovebox. The flask was removed to the Schlenk line, freeze-pump-thaw degassed (3x) to remove N_2,[39] and on the final cycle, thawed under an atmosphere of Ar. The reaction was then allowed to come to thermal equilibrium at RT for 30 min, after which catalyst **GII** (84.9 μL of a 0.118 mM stock solution prepared in the glovebox) was added via gas-tight syringe. The solution was stirred at room temperature for 4 h. (For slowly-initiating **HC**, the reaction was stirred at room temperature for 24 h, instead of 4 h). A sample was then removed, quenched[46] with KTp (10 mg/mL in THF), and analyzed by GC-FID to determine the final ratio of **2'**:IS. Note: the O_2 decomposition experiments shown as Trial C in Appendix A, Table A-2 were repeated on the same day as these control experiments, using the same stock solutions.

Control RCM Experiments (Glovebox, in vials; N_2 Atmosphere). In the glovebox, a 4 mL vial was charged with DDM **2** (96 mg, 97 μL, 0.40 mmol), dodecane (68 mg, 91 μL, 0.40 mmol; internal standard), and benzene (1.8 mL). An aliquot was removed for GC-FID analysis to establish the starting ratio of DDM to dodecane, after which **GII** was added and the reaction was stirred for 4 h prior to analysis as above. Data from these experiments are in good agreement with those in Schlenk flasks (see Appendix A, Tables A-1, A-2).

RCM O_2 Decomposition Experiments (Schlenk Line; 8% O_2 in Ar Atmosphere). A 10 ml Schlenk tube was charged with DDM **2** (96 mg, 97 μL, 0.40 mmol), dodecane (68 mg, 91 μL, 0.40 mmol; internal standard), and benzene (1.8 mL) in the glovebox. The flask was removed to the Schlenk line, attached to a T-joint connecting the Schlenk line to a cylinder of 8% O_2 in Ar. The flask was then freeze-pump-thaw degassed (3x) to remove N_2.[39] On the final cycle, the frozen solution was thawed under an atmosphere of 8% O_2 in Ar, and the solution was stirred open to the reagent gas at RT for 30 min to establish thermal equilibrium, after which catalyst was added, and the solution was conducted and analyzed as above. (For slowly-initiating **HC**, however, the solution was stirred at room temperature for 24 h instead of 4 h). Data for reactions aimed at identifying suitable catalyst loadings appear in Figure 2.2. These correspond to loadings that are in general too low or too high, respectively.

RCM Air-Induced Decomposition Experiments (Benchtop, in vials; Air Atmosphere). A 4 mL vial was charged with DDM **2** (96 mg, 97 μL, 0.40 mmol), dodecane (68 mg, 91 μL, 0.40 mmol; internal standard) in the glovebox. The vial was removed to the fumehood, where the solution was diluted with 1.8 mL benzene (HPLC grade C_6H_6; stirred in air overnight) to a final concentration of 200 mM. Reaction and analysis was then carried out as for the control experiment in vials above.

2.5.3 Probing Catalyst Decomposition via NMR Experiments

Decomposition of GII by O_2; Replenishing O_2 Atmosphere. See Figures 2.4 and A1-A3. A solution of **GII** (13 mg, 0.015 mmol) and anthracene (ca. 2 mg, internal standard for ^{1}H NMR integration) in C_6D_6 (0.75 mL) was transferred to a J. Young-valved NMR tube. A flame-sealed

capillary containing 1,4-bis(diphenylphosphino)butane (dppb) as a ^{31}P NMR integration standard (70 μL of a 10.6 mg/mL, 25 mM stock solution in C_6D_6) was added and a spectrum was taken to establish the initial ratio of **GII**:anthracene (^1H NMR) and **GII**:dppb ($^{31}P\{^1H\}$ NMR). The sample was then transferred to the Schlenk line, degassed and thawed under 8% O_2 as above, then attached to a rotary mixer and mixed (15 rpm) at RT, with periodic ^1H NMR analysis. The tube was recharged with O_2 at 24 h intervals. Over the course of 72 h, the solution changed in colour from deep-red to black, and a black precipitate formed. After 48 h: 5% **GII**, 27% benzaldehyde, 56% stilbene (E)-PhC*H*=C*H*Ph. After 72 h: no remaining **GII**, 30% PhCHO, 55% stilbene. ^1H NMR (C_6D_6, 300 MHz; diagnostic signals only): δ 9.64 (s, 1H, *H*C(O)Ph), 8.16 (s, 2H, ArC*H* of anthracene), 7.00 (s, 2H, =C*H*Ph of stilbene). For the corresponding spectrum without dppb, to enable accurate quantitation of stilbene, see Appendix B, Figure B-3.

Impact of Added PCy_3 on Rate of Decomposition of GII by O_2. ^1H NMR experiment: see Figure 2.4c. As for the preceding experiment, but without recharging with O_2, in the presence of 0 or 1 equiv PCy_3 (100 μL of a 42 mg/mL stock solution in benzene, 0.015 mmol) and without the dppb capillary.

Quantification of Ru-16, Ru-17 and O=PCy_3. See Appendix B, Figure B-2. Quantitative $^{31}P\{^1H\}$ NMR spectrum were recorded using an inverse-gated 30° pulse sequence. An 18 s relaxation delay was used (>3x T_1 for free PCy_3; Appendix A, Table A-6). After 72 h: no **GII**, 7% **Ru-16**, 4% **Ru-17** and 58% O=PCy_3. $^{31}P\{^1H]$ NMR (C_6D_6, 121 MHz): δ 48.3 (O=PCy_3), 32.6 (**Ru-17**), 22.4 (**Ru-16**), –15.7 (dppb).

Decomposition of HII by O_2. See Appendix B, Figure B-4. As for **GII**, using 12.5 mg **HII** (0.02 mmol) and DMT (ca. 2 mg, ^1H NMR integration standard) in C_6D_6 (1 mL). After 14 d: 0% decomposition. ^1H NMR (C_6D_6, 300 MHz; diagnostic signals only): δ 16.70 (s, 1H, [Ru]=C*H*R of **HII**), 7.99 (s, 4H, ArC*H* of DMT).

Decomposition of UC by O_2. See Appendix B, Figure B-5. As for **GII**, using 15 mg **UC** (0.015 mmol) and DMT (ca. 2 mg, internal standard for ^1H NMR integration) in C_6D_6 (0.75 mL). After

36 h: 62% loss. ^{1}H NMR (C_6D_6, 300 MHz; diagnostic signals only): δ 9.60 (d, 1H, ArC*H* of **UC**), 8.00 (s, 4H, ArC*H* of DMT).

2.6 References

(1) Grela, K., *Olefin Metathesis-Theory and Practice*. Wiley: Hoboken, NJ, 2014.

(2) Grubbs, R. H.; Wenzel, A. G., *Handbook of Metathesis*. 2nd ed.; Wiley-VCH: Weinheim, 2015.

(3) Schwab, P.; Grubbs, R. H.; Ziller, J. W., Synthesis and Applications of $RuCl_2(=CHR')(PR_3)_2$: The Influence of the Alkylidene Moiety on Metathesis Activity. *J. Am. Chem. Soc.* **1996**, *118*, 100–110.

(4) (a) Higman, C. S.; Lummiss, J. A. M.; Fogg, D. E. Olefin Metathesis at the Dawn of Uptake in Pharmaceutical and Specialty Chemicals Manufacturing. *Angew. Chem., Int. Ed.* **2016**, *55*, 3552–3565. (b) Fandrick, K. R.; Savoie, J.; Jinhua, N. Y.; Song, J. J.; Senanayake, C. H., Challenges and Opportunities for Scaling the Ring-Closing Metathesis Reaction in the Pharmaceutical Industry. In *Olefin Metathesis – Theory and Practice*, Grela, K., Ed. Wiley: Hoboken, 2014; pp 349-366. (c) Farina, V.; Horváth, A., Ring-Closing Metathesis in the Large-Scale Synthesis of Pharmaceuticals. In *Handbook of Metathesis*, Grubbs, R. H.; Wenzel, A. G., Eds. Wiley-VCH: Weinheim, 2015; Vol. 2, pp 633–658.

(5) Ruthenium metathesis catalysts stabilized by ligands that show low lability in the absence of substrate are often oxygen-stable as the precatalysts. See, for example: (a) Kingsbury, J. S.; Harrity, J. P. A.; Bonitatebus, P. J.; Hoveyda, A. H., A Recyclable Ru-Based Metathesis Catalyst. *J. Am. Chem. Soc.* **1999**, *121*, 791–799. Oxygen may have an initially activating effect in metathesis by phosphine–stabilized precatalysts, owing to trapping of released PR_3 as the phosphine oxide. See: (b) Drouin, S. D.; Foucault, H. M.; Yap, G. P. A.; Fogg, D. E., New Pseudohalide Ligands in Ru-Catalyzed Olefin Metathesis: A Robust, Air-Activated Iminopyrrolato Catalyst. *Can. J. Chem.* **2005**, *83*, 748–754, and references therein). The productivity of any Ru catalyst in aerobic metathesis is determined by the relative rates of metathesis and decomposition.

(6) Piola, L.; Nahra, F.; Nolan, S. P., Olefin Metathesis in Air. *Beilstein J. Org. Chem.* **2015**, *11*, 2038–2056.

(7) Guidone, S.; Songis, O.; Nahra, F.; Cazin, C. S. J., Conducting Olefin Metathesis Reactions in Air: Breaking the Paradigm. *ACS Catal.* **2015**, *5*, 2697–2701.

(8) Skowerski, K.; Bialecki, J.; Tracz, A.; Olszewski, T. K., An Attempt to Provide an Environmentally Friendly Solvent Selection Guide for Olefin Metathesis. *Green Chem.* **2014**, *16*, 1125–1130.

(9) Kniese, M.; Meier, M. A. R., A Simple Approach to Reduce the Environmental Impact of Olefin Metathesis Reactions: A Green and Renewable Solvent Compared to Solvent-Free Reactions. *Green Chem.* **2010**, *12*, 169-173.

(10) Michrowska, A.; Gulajski, L.; Kaczmarska, Z.; Mennecke, K.; Kirschning, A.; Grela, K., A Green Catalyst for Green Chem.: Synthesis and Application of an Olefin Metathesis Catalyst Bearing a Quaternary Ammonium Group. *Green Chem.* **2006**, *8*, 685–688.

(11) van Lierop, B. J.; Lummiss, J. A. M.; Fogg, D. E., Ring-Closing Metathesis. In *Olefin Metathesis-Theory and Practice*, Grela, K., Ed. Wiley: Hoboken, NJ, 2014; pp 85–152.

(12) Anderson, N. G., Final Product Form and Impurities. In *Practical Process Research and Development*, 2nd ed.; Elsevier: New York, 2012; p 378.

(13) Various contaminants have been shown to negatively affect metathesis reactions conducted at low catalyst loadings. For the impact of trace morpholine (a contaminant in technical-grade toluene) on metathesis via a phosphine-free catalyst, see: (a) Nicola, T.; Brenner, M.; Donsbach, K.; Kreye, P., First Scale-Up to Production Scale of a Ring Closing Metathesis Reaction Forming a 15-Membered Macrocycle as a Precursor of an Active Pharmaceutical Ingredient. *Org. Process Res. Dev.* **2005**, *9*, 513–515. For mechanistic studies showing that the incompatibility of such catalysts with various Bronsted bases originates in metallacyclobutane deprotonation, see: (b) Bailey, G. A.; Lummiss, J. A. M.; Foscato, M.; Occhipinti, G.; McDonald, R.; Jensen, V. R.; Fogg, D. E., Decomposition of Olefin Metathesis Catalysts by Brønsted Base: Metallacyclobutane Deprotonation as a Primary Deactivating Event. *J. Am. Chem. Soc.* **2017**, *139*, 16446–16449. (c) Ireland, B. J.; Dobigny, B. T.; Fogg, D. E., Decomposition of a Phosphine-Free Metathesis Catalyst by Amines and Other Nitrogen Bases: Metallacyclobutane Deprotonation as a Major Deactivation Pathway. *ACS Catal.* **2015**, *5*, 4690−4698. For the negative impact of nucleophiles on phosphine-free *or* phosphine-stabilized catalysts, see: ref (c) and: (d) Lummiss, J. A. M.; Ireland, B. J.; Sommers, J. M.; Fogg, D. E., Amine-Mediated Degradation in Olefin Metathesis Reactions that Employ the Second-Generation Grubbs Catalysts. *ChemCatChem* **2014**, *6*, 459–463. For the impact of contaminants present in commercial diethyl diallyl malonate (DDM, **2**), see: (e) Lübbe, C.; Dumrath, A.; Neumann, H.; Schäffer, M.; Zimmermann, R.; Beller, M.; Kadyrov, R., How Important are Impurities in Catalysis? An Example from Ring-Closing Metathesis. *ChemCatChem* **2014**, *6*, 684–688. For a discussion of the impact of contaminants in technical-grade ethylene, see: (f) Nascimento, D. L.; Gawin, A.; Gawin, R.; Guńka, P. A.; Zachara, J.; Skowerski, K.; Fogg, D. E., A Highly Reactive Ruthenium-Indenylidene Catalyst for Olefin Metathesis. *J. Am. Chem. Soc.* **2019**, *141*, 10626–10631.

(14) For a study demonstrating that hydroperoxides are incompatible with **HII** and **nG** even at loadings of 2.5 mol%, see: Jana, A.; Grela, K., Mild Functionalization of Tetraoxane Derivatives via Olefin Metathesis: Compatibility of Ruthenium Alkylidene Catalysts with Peroxides. *Org. Lett.* **2017**, *19*, 520−523.

(15) Gawin, R.; Tracz, A.; Chwalba, M.; Kozakiewicz, A.; Trzaskowski, B.; Skowerski, K., Cyclic Alkyl Amino Ruthenium Complexes—Efficient Catalysts for Macrocyclization and Acrylonitrile Cross Metathesis. *ACS Catal.* **2017**, *7*, 5443–5449.

(16) (a) Conrad, J. C.; Eelman, M. D.; Duarte Silva, J. A.; Monfette, S.; Parnas, H. H.; Snelgrove, J. L.; Fogg, D. E., Oligomers as Intermediates in Ring-Closing Metathesis. *J. Am. Chem. Soc.* **2007**, *129*, 1024–1025. (b) Monfette, S.; Fogg, D. E., Equilibrium Ring-Closing Metathesis. *Chem. Rev.* **2009**, *109*, 3783–3816. (c) Higman, C. S.; Nascimento, D.; Ireland, B. J.; Audorsch, S.; Bailey, G. A.; Fogg, D. E., Chelate-Assisted Ring-Closing

Metathesis: A Strategy for Accelerating Macrocyclization at Ambient Temperatures. *J. Am. Chem. Soc.* **2018**, *140*, 1604−1607.

(17) Grela, K.; Harutyunyan, S.; Michrowska, A., A Highly Efficient Ruthenium Catalyst for Metathesis Reaction. *Angew. Chem. Int. Ed.* **2002**, *41*, 4038–4040.

(18) Marx, V. M.; Sullivan, A. H.; Melaimi, M.; Virgil, S. C.; Keitz, B. K.; Weinberger, D. S.; Bertrand, G.; Grubbs, R. H., Cyclic Alkyl Amino Carbene (CAAC) Ruthenium Complexes as Remarkably Active Catalysts for Ethenolysis. *Angew. Chem., Int. Ed.* **2015**, *54*, 1919–1923.

(19) Gawin, R.; Kozakiewicz, A.; Guńka, P. A.; Dąbrowski, P.; Skowerski, K., Bis(Cyclic Alkyl Amino Carbene) Ruthenium Complexes: A Versatile, Highly Efficient Tool for Olefin Metathesis. *Angew. Chem., Int. Ed.* **2017**, *56*, 981–986.

(20) Soleilhavoup, M.; Bertrand, G., Cyclic (Alkyl)(Amino)Carbenes (CAACs): Stable Carbenes on the Rise. *Acc. Chem. Res.* **2015**, *48*, 256–266.

(21) Melaimi, M.; Jazzar, R.; Soleilhavoup, M.; Bertrand, G., Cyclic (Alkyl)(amino)carbenes (CAACs): Recent Developments. *Angew. Chem., Int. Ed.* **2017**, *56*, 10046–10068.

(22) Lummiss, J. A. M.; Perras, F. A.; Bryce, D. L.; Fogg, D. E., Sterically-Driven Metathesis: The Impact of Alkylidene Substitution on the Reactivity of the Grubbs Catalysts. *Organometallics* **2016**, *35*, 691–698.

(23) For the original bis-NHC catalysts, see: (a) Weskamp, T.; Schattenmann, W. C.; Spiegler, M.; Herrmann, W. A., A Novel Class of Ruthenium Catalysts for Olefin Metathesis. *Angew. Chem., Int. Ed.* **1998**, *37*, 2490–2493. For the original synthesis of **HC**, see: (b) Trnka, T. M.; Morgan, J. P.; Sanford, M. S.; Wilhelm, T. E.; Scholl, M.; Choi, T.-L.; Ding, S.; Day, M. W.; Grubbs, R. H., Synthesis and Activity of Ruthenium Alkylidene Complexes Coordinated with Phosphine and N-Heterocyclic Carbene Ligands. *J. Am. Chem. Soc*. **2003**, *125*, 2546–2558. For recent applications of **HC** in visible-light-controlled metathesis, see: (c) Theunissen, C.; Ashley, M. A.; Rovis, T., Visible-Light-Controlled Ruthenium-Catalyzed Olefin Metathesis. *J. Am .Chem. Soc.* **2019**, *141*, 6791–6796.

(24) In the present context, lability refers to the ease with which a binding site for olefin is created by loss of a stabilizing donor ligand from the precatalyst or resting state. Exemplary values, in s^{-1} (in C_7D_8 or C_6D_6 at 80 °C): **GI** (ca. 10), **GII** (0.13), **GIIm** (ca. 0.0005). For **GI**, **GII**, see: (a) Sanford, M. S.; Love, J. A.; Grubbs, R. H., Mechanism and Activity of Ruthenium Olefin Metathesis Catalysts. *J. Am. Chem. Soc.* **2001**, *123*, 6543–6554. For **GIIm**, see: (b) Lummiss, J. A. M.; Higman, C. S.; Fyson, D. L.; McDonald, R.; Fogg, D. E., The Divergent Effects of Strong NHC Donation in Catalysis. *Chem. Sci.* **2015**, *6*, 6739–6746. Steric pressure exerted by the benzylidene ligand is a major contributor to the ca. 275x faster loss of the PCy_3 ligand from **GII**, vs. its resting-state methylidene complex **GIIm**. See: ref 24. Effecting complete displacement of sterically undemanding donors from Ru centers can be challenging even in less congested environments. See: (d) Fogg, D. E.; James, B. R., Chiral and Achiral Diphosphine Complexes of Ruthenium(II) Incorporating Labile Nitrile Ligands. *Inorg. Chem.* **1997**, *36*, 1961–1966.

(25) See ref 11 and: (a) Schrodi, Y. In ref 2; pp 323–342. (b) Crabtree, R. H., Deactivation in Homogeneous Transition Metal Catalysis: Causes, Avoidance, and Cure. *Chem. Rev.* **2015**,

115, 127–150. (c) Chadwick, J. C.; Duchateau, R.; Freixa, Z.; van Leeuwen, P. W. N. M. *Homogeneous Catalysts: Activity – Stability – Deactivation*, Wiley-VCH: Weinheim, 2011; pp 347–396.

(26) Dinger, M. B.; Mol, J. C., Degradation of the Second-Generation Grubbs Metathesis Catalyst with Primary Alcohols and Oxygen. *Eur. J. Inorg. Chem.* **2003**, 2827–2833.

(27) The corresponding reaction of **GI** afforded RuCl(Ph)(CO)(PCy_3)$_2$ in 75% yield. See: Dinger, M. B.; Mol, J. C., Degradation of the First-Generation Grubbs Metathesis Catalyst with Primary Alcohols, Water, and Oxygen. Formation and Catalytic Activity of Ruthenium(II) Monocarbonyl Species. *Organometallics* **2003**, *22*, 1089–1095.

(28) Espinal-Viguri, M.; Varela-Izquierdo, V.; Miloserdov, F. M.; Riddlestone, I. M.; Mahon, M. F.; Whittlesey, M. K., Heterobimetallic Ruthenium-Zinc Complexes with Bulky N-Heterocyclic Carbenes: Syntheses, Structures and Reactivity. *Dalton Trans.* **2019**, *48*, 4176–4189.

(29) Dumas, A.; Tarrieu, R.; Vives, T.; Roisnel, T.; Dorcet, V.; Basle, O.; Mauduit, M., A Versatile and Highly Z-Selective Olefin Metathesis Ruthenium Catalyst Based on a Readily Accessible N-Heterocyclic Carbene. *ACS Catal.* **2018**, *8*, 3257–3262.

(30) McClennan, W. L.; Rufh, S. A.; Lummiss, J. A. M.; Fogg, D. E., A General Decomposition Pathway for Phosphine-Stabilized Metathesis Catalysts: Lewis Donors Accelerate Methylidene Abstraction. *J. Am. Chem. Soc.* **2016**, *138*, 14668−14677.

(31) Endo, K.; Grubbs, R. H., Chelated Ruthenium Catalysts for Z-Selective Olefin Metathesis. *J. Am. Chem. Soc.* **2011**, *133*, 8525–8527.

(32) Burling, S.; Paine, B. M.; Nama, D.; Brown, V. S.; Mahon, M. F.; Prior, T. J.; Pregosin, P. S.; Whittlesey, M. K.; Williams, J. M. J., C-H Activation Reactions of Ruthenium N-Heterocyclic Carbene Complexes: Application in a Catalytic Tandem Reaction Involving C-C Bond Formation from Alcohols. *J. Am. Chem. Soc.* **2007**, *129*, 1987–1995.

(33) Abdur-Rashid, K.; Fedorkiw, T.; Lough, A. J.; Morris, R. H., Coordinatively Unsaturated Hydridoruthenium(II) Complexes of N-Heterocyclic Carbenes. *Organometallics* **2004**, *23*, 86–94.

(34) Jazzar, R. F. R.; Macgregor, S. A.; Mahon, M. F.; Richards, S. P.; Whittlesey, M. K., C-C and C-H Bond Activation Reactions in N-Heterocyclic Carbene Complexes of Ruthenium. *J. Am. Chem. Soc.* **2002**, *124*, 4944–4945.

(35) Feast, W. J.; Gibson, V. C.; Khosravi, E.; Marshall, E. L.; Mitchell, J. P., Bimolecular Termination in Living Ring Opening Metathesis Polymerization. *Polymer* **1992**, *33*, 872–873.

(36) Isotopically-labelled [Ru]=CHR groups have also proved invaluable. See refs 26, 31 and: (a) Lummiss, J. A. M.; Botti, A. G. G.; Fogg, D. E., Isotopic Probes for Ruthenium-Catalyzed Olefin Metathesis. *Catal. Sci. Technol.* **2014**, *4*, 4210–4218. (b) Bates, J. M.; Lummiss, J. A. M.; Bailey, G. A.; Fogg, D. E., Operation of the Boomerang Mechanism in Olefin Metathesis Reactions Promoted by the Second-Generation Hoveyda Catalyst. *ACS Catal.* **2014**, *4*, 2387−2394. (c) Jimenez, L. R.; Tolentino, D. R.; Gallon, B. J.; Schrodi, Y. Development of a Method for the Preparation of Ruthenium Indenylidene-Ether Olefin Metathesis Catalysts. *Molecules* **2012**, *17*, 5675–5689. (d) Pietraszuk, C.;

Fischer, H., Reactions of Ruthenium-Benzylidene Complexes with Bis(trimethylsilyl)ethene and Trimethylsilylstyrenes: Olefin Metathesis versus b-$SiMe_3$ Elimination/Reductive Elimination. *Organometallics* **2001**, *20*, 4641–4646. (e) Ulman, M.; Grubbs, R. H., Ruthenium Carbene-Based Olefin Metathesis Initiators: Catalyst Decomposition and Longevity. *J. Org. Chem.* **1999**, *64*, 7202–7207.

(37) Formation of benzaldehyde was also reported in a mass spectrometric study in which **GII** or, particularly, $[Ru(H_2IMes)(MeCN)_3(=CHPh)]^{2+}$ were exposed to water. Nucleophilic attack by water on the benzylidene carbon was proposed. See: (a) Kim, M.; Eum, M. S.; Jin, M. Y.; Jun, K. W.; Lee, C. W.; Kuen, K. A.; Kim, C. H.; Chin, C. S., Reactions of Ruthenium Benzylidenes with H_2O to Give Benzaldehyde and (Aqua)ruthenium Complex. *J. Organomet. Chem.* **2004**, *689*, 3535–3540. (In the present work, standard precautions were taken to ensure that <5 ppm H_2O was present, as indicated by Karl-Fischer titration prior to drying over freshly-activated molecular sieves: see SI). The minor amounts (<2%) of *o*-isopropoxybenzaldehyde detected in an early study on heating **HII** in toluene (0.05 M) at 80 °C for 12 h may thus have been due to trace O_2 or water. See: (b) Garber, S. B.; Kingsbury, J. S.; Gray, B. L.; Hoveyda, A. H., Efficient and Recyclable Monomeric and Dendritic Ru-Based Metathesis Catalysts. *J. Am. Chem. Soc.* **2000**, *122*, 8168–8179.

(38) Bailey, G. A.; Foscato, M.; Higman, C. S.; Day, C. S.; Jensen, V. R.; Fogg, D. E., Bimolecular Coupling as a Vector for Decomposition of Fast-Initiating Olefin Metathesis Catalysts. *J. Am. Chem. Soc.* **2018**, *140*, 6931–6944.

(39) Shriver, D. F.; Drezdzon, M. A., *The Manipulation of Air-Sensitive Compounds*. 2nd Ed. ed.; John Wiley & Sons: New York, 1986.

(40) Nascimento, D. L.; Davy, E. C.; Fogg, D. E., Merrifield Resin-Assisted Routes to Second-Generation Catalysts for Olefin Metathesis. *Catal. Sci. Technol.* **2018**, 1535–1544.

(41) Nascimento, D. L.; Gawin, A.; Gawin, R.; Guńka, P. A.; Zachara, J.; Skowerski, K.; Fogg, D. E., A Highly Reactive Ruthenium-Indenylidene Catalyst for Olefin Metathesis. *J. Am. Chem. Soc.* **2019**, *141*, 10626–10631.

(42) Day, C. S.; Fogg, D. E., High-Yield Synthesis of a Long-Sought, Labile Ru-NHC Complex and Its Application to the Concise Synthesis of Second-Generation Olefin Metathesis Catalysts. *Organometallics* **2018**, *24*, 4551–4555.

(43) Trnka, T. M.; Morgan, J. P.; Sanford, M. S.; Wilhelm, T. E.; Scholl, M.; Choi, T.-L.; Ding, S.; Day, M. W.; Grubbs, R. H., Synthesis and Activity of Ruthenium Alkylidene Complexes Coordinated with Phosphine and N-Heterocyclic Carbene Ligands. *J. Am. Chem. Soc.* **2003**, *125*, 2546–2558.

(44) Fürstner, A.; Langemann, K., Macrocycles by Ring-Closing Metathesis. *Synthesis* **1997**, 792–803.

(45) Clavier, H.; Nolan, S. P., N-Heterocyclic Carbene and Phosphine Ruthenium Indenylidene Precatalysts: A Comparative Study in Olefin Metathesis. *Chem. – Eur. J.* **2007**, *13*, 8029–8036.

(46) Blacquiere, J. M.; Jurca, T.; Weiss, J.; Fogg, D. E., Time as a Dimension in High-Throughput Homogeneous Catalysis. *Adv. Synth. Catal.* **2008**, *350*, 2849–2855.

3 Encapsulation of Ruthenium Olefin Metathesis Catalysts Within a Self-Assembled Capsule

3.1 Context, Objectives, and Overview of Content

As discussed in Chapter 1, uptake of ruthenium-catalyzed olefin metathesis in industry is now under way.[1] Of particular relevance is ring-closing metathesis (RCM), a key synthetic step in the production of active pharmaceutical ingredients, including the hepatitis C virus (HCV) inhibitors Simeprevir and Vaniprevir.[1-3] Indeed, RCM is a technology of major potential importance for the production of antiviral drugs, within which macrocycles represent a fast-moving frontier.[4-7] The COVID crisis has brought unprecedented global awareness to the devastating potential of emerging viral diseases,[8] an awareness that has catapulted vaccines and antiviral therapeutics to the top of the global priority list for development.[9] In particular, the RCM-derived HCV drug Simeprevir is currently being investigated as a promising COVID antiviral candidate.[10]

Within this context, improving the reliability of metathesis methodologies takes on new urgency. Studies focusing on deactivation of high-performing metathesis catalysts, including those presented in Chapter 2, have revealed potential contaminants that limit catalyst lifetime.[11-15] In an industrial setting, many contaminants may be present in the reaction medium.[1] This chapter explores a strategy for limiting catalyst decomposition via use of a protective cage: specifically, by encapsulating the metathesis catalyst within a self-assembled cage that can permit entry and exit of substrate and product.[16]

3.2 Published Contributions

Jongkind L.J., Rahimi M.R., Poole D., **Ton S.J.**, Fogg D. E., Reek J.N.H. "Protection of Ruthenium Olefin Metathesis Catalysts by Encapsulation in a Self-Assembled Resorcinarene Capsule." *ChemCatChem,* 2020; Early View Article. Weblink: https://chemistry-europe.onlinelibrary.wiley.com/doi/full/10.1002/cctc.202000111

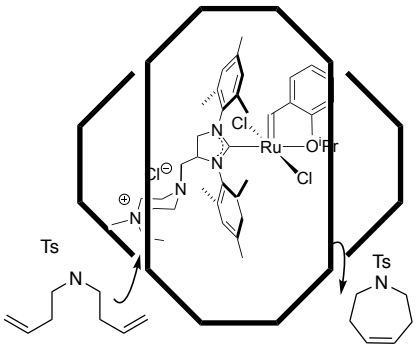

Abstract: Catalyst encapsulation is examined as a means of increasing the productivity of olefin metathesis catalysts. Commercially available, cationic ruthenium metathesis catalysts were incorporated into a supramolecular resorcin[4]arene capsule. Encapsulation increased catalyst stability in the presence of water, delivering higher metathesis yields than the parent, non-encapsulated Hoveyda catalyst in the same reaction medium.

Author contributions: This manuscript was written by DEF, LJJ, and JNHR; SJT contributed critiques of the text, graphics, and data interpretation. The concept was initially investigated by MRR, a visiting M.Sc. thesis student from the University of Amsterdam, in a research stage at Ottawa in which she was supported by SJT. MRR demonstrated the successful encapsulation of metathesis catalysts, and explored the potential of the cage to inhibit oligomerization during macrocyclization. Metathesis experiments with encapsulated catalysts, including tracking decomposition by UV-Vis analysis, were carried out by MRR and LJJ. Molecular dynamic simulations were carried out by DP. SJT conceived of and carried out key control experiments with catalyst **HII** in anhydrous toluene, which revealed the impact of decomposition in water-saturated toluene and substantiated the proposed protective role of the capsule. SJT also carried out experiments with the cationic catalysts in anhydrous solvents, which demonstrated that their activity is near-zero in the absence of the capsule, owing to low solubility.

3.3 Introduction

Olefin metathesis is now a core methodology in organic synthesis.[17,18] RCM is beginning to see uptake in process chemistry,[19] while advances in chemical biology represent an expanding interdisciplinary frontier.[20] These and other challenging applications exert considerable pressure on catalyst productivity. While breakthrough turnover numbers (TON)[21] have recently been achieved via improvements in catalyst design that inhibit unimolecular decomposition,[22] bimolecular decomposition[23-27] remains a challenge. Bimolecular degradation is operative even at ppm-level catalyst loadings,[21,28] pointing toward the merits of site-isolation (by, for example, immobilizing the molecular catalysts on a solid support).[29] To date, the problem of *induced* catalyst decomposition can be addressed only by pre-purification[19,30,31] or quenching deleterious entities as they form.[19]

Metathesis in confined environments offers an intriguing alternative approach. Supramolecular capsules are an increasingly popular design element in homogeneous catalysis.[32-36] Encapsulation creates a second coordination sphere around the catalyst,[37-40] creating confinement effects similar to those ubiquitous in enzyme catalysis. Substrate preorganization in such confined environments[16,41,42] can accelerate desired intramolecular reactions, relative to intermolecular reactions.[43-46]

Within the context of olefin metathesis, catalyst confinement in porous materials[47,48] has been deployed to improve selectivity for macrocyclization over oligomerization.[49-51] To the best of our knowledge, however, encapsulation of molecular metathesis catalysts has not been explored as a strategy for stabilizing reactive intermediates against decomposition. We anticipated that encapsulation would aid in suppressing bimolecular catalyst decomposition.[23,24] Of added interest, however, is the potential capacity of the cage to protect the catalyst from attack by contaminants in the bulk solution.

Motivated by these opportunities, we sought to assess the impact of encapsulation in a resorcin[4]arene capsule[52-55] on the performance of Ru metathesis catalysts. We report the successful encapsulation of two cationic metathesis catalysts, and demonstrate that the

encapsulated catalysts are more stable and productive than the leading second-generation Hoveyda catalyst (**HII**)[56] in water-saturated toluene. Here water should be recognized both as an agent of decomposition in its own right (see below), and as a model for other contaminants in the bulk reaction medium.

3.4 Results and Discussion

Formation of a stable host-guest structure requires a structural element in the catalyst that can bind to the capsule interior. Cationic guest molecules, including gold-NHC catalysts[43,44] (NHC = N-heterocyclic carbene) have been successfully incorporated within the hexameric resorcin[4]arene array (Scheme 3.1), via electrostatic π-interactions with the internal aromatic surfaces of the capsule.[53,55] Importantly, these interactions are maintained in the aromatic solvents routinely used for metathesis. We therefore considered encapsulating cationic analogues of **HII**: specifically, the trimethylammonium[57] and piperazinylammonium[58] catalysts **SC** and **AM** (Figure 3.1a),[59] which we anticipated could form host-guest structures with the hexameric resorcin[4]arene capsule. A reverse ship-in-a-bottle synthesis was envisaged, involving assembly of the cage around the catalyst molecules by equilibration with the resorcin[4]arene monomers in water-saturated toluene. Of interest is the impact of encapsulation on catalyst stability in a water-rich environment. Despite successes in aqueous metathesis at high catalyst loadings,[60,61] evidence is beginning to accumulate that water exerts an unexpectedly potent negative impact on Ru-catalyzed metathesis.[11,12,62]

Scheme 3.1 Resorcin[4]arene Molecules Form Hexameric Capsules in Water-Saturated Apolar Solvents (Toluene, Benzene, CH_2Cl_2, $CHCl_3$).

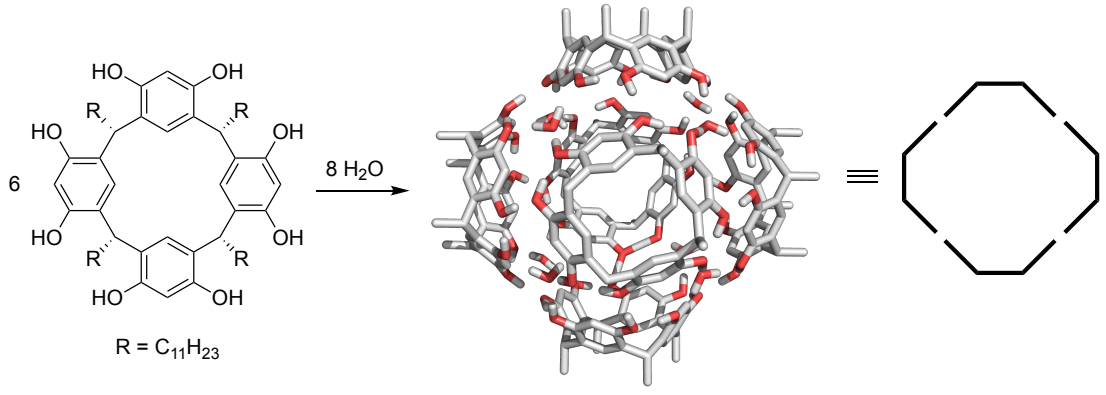

To confirm that the ruthenium complexes fit within the self-assembled hexameric cage, molecular dynamics simulations were carried out with **SC**. As shown in Figure 3.1b, these demonstrate that the catalyst fits readily within the cage (for details, see Appendix D, Figures D-1-D-2). The diffusion constant of –9.57 calculated from the dynamics simulation is in good agreement with the reported value of –9.62 for the capsule,[43,52] and the value determined experimentally below. A key feature of these self-assembled structures, relative to rigid three-dimensional cages, is facile dynamic reconfiguration of the H-bonded capsule. This permits expansion and dynamic reconfiguration of the empty cage to accommodate substrate **3** and the required alkylidene intermediate (Scheme 3.2), as well as the exit of the product.

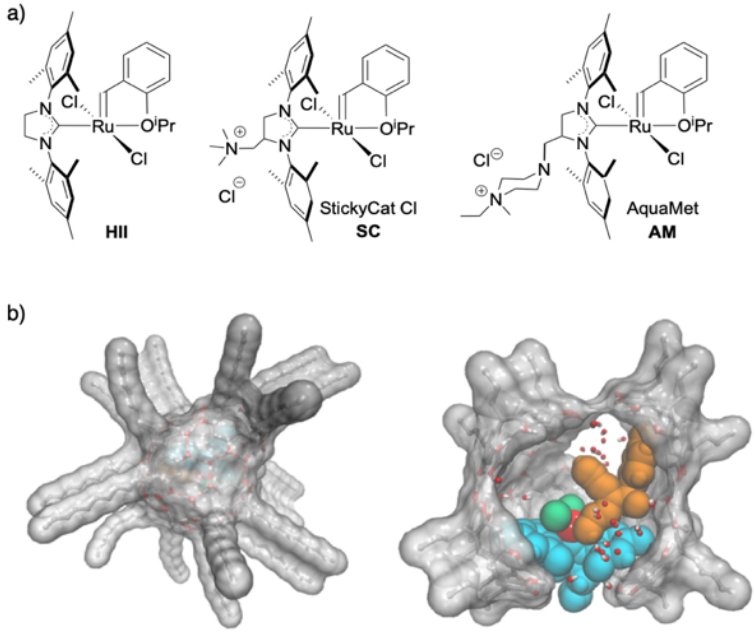

Figure 3.1 (a) The Hoveyda catalyst **HII**, and its cationic derivatives **SC** and **AM**. b) Images from molecular dynamics simulations of the alkylidene intermediate **SC'** (see Scheme 3.2) within the hexameric resorcin[4]arene capsule. (b) Left: full model; carbon-bound hydrogen atoms and explicit solvent omitted for clarity. right: alkyl side-chains and occluding capsule face also omitted. gray: resorcin[4]arene; green: Cl; red: Ru; blue: NHC; orange: alkylidene ligand.

The solvent of choice for the catalysis experiments is water-saturated toluene, both because the resorcin[4]arene capsule is known to form in this medium,[43,54] and because toluene is a standard

solvent for metathesis, including in pharmaceutical manufacturing.[19] Successful encapsulation of the **SC** and **AM** catalysts was indicated by ^{1}H NMR and ^{1}H 2D-DOSY NMR analysis. Diffusion constants were first evaluated for the free catalysts in $CDCl_3$, as **AM** and **SC** are not soluble in toluene. Diffusion constants in these solvents can be compared directly, given the similarity in viscosity (0.54 vs. 0.56 mPa-s, respectively, at 25 ºC).[63] Very similar diffusion constants were determined for **HII**, **SC**, and **AM**, with $\log_D$ values of –9.08, –9.22, and –9.11, respectively. In comparison, a $\log_D$ value of –9.57 was measured for the empty hexameric capsule. The latter, significantly lower diffusion constant reflects the much larger size of this hexameric assembly.

In the presence of the resorcin[4]arene (7.5 equiv), the diffusion constants measured for **SC** and **AM** were in line with those for the empty capsule (**SC**, –9.52; **AM**, –9.60), consistent with confinement within the cage. As typically observed for encapsulated species in these self-assembled structures,[43,53,55] a dramatic, complexation-induced upfield shift is seen for the alkylammonium ^{1}H NMR signals, confirming binding of the catalysts inside the hexameric cage (–0.9 ppm for the NMe_3 groups of **SC**, vs. 3.24 for free **SC**; –2.3 ppm for the $NCH_2\mathit{CH_3}$ groups of **AM**, vs. 1.34 ppm for free **AM**). In contrast, no change in chemical shifts is seen for **HII** under the same conditions, and its diffusion constant is essentially unaffected by the presence of the hexameric assembly ($\log_D$ –9.20; the signals for the capsule are detected separately). We infer that the cationic catalysts are encapsulated in the resorcin[4]arene cage, but that **HII** is not. This difference has important consequences for catalysis, as discussed below.

RCM of the model diene **3** (Scheme 3.2a) in water-saturated toluene was performed to assess the impact of encapsulation on catalyst performance, relative to **HII** as a non-encapsulated benchmark catalyst. Reaction of **HII** with **3** yielded 99% **3'** over 2 h (Table 3.1), with no observable oligomerization (Scheme 3.2b).[49,50] Encapsulated **SC** and **AM** afforded ca. 96% **3'** over the same period. A control experiment carried out with **AM** in anhydrous toluene indicated no reaction, consistent with catalyst insolubility.

Scheme 3.2 (a) RCM of 3 to Form Product 3'. (b) Oligomers Potentially Arising from Intermolecular Metathesis (Not Observed).[a]

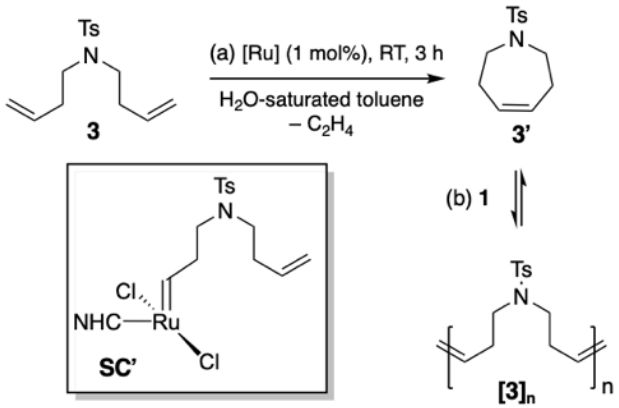

[a] Inset depicts the 4-coordinate active alkylidene species derived from **SC**, modelled in Figure 3.1b.

Table 3.1 RCM of 1 by HII and encapsulated catalysts.[a]

Catalyst[a]	Conversion[b]	RCM yield[b]
HII	99%	99%
SC@resorcin[4]arene	96%	95%
AM@resorcin[4]arene	99%	97%

[a]Conditions: [**3**]=200 mM in water-saturated toluene, [Ru]=1 mol% (2.0 mM), T=20 °C, t=2 h. For **SC**, **AM**, [resorcin[4]arene]=15.0 mM. [b] GC analysis.

While these data suggest little benefit to encapsulation in terms of selectivity and productivity, a very different perspective emerged when a second dose of substrate, without further catalyst, was added. Figure 3.2 shows the time profiles for metathesis by **HII** in both stages, relative to the corresponding reaction of **HII** in *anhydrous* toluene. In dry toluene (Figure 3.2a), RCM of the initial substrate charge reached 97% within 5 minutes, and was complete by the next timepoint (30 min). To test the stability of **HII**, the solution was allowed to stand for another 2.5 h before adding the second, equivalent proportion of substrate. Consumption of **3** was slightly slower, but the RCM reaction was essentially complete within 30 min, with a turnover number (TON) of 198.

The corresponding reaction in water-saturated toluene (Figure 3.2b) shows slower cyclization of the initial substrate charge relative to the anhydrous reaction (75% at 5 min), although RCM was quantitative by 3 h, as expected from the data in Table 3.1. Following addition of a second dose of **3**, however, RCM was very sluggish, ultimately resulting in only a 4% increase in yield (total TON 104; Figure 3.2b). These data clearly indicate accelerated catalyst decomposition in the presence of water, consistent with the literature reports noted above.[11,12,62]

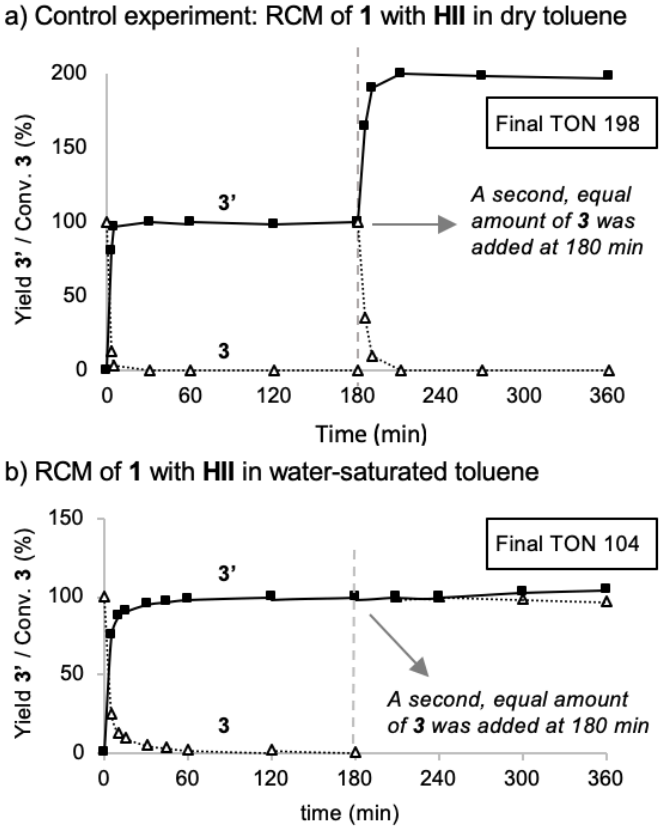

Figure 3.2 Rate profiles for RCM of **3** by **HII** in: (a) dry toluene; (b) water-saturated toluene. Conditions: [$\mathbf{3}_{initial}$]=200 mM, [$Ru_{initial}$]=2.0 mM. After 3 h, a second bolus of **3** was added, such that [Ru]=1.0 mM.

Catalyst decomposition was confirmed by UV-vis analysis of aliquots from the reaction in water-saturated toluene. Shown in Figure 3.3 is the rate of decrease in the intensity of the principal absorption band for **HII** (380 nm). An immediate, drastic drop in intensity occurred within the first

10 min of catalysis, with little further change after 30 min. Near-complete catalyst decomposition is consistent with the minimal increase in TON observed on adding the second dose of substrate.

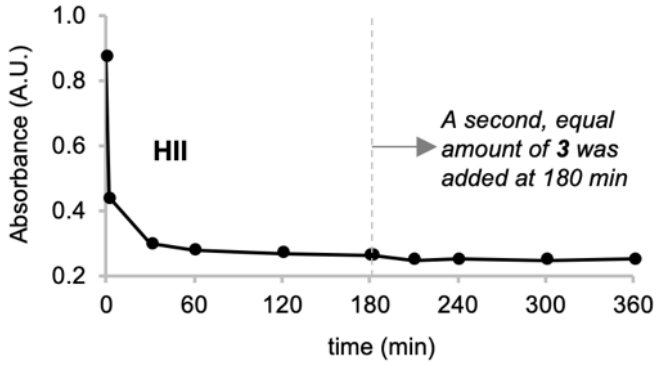

Figure 3.3 Rate of decrease in intensity of UV-vis absorbance band for **HII** (380 nm) during RCM of **3** in water-saturated toluene (experiment in Figure 3.2b). For details, see Appendix C, Figure C-1.

In striking contrast, both encapsulated catalysts exhibited sustained RCM following addition of the second bolus of substrate. With **SC**@resorcin[4]arene (Figure 3.4a), a total TON of 142 was achieved after 6 h. For **AM**@resorcin[4]arene (Figure 3.4b), the rate of RCM is only slightly slower than that seen for free **HII** in anhydrous toluene, and the ultimate RCM yield was near-quantitative (total TON of 192). The latter value is nearly double that ultimately achieved with **HII** in water-saturated toluene. We speculate that the improved performance of **AM** relative to **SC** may reflect the larger catalyst size. Greater constraint by the cage may increase the conformational bias toward cyclization, and/or accelerate cycloreversion of the vulnerable metallacyclobutane intermediate. Clearly, however, the cage serves to shield the catalyst (particularly **AM**) against decomposition of the active species by water, as also evidenced by UV-vis analysis (Figure 3.5a).

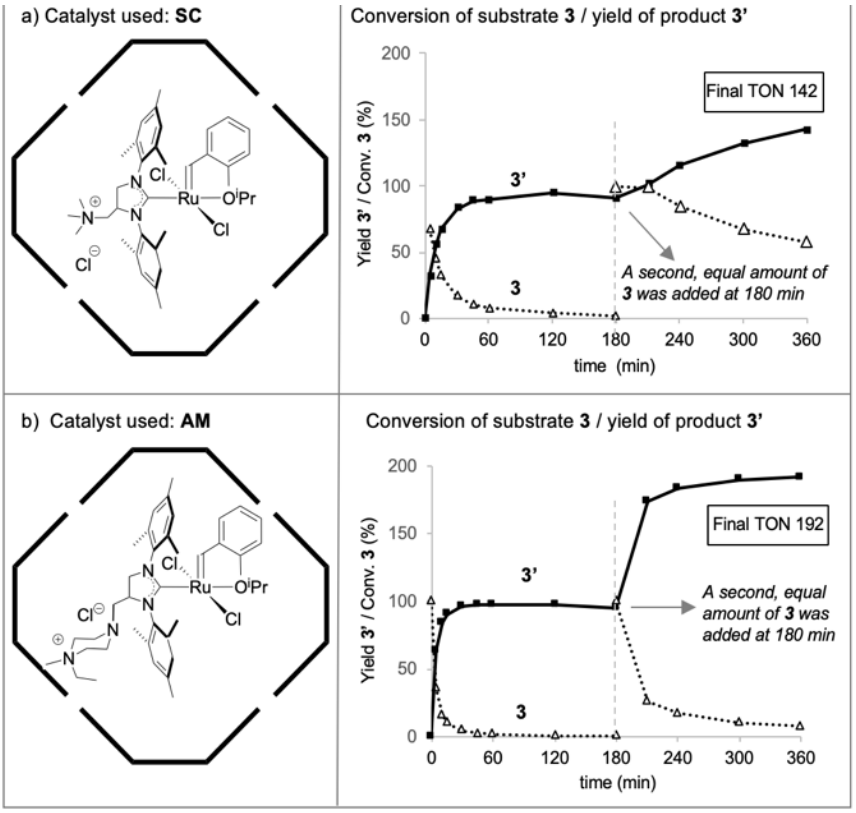

Figure 3.4 RCM rate profiles. (a) **SC**@resorcin[4]arene; (b) **AM**@resorcin[4]arene. Conditions as in Figure 3.2, with 15.0 mM resorcin[4]arene and the catalyst indicated.

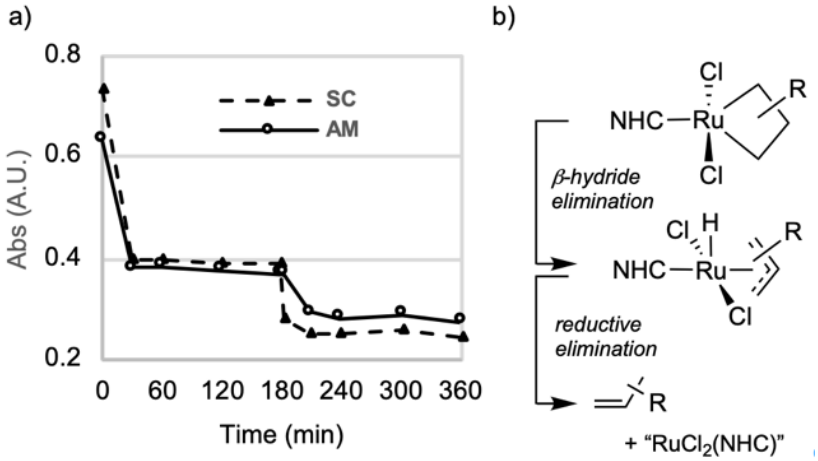

Figure 3.5 (a) Rate profiles for decomposition of **SC**@resorcin[4]arene and **AM**@resorcin[4]arene, assessed by UV-vis analysis. (b) Unimolecular decomposition of the metallacyclobutane intermediate. For details, see Appendix C, Figures C-2-C-3.

Several factors may contribute to the improved lifetime of the encapsulated catalysts. First, site-isolation prevents bimolecular coupling of the [Ru]=CH_2 intermediate, an important contributor to decomposition of **HII**.[23,24] Intrinsic decomposition is then limited chiefly to β-hydride elimination from the metallacyclobutane intermediate (see Figure 3.5b). Second, as decomposition by water is concentration-dependent,[12,62] and the hydrophobic properties of the capsule interior are well documented,[34,43] a protective effect is anticipated from the reduced proportion of water within the capsule. Finally, confinement may exert conformational constraints that promote cyclization, as noted above, while destabilizing coordination modes that contribute to catalyst deactivation.

3.5 Conclusions

The foregoing demonstrates that the hexameric resorcin[4]arene capsule can be successfully used to encapsulate cationic metathesis catalysts. The encapsulated catalysts are not merely metathesis-active, but deliver turnover numbers significantly higher than the parent, uncaged catalyst **HII** in the presence of water. Improved catalyst stability is attributed, in part, to the capacity of the capsule to prevent inter-catalyst contact, and hence catalyst degradation via bimolecular coupling. In addition, however, the cage protects from attack by water, by introducing a barrier between the catalyst and the bulk, water-saturated solvent. Site-isolation, notwithstanding its importance, has long been attainable via established surface-anchoring methods. The additional capacity of the cage to shield the catalyst against attack by deleterious agents in the solvent medium represents a unique further advantage that merits further study.

3.6 Experimental Procedures

3.6.1 General Procedures

All reactions were performed under inert atmosphere (N_2 or Ar) using standard Schlenk techniques. Water-saturated toluene was obtained by shaking degassed toluene and degassed, deionized water, and removing the desired volume of toluene once phase-separation was complete. All reagents were purchased from commercial sources and used without purification. The catalysts

SC and **AM** were purchased from Strem. The resorcin[4]arene monomer[64] and substrate **3**[65] were prepared by literature procedures.

NMR spectra were recorded on Bruker AMX 300, 400 or 500 spectrometers (300.1, 400.1, or 500.1 MHz, respectively, for ^{1}H NMR), and referenced to the residual signal for the protio-solvent. 2D ^{1}H DOSY-NMR spectra were recorded with a calibrated gradient at 298 K. UV-vis spectra were measured on Shimadzu UV-1800 and UV-2600 Double Beam spectrophotometers over the range of 190-700 nm. RCM experiments were analyzed using an Agilent 7890A gas chromatograph (GC) equipped with auto-sampler, flame ionization detector (FID) and Agilent HP-5 polysiloxane column (30 m length, 320 μm diameter) or on an Interscience Trace GC Ultra instrument with a RTX-1 column (30 m column, 0.25 mm internal diameter, 0.25 μm film thickness), initial temperature: 100 °C, hold 1 min, ramp at 20 °C/min to 140 °C, hold 12 min, ramp at 10 °C/min to 180 °C, hold 5 min. Response factors were determined for substrate **3** and its cyclic product **3'** versus decane or dodecane.

3.6.2 Encapsulation of Cationic Catalysts SC and AM.

The resorcin[4]arene monomer and the catalyst guest were added to a Schlenk flask, which was then evacuated and refilled with argon (3x). The water-saturated solvent was added by syringe against a flow of argon. The solution was stirred for 2 h at RT, at which point successful encapsulation was confirmed by ^{1}H NMR analysis from the absence of any NMR signals for the free catalyst.

3.6.3 General Procedure for Ring-Closing Metathesis of 3.

RCM reactions were performed in 4 mL vials equipped with a stirring bar inside Schlenk flasks under argon. To solutions of **AM**@resorcin[4]arene, **SC**@resorcin[4]arene, or **HII** in H_2O-saturated toluene prepared as above (4.0 μmol catalyst, 30.0 μmol resorcin[4]arene), substrate **3** (0.4 mmol) and decane (I.S., 0.2 mmol) were added from a stock solution against a flow of argon to give a final sample volume of 2.0 mL. Conversions of **3** and yields of **3'** were determined by removing aliquots, quenching with potassium tris-pyrazolyl borate (KTp)[66] in THF, then diluting

for GC-FID analysis. UV-vis samples were prepared without quenching ([$catalyst_{UV\text{-}Vis}$] = 0.04 mM, measured in a 2 mm cuvette).

3.6.4 Control RCM Reactions in Anhydrous toluene.

a) RCM by **HII**. RCM by **HII**. A mixture of diene **3** (112 mg, 0.4 mmol) and dodecane (68 μL, 0.4 mmol; internal standard for GC analysis) was diluted in 1.80 mL C_7H_8 to give a final concentration of 200 mM substrate. A 10.0 μL aliquot was removed for GC-FID analysis to establish the starting ratio of **3** to IS. **HII** (4.0 μmol, 1 mol%) (118 μL of a 10.6 mg/mL stock in toluene) was added to the stirred solution. Aliquots were removed periodically, quenched with 100 μL KTp in THF (10.0 mg/mL), and analyzed by GC-FID

b) RCM by **AM.** A mixture of diene **3** (335 mg, 1.20 mmol) and dodecane (204 μL, 1.20 mmol; internal standard for GC analysis) was diluted in 4.40 mL C_7H_8 to give a final concentration of 200 mM substrate. A 10.0 μL aliquot was removed for GC-FID analysis to establish the starting ratio of **1** to IS. Solid **AM** (10.0 mg, 0.012 mmol, 1 mol%) was added to the stirred solution. Aliquots were removed periodically, quenched with 100 μL KTp in THF (10.0 mg/mL), and analyzed by GC-FID. No product was observed after 4 h (no new peaks by GC), 3% conversion by GC.

3.6.5 Molecular Dynamics Simulations

Molecular dynamics simulations were carried out on the alkylidene intermediate **SC'** (Appendix D, Figure D-1) using the CUDA-enabled Amber14 software suite. Simulations included explicit solvation in a water-chloroform mixture (30:1,000), with the complex pre-encapsulated. Initial minimization was carried out over 10,000 steps followed by heating the system over 1 ns at constant volume. The simulation was then equilibrated at constant pressure for 10 ns followed by 500 ns of productive simulation carried out at constant volume. Molecular illustrations (Appendix D, Figure D-2) were then rendered using VMD.

3.7 References

(1) Higman, C. S.; Lummiss, J. A. M.; Fogg, D. E., Olefin Metathesis at the Dawn of Uptake in Pharmaceutical and Specialty Chemicals Manufacturing. *Angew. Chem., Int. Ed.* **2016**, *55*, 3552–3565.

(2) Yee, N. K.; Farina, V.; Houpis, I. N.; Haddad, N.; Frutos, R. P.; Gallou, F.; Wang, X.-J.; Wei, X.; Simpson, R. D.; Feng, X.; Fuchs, V.; Xu, Y.; Tan, J.; Zhang, L.; Xu, J.; Smith-Keenan, L. L.; Vitous, J.; Ridges, M. D.; Spinelli, E. M.; Johnson, M.; Donsbach, K.; Nicola, T.; Brenner, M.; Winter, E.; Kreye, P.; Samstag, W., Efficient Large-Scale Synthesis of BILN 2061, a Potent HCV Protease Inhibitor, by a Convergent Approach Based on Ring-Closing Metathesis. *J. Org. Chem.* **2006**, *71*, 7133–7145.

(3) Nicola, T.; Brenner, M.; Donsbach, K.; Kreye, P., First Scale-Up to Production Scale of a Ring Closing Metathesis Reaction Forming a 15-Membered Macrocycle as a Precursor of an Active Pharmaceutical Ingredient. *Org. Process Res. Dev.* **2005**, *9*, 513–515.

(4) Marsault, E.; Peterson, M. L., Macrocycles Are Great Cycles: Applications, Opportunities, and Challenges of Synthetic Macrocycles in Drug Discovery. *J. Med. Chem.* **2011**, *54*, 1961–2004.

(5) Giordanetto, F.; Kihlberg, J., Macrocyclic Drugs and Clinical Candidates: What Can Medicinal Chemists Learn from Their Properties? *J. Med. Chem.* **2014**, *57*, 278-295.

(6) Driggers, E. M.; Hale, S. P.; Lee, J.; Terrett, N. K., The Exploration of Macrocycles for Drug Discovery - An Underexploited Structural Class. *Nat. Rev. Drug Discov.* **2008**, *7*, 608–624.

(7) Chang, K.-O.; Kim, Y.; Lovell, S.; Rathnayake, A. D.; Groutas, W. C., Antiviral Drug Discovery: Norovirus Proteases and Development of Inhibitors. *Viruses* **2019**, *11*, 197.

(8) Schwartz, A. D.; Graham, L. A., Potential Maternal and Infant Outcomes from Coronavirus 2019-nCoV (SARS-CoV-2) Infecting Pregnant Women: Lessons from SARS, MERS, and Other Human Coronavirus Infections. *Viruses* **2020**, *12*.

(9) Morse, J. S.; Lalonde, T.; Xu, S.; Liu, W. R., Learning from the Past: Possible Urgent Prevention and Treatment Options for Severe Acute Respiratory Infections Caused by 2019-nCoV. *ChemBioChem* **2020**, *21*, 730–738.

(10) Calligari, P.; Bobone, S.; Ricci, G.; Bocedi, A., Molecular Investigation of SARS–CoV-2 Proteins and Their Interactions with Antiviral Drugs. *Viruses* **2020**, *12*.

(11) Ton, S. J.; Fogg, D. E., The Impact of Oxygen on Leading and Emerging Ru-Carbene Catalysts for Olefin Metathesis: An Unanticipated Correlation Between Robustness and Metathesis Activity *ACS Catal.* **2019**, *9*, 11329−11334.

(12) Guidone, S.; Songis, O.; Nahra, F.; Cazin, C. S. J., Conducting Olefin Metathesis Reactions in Air: Breaking the Paradigm. *ACS Catal.* **2015**, *5*, 2697–2701.

(13) Goudreault, A. Y.; Walden, D. M.; Nascimento, D. L.; Botti, A. G.; Steinmann, S. N.; Michel, C.; Fogg, D. E., Hydroxide-Induced Degradation of Olefin Metathesis Catalysts: A Challenge for Metathesis in Alkaline Media. *ACS Catal.* **2020**, *10*, 3838−3843.

(14) Ireland, B. J.; Dobigny, B. T.; Fogg, D. E., Decomposition of a Phosphine-Free Metathesis Catalyst by Amines and Other Nitrogen Bases: Metallacyclobutane Deprotonation as a Major Deactivation Pathway. *ACS Catal.* **2015**, *5*, 4690−4698.

(15) Bailey, G. A.; Lummiss, J. A. M.; Foscato, M.; Occhipinti, G.; McDonald, R.; Jensen, V. R.; Fogg, D. E., Decomposition of Olefin Metathesis Catalysts by Brønsted Base: Metallacyclobutane Deprotonation as a Primary Deactivating Event. *J. Am. Chem. Soc.* **2017**, *139*, 16446–16449.

(16) Koblenz, T. S.; Wassenaar, J.; Reek, J. N. H., Reactivity Within a Confined Self-Assembled Nanospace. *Chem. Soc. Rev.* **2008**, *37*, 247–262.

(17) Grubbs, R. H.; Wenzel, A. G., *Handbook of Metathesis*. 2nd ed.; Wiley-VCH: Weinheim, 2015.

(18) Grela, K., *Olefin Metathesis-Theory and Practice*. Wiley: Hoboken, NJ, 2014.

(19) For recent reviews of Ru-catalyzed olefin metathesis in pharmaceutical manufacturing, see: a) Higman, C. S.; Lummiss, J. A. M.; Fogg, D. E. Olefin Metathesis at the Dawn of Uptake in Pharmaceutical and Specialty Chemicals Manufacturing. *Angew. Chem., Int. Ed.* **2016**, *55*, 3552–3565. b) Farina, V.; Horváth, A., Ring-Closing Metathesis in the Large-Scale Synthesis of Pharmaceuticals. In *Handbook of Metathesis*, Grubbs, R. H.; Wenzel, A. G., Eds. Wiley-VCH: Weinheim, **2015**; Vol. 2, pp 633–658. c) Fandrick, K. R.; Savoie, J.; Jinhua, N. Y.; Song, J. J.; Senanayake, C. H., Challenges and Opportunities for Scaling The Ring-Closing Metathesis Reaction In The Pharmaceutical Industry. In *Olefin Metathesis – Theory and Practice*, Grela, K., Ed. Wiley: Hoboken, **2014**; pp 349-366.

(20) For selected recent examples of metathesis in chemical biology, see: (a) Bhushan, B.; Lin, Y. A.; Bak, M.; Phanumartwiwath, A.; Yang, N.; Bilyard, M. K.; Tanaka, T.; Hudson, K. L.; Lercher, L.; Stegmann, M.; Mohammed, S.; Davis, B. G., Genetic Incorporation of Olefin Cross-Metathesis Reaction Tags for Protein Modification. *J. Am. Chem. Soc.* **2018**, *140*, 14599–14603. (b) Lu, X.; Fan, L.; Phelps, C. B.; Davie, C. P.; Donahue, C. P., Ruthenium Promoted On-DNA Ring-Closing Metathesis and Cross-Metathesis. *Bioconjugate Chem.* **2017**, *28*, 1625–1629. (c) Grison, C. M.; Burslem, G. M.; Miles, J. A.; Pilsl, L. K. A.; Yeo, D. J.; Imani, Z.; Warriner, S. L.; Webb, M. E.; Wilson, A. J., Double Quick, Double Click Reversible Peptide "Stapling". *Chem. Sci.* **2017**, *8*, 5166–5171. (d) Cromm, P. M.; Spiegel, J.; Kuchler, P.; Dietrich, L.; Kriegesmann, J.; Wendt, M.; Goody, R. S.; Waldmann, H.; Grossmann, T. N., Protease-Resistant and Cell-Permeable Double-Stapled Peptides Targeting the Rab8a GTPase. *ACS Chem. Biol.* **2016**, *11*, 2375–2382.

(21) a) Marx, V. M.; Sullivan, A. H.; Melaimi, M.; Virgil, S. C.; Keitz, B. K.; Weinberger, D. S.; Bertrand, G.; Grubbs, R. H., Cyclic Alkyl Amino Carbene (CAAC) Ruthenium Complexes as Remarkably Active Catalysts for Ethenolysis. *Angew. Chem., Int. Ed.* **2015**, *54*, 1919–1923; b) Gawin, R.; Tracz, A.; Chwalba, M.; Kozakiewicz, A.; Trzaskowski, B.; Skowerski, K., Cyclic Alkyl Amino Ruthenium Complexes—Efficient Catalysts for Macrocyclization and Acrylonitrile Cross Metathesis. *ACS Catal.* **2017**, *7*, 5443–5449; c) Gawin, R.; Kozakiewicz, A.; Guńka, P. A.; Dąbrowski, P.; Skowerski, K., Bis(Cyclic Alkyl Amino Carbene) Ruthenium Complexes: A Versatile, Highly Efficient Tool for Olefin Metathesis. *Angew. Chem., Int. Ed.* **2017**, *56*, 981–986; d) Nascimento, D. L.;

Gawin, A.; Gawin, R.; Guńka, P. A.; Zachara, J.; Skowerski, K.; Fogg, D. E., A Highly Reactive Ruthenium-Indenylidene Catalyst for Olefin Metathesis. *J. Am. Chem. Soc.* **2019**, *141*, 10626–10631. (22) Nascimento, D. L.; Gawin, A.; Gawin, R.; Guńka, P. A.; Zachara, J.; Skowerski, K.; Fogg, D. E., Integrating Activity with Accessibility in Olefin Metathesis: An Unprecedentedly Reactive Ruthenium-Indenylidene Catalyst Bearing a Cyclic Alkyl Amino Carbene. *J. Am. Chem. Soc.* **2019**, *141*, 10626–10631.

(23) Bailey, G. A.; Foscato, M.; Higman, C. S.; Day, C. S.; Jensen, V. R.; Fogg, D. E., Bimolecular Coupling as a Vector for Decomposition of Fast-Initiating Olefin Metathesis Catalysts. *J. Am. Chem. Soc.* **2018**, *140*, 6931–6944.

(24) Thiel, V.; Wannowius, K.-J.; Wolff, C.; Thiele, C. M.; Plenio, H., Ring-Closing Metathesis Reactions: Interpretation of Conversion–Time Data. *Chem. - Eur. J.* **2013**, *19*, 16403–16414.

(25) Lopez, L. P. H.; Schrock, R. R.; Muller, P., Dimers that Contain Unbridged W(IV)/W(IV) Double Bonds. *Organometallics* **2006**, *25*, 1978–1986.

(26) Tsang, W. C. P.; Schrock, R. R.; Hoveyda, A. H., Evaluation of Enantiomerically Pure Binaphthol-Based Molybdenum Catalysts for Asymmetric Olefin Metathesis Reactions that Contain 3,3'-Diphenyl- or 3,3'-Dimesityl-Substituted Binaphtholate Ligands. Generation and Decomposition of Unsubstituted Molybdacyclobutane Complexes. *Organometallics* **2001**, *20*, 5658–5669.

(27) Pilyugina, T. S.; Schrock, R. R.; Hock, A. S.; Muller, P., Synthesis of Molybdenum(VI) Monoimido Alkyl and Alkylidene Complexes. *Organometallics* **2005**, *24*, 1929-1937.

(28) Nascimento, D. L.; Fogg, D. E., Origin of the Breakthrough Productivity of Ruthenium-CAAC Catalysts in Olefin Metathesis (CAAC = Cyclic Alkyl Amino Carbene). *J. Am. Chem. Soc.* **2019**, *141*, 19236–19240.

(29) For comprehensive overviews of strategies employed in immobilizing molecular olefin metathesis catalysts, see: a) Dewaele, A.; Verpoort, F.; Sels, B., Opportunities of Immobilized Homogeneous Metathesis Complexes as Prominent Heterogeneous Catalysts. *ChemCatChem* **2016**, *8*, 3010-3030; b) Coperet, C.; Basset, J. M., Strategies to Immobilize Well-Defined Olefin Metathesis Catalysts: Supported Homogeneous Catalysis *vs.* Surface Organometallic Chemistry *Adv. Synth. Catal.* **2007**, *349*, 78–92; c) Buchmeiser, M. R.; in *Olefin Metathesis-Theory and Practice* (Ed.: Grela, K.), Wiley, Hoboken, NJ, **2014**, pp. 495–514. For a discussion of challenges, particularly in terms of productivity and leaching from the support, see: d) Hubner, S.; de Vries, J. G.; Farina, V., Why Does Industry Not Use Immobilized Transition Metal Complexes as Catalysts? *Adv. Synth. Catal.* **2016**, *358*, 3–25.

(30) Lübbe, C.; Dumrath, A.; Neumann, H.; Schäffer, M.; Zimmermann, R.; Beller, M.; Kadyrov, R., How Important are Impurities in Catalysis? An Example from Ring-Closing Metathesis. *ChemCatChem* **2014**, *6*, 684–688.

(31) Kadyrov, R., Low Catalyst Loading in Ring-Closing Metathesis Reactions. *Chem. – Eur. J.* **2013**, *19*, 1002–1012.

(32) Hong, C. M.; Bergman, R. G.; Raymond, K. N.; Toste, F. D., Self-Assembled Tetrahedral Hosts as Supramolecular Catalysts. *Acc. Chem. Res.* **2018** *51*, 2447–2455.

(33) Brown, C. J.; Toste, F. D.; Bergman, R. G.; Raymond, K. N., Supramolecular Catalysis in Metal–Ligand Cluster Hosts. *Chem. Rev.* **2015**, *115*, 3012–3035.

(34) Catti, L.; Zhang, Q.; Tiefenbacher, K., Advantages of Catalysis in Self-Assembled Molecular Capsules. *Chem. Eur. J.* **2016**, *22*, 9060–9066.

(35) Wiester, M. J.; Ulmann, P. A.; Mirkin, C. A., Enzyme Mimics Based Upon Supramolecular Coordination Chemistry. *Angew. Chem. Int. Ed.* **2011**, *50*, 114–137.

(36) Zhang, Q.; Catti, L.; Tiefenbacher, K., Catalysis inside the Hexameric Resorcinarene Capsule. *Acc. Chem. Res.* **2018**, *51*, 2107−2114.

(37) Leenders, S. H. A. M.; Gramage-Doria, R.; de Bruin, B.; Reek, J. N. H., Transition metal Catalysis in Confined Spaces. *Chem. Soc. Rev.* **2015**, *44*, 433–448.

(38) Raynal, M.; Ballester, P.; Vidal-Ferran, A.; Van Leeuwen, P. W. N. M., Supramolecular Catalysis. Part 1: Non-Covalent Interactions as a Tool for Building and Modifying Homogeneous Catalysts. *Chem. Soc. Rev.* **2014**, *43*, 660–1733.

(39) Raynal, M.; Ballester, P.; Vidal-Ferran, A.; van Leeuwen, P. W. N. M., Supramolecular Catalysis. Part 2: Artificial Enzyme Mimics. *Chem. Soc. Rev.* **2014**, *43*, 1734–1787.

(40) Jongkind, L. J.; Caumes, X.; Hartendorp, A. P. T.; Reek, J. N. H., Ligand Template Strategies for Catalyst Encapsulation. *Acc. Chem. Res.* **2018**, *51*, 2115–2128.

(41) Meeuwissen, J.; Reek, J. N. H., Supramolecular catalysis beyond enzyme mimics. *Nat. Chem.* **2010**, *2*, 615–621.

(42) Yoshizawa, M.; Klosterman, J. K.; Fujita, M., Functional Molecular Flasks: New Properties and Reactions Within Discrete, Self-Assembled Hosts. *Angew. Chem., Int. Ed.* **2009**, *48*, 3418–3438.

(43) a) Cavarzan, A.; Scarso, A.; Sgarbossa, P.; Strukul, G.; Reek, J. N. H., Supramolecular Control on Chemo- and Regioselectivity via Encapsulation of (NHC)-Au Catalyst within a Hexameric Self-Assembled Host *J. Am. Chem. Soc.* **2011**, *133*, 2848–2851; b) Jans, A. C. H.; Gómez-Suárez, A.; Nolan, S. P.; Reek, J. N. H., A Switchable Gold Catalyst by Encapsulation in a Self-Assembled Cage. C*hem. – Eur. J.*. **2016**, *22*, 14836–14839; c) Adriaenssens, L.; Escribano-Cuesta, A., Homs, A. Echavarren, M.; Ballester, P., Encapsulation Studies of Cationic Gold Complexes within a Self-Assembled Hexameric Resorcin[4]arene Capsule. *Eur. J. Org. Chem.* **2013**, 1494–1500.

(44) For a review on gold catalysis in capsules, see: Jans, A. C. H.; Caumes, X.; Reek, J. N. H., Gold Catalysis in (Supra)Molecular Cages to Control Reactivity and Selectivity. *ChemCatChem*. **2019**, *11*, 287–297.

(45) Wang, Z. J.; Brown, C. J.; Bergman, R. G.; Raymond, K. N.; Toste, F. D., Hydroalkoxylation Catalyzed by a Gold(I) Complex Encapsulated in a Supramolecular Host. *J. Am. Chem. Soc.* **2011**, *133*, 7358–7360.

(46) Wang, Q. Q.; Gonell, S.; Leenders, S. H. A. M.; Dürr, M.; Ivanovic-Burmazovic, I.; Reek, J. N. H., Self-Assembled Nanospheres with Multiple Endohedral Binding Sites Pre-Organize Catalysts and Substrates for Highly Efficient Reactions. *Nat. Chem.* **2016**, *8*, 225–230.

(47) Ziegler, F.; Teske, J.; Elser, I.; Dyballa, M.; Frey, W.; Kraus, H.; Hansen, N.; Rybka, J.; Tallarek, U.; Buchmeiser, M. R., Olefin Metathesis in Confined Geometries: A Biomimetic Approach toward Selective Macrocyclization. *J. Am. Chem. Soc.* **2019**, *141*, 19014−19022.

(48) Jee, J.-E.; Cheong, J. L.; Lim, J.; Chen, C.; Hong, S. H.; Lee, S. S., Highly Selective Macrocycle Formations by Metathesis Catalysts Fixated in Nanopores. *J. Org. Chem.* **2013**, *78*, 3048−3056.

(49) Conrad, J. C.; Eelman, M. D.; Duarte Silva, J. A.; Monfette, S.; Parnas, H. H.; Snelgrove, J. L.; Fogg, D. E., Oligomers as Intermediates in Ring-Closing Metathesis. *J. Am. Chem. Soc.* **2007**, *129*, 1024–1025.

(50) Monfette, S.; Fogg, D. E., Equilibrium Ring-Closing Metathesis. *Chem. Rev.* **2009**, *109*, 3783–3816.

(51) Alternatively, macrocyclic lactones have been distilled from the reaction mixture as they form. See: Sytniczuk, A.; Dąbrowski, M.; Banach, Ł.; Urban, M.; Czarnocka-Śniadała, S.; Milewski, M.; Kajetanowicz, A.; Grela, K., At Long Last: Olefin Metathesis Macrocyclization at High Concentration. *J. Am. Chem. Soc.* **2018**, *40*, 8895–8901

(52) a) L. Avram, Y. Cohen, *J. Am. Chem. Soc.* **2002**, *124*, 15148–15149; b) L. Avram, Y. Cohen, *Org. Lett.,* **2002**, *4,* 4365-4368.

(53) For reports of encapsulation by self-assembling resorcinarene subunits, see: a) Shivanyuk, A.; Rebek, J., Reversible encapsulation by self-assembling resorcinarene subunits. *Proc. Natl. Acad. Sci.* **2001**, *98*, 7662–7665; b) Beyeh, N. K.; Kogej, M.; Åhman, A.; Rissanen, K.; Schalley, C. A., Flying Capsules: Mass Spectrometric Detection of Pyrogallarene and Resorcinarene Hexamers. *Angew. Chem. Int. Ed.* **2006**, *45*, 5214–5218.

(54) Atwood, J. J. L.; MacGillivray, L. R., A Chiral Spherical Molecular Assembly Held Together by 60 Hydrogen Bonds. *Nature* **1997**, *389*, 469–472.

(55) For a review on the applications of hexameric resorcinarene capsules in catalysis, see: Gaeta, C.; Talotta, C.; De Rosa, M.; La Manna, P., Soriente, A.; Neri, P., The Hexameric Resorcinarene Capsule at Work: Supramolecular Catalysis in Confined Spaces. *Chem. Eur. J.* **2019**, *25*, 4899–4913.

(56) Garber, S. B.; Kingsbury, J. S.; Gray, B. L.; Hoveyda, A. H., Efficient and Recyclable Monomeric and Dendritic Ru-Based Metathesis Catalysts. *J. Am. Chem. Soc.* **2000**, *122*, 8168–8179.

(57) Skowerski, K.; Wierzbicka, C.; Szczepaniak, G.; Gułajski, Ł.; Bienieka, M.; Grela, K., Easily Removable Olefin Metathesis Catalysts. *Green Chem.* **2012**, *14*, 3264–3268.

(58) Skowerski, K.; Szczepaniak, G.; Wierzbicka, C.; Gulajski, L.; Bieniek, M.; Grela, K., Highly Active Catalysts for Olefin Metathesis in Water. *Catal. Sci. Technol.* **2012**, *2*, 2424–2427.

(59) For a recent review, including alternative immobilization strategies deployed with these catalysts, see: Olszewski, T. K.; Bieniek, M.; Skowerski, K., Practical Use of Continuous Processing in Developing and Scaling Up Laboratory Processes. *Org. Process Res. Dev.* **2020**, *24*, 125−145.

(60) Lipshutz, B. H., Ghorai, S., Olefin Metathesis in Water and Aqueous Media. In *Olefin Metathesis – Theory and Practice*, Grela, K., Ed. 2014; pp 515-521.

(61) Grela, K.; Gulajski, L.; Skowerski, K., Alkene Metathesis in Water. In *Metal-Catalyzed Reactions in Water*, Dixneuf, P. H.; Cadierno, V., Eds. Wiley-VCH: Weinheim, 2013; pp 291–336.

(62) McClennan, W. L.; Rufh, S. A.; Lummiss, J. A. M.; Fogg, D. E., A General Decomposition Pathway for Phosphine-Stabilized Metathesis Catalysts: Lewis Donors Accelerate Methylidene Abstraction. *J. Am. Chem. Soc.* **2016**, *138*, 14668−14677.

(63) Haynes, W. M., *CRC Handbook of Chemistry and Physics*. 95th ed.; CRC Press: Boca Raton, FL, 2014; p viscosity at 25 ˚C: CDCl3, 0.54. toluene 0.56 mPa-s.

(64) Aoyama, Y.; Tanaka, Y.; Sugahara, S., Resorcin[4]arene Monomer Synthesis. *J. Am. Chem. Soc.* **1989**, *111*, 5397–5404.

(65) Clavier, H.; Nolan, S. P., N-Heterocyclic Carbene and Phosphine Ruthenium Indenylidene Precatalysts: A Comparative Study in Olefin Metathesis. *Chem. – Eur. J.* **2007**, *13*, 8029–8036.

(66) Blacquiere, J. M.; Jurca, T.; Weiss, J.; Fogg, D. E., Time as a Dimension in High-Throughput Homogeneous Catalysis. *Adv. Synth. Catal.* **2008**, *350*, 2849–2855.

4 Investigation of New Electron-Rich Phosphines as Ligands for Ruthenium-Catalyzed Olefin Metathesis

4.1 Publication Pending

Ton, S.J., Rotterig, P., Löwe, P., Dielmann F., Fogg, D. E. "Pyridinylide Aminophosphine Ligands: Lessons in Ligation for Ruthenium-Catalyzed Olefin Metathesis." (Manuscript in preparation)

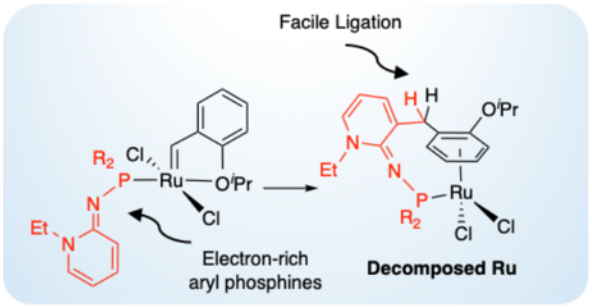

Abstract: Ubiquitous in high-performing metathesis catalysts are strongly-donating carbene ligands, most commonly N-heterocyclic carbenes (NHCs). With an eye to increasing the diversity of the available catalyst structures, a new class of highly electron-rich phosphines is explored as an alternative to NHCs. Pyridinylide aminophosphine (PyAP) ligands have been shown to be stronger σ-donors than NHCs, and to possess a readily modified backbone, which facilitates stereoelectronic tuning. Strategies are described that enable access to the target PyAP derivatives. Catalytic studies demonstrate, however, that the increased donicity of the PyAP ligands does not translate into higher metathesis activity relative to the NHC analogues. This unexpected behaviour is traced to facile *o*-metalation of the electron-rich aryl ring in the PyAP ligand, which results in rapid catalyst decomposition. These data establish a basis for redesign of the PyAP ligand. More fundamentally, they underscore the point that informed understanding of catalyst structure-decomposition relationships is fundamental to the interpretation of catalyst activity.

Author Contributions: This manuscript was written by SJT and DEF. Experiments were conceived by SJT, DEF and FD. Phosphine ligands were synthesized by PR. X-ray quality crystals of **Ru-25** were obtained by SJT, and analyzed by PL. All other experiments were conducted by SJT.

4.2 Introduction

Olefin metathesis offers exceptional power and versatility in the catalytic formation of carbon-carbon bonds.[1,2] Metathesis methodologies based on ruthenium catalysis have been embraced for their versatility and functional-group tolerance. Pioneering work by Schwab and Grubbs established that replacing PPh_3 ligands by PCy_3 ligands in Ru metathesis catalysts (see **GI**, Chart 4.1) opened the door to synthetically relevant activity.[3] Following the discovery that strongly-donating N-heterocyclic carbene (NHC) ligands confer dramatically higher reactivity,[4-6] efforts in the field shifted to "second-generation" Ru-NHC catalysts such as the Grubbs and Hoveyda catalysts **GII**[7] and **HII**.[8] Much ensuing work, up to the present,[2,9] has focused on improving activity by increasing initiation rates: that is, accelerating loss of the ligand shown in red in Chart 4.1, which opens a coordination site for olefin binding.[10-12] In the high-performing nitro-Grela catalyst **nG**, for example, the lability of the chelating ether donor is increased by the inductive effect of the *p*-NO_2 group.[10]

Chart 4.1 Metathesis Catalysts Discussed

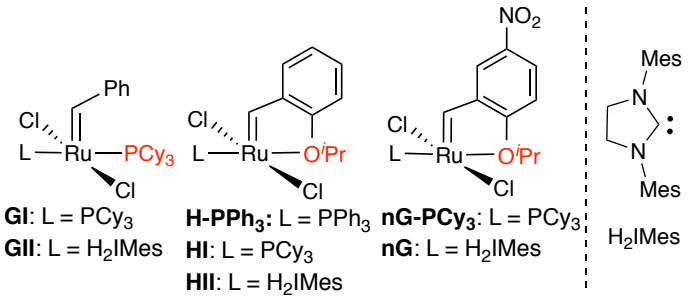

Concurrent developments have greatly expanded the σ-donor abilities of tertiary phosphines. Multiple examples now exist of phosphines that are stronger σ-donors than NHCs, as judged from the Tolman electronic parameter (TEP).[13] Shown in Chart 4.2a are leading selected examples, a number of which have led to advances in catalysis. Among these, Carrow's tri(1-adamantyl)phosphine was shown to double yields in Suzuki cross-coupling, relative to P^tBu_3 analogues.[14] Gessner's ylide-phosphines, which combine high donicity with a steric demand comparable to that of Buchwald-class biaryl phosphines, increased activity in gold-catalyzed hydroamination, relative to classic Buchwald-phosphines.[15,16] Sundermeyer's recently reported

phosphazenyl phosphine has the lowest TEP value of any phosphine reported to date.[17] While these have not, to our knowledge, yet been deployed in catalysis, related N-superbases developed by Schwesiger are widely used in Brønsted-base catalysis.[18-20] The present work focuses on Dielmann's imidazole ylide aminophosphine (IAP) ligands, in which a π-donor nitrogen substituent on the phosphorus atom increases the electron-density at phosphorus.[21-23] This ligand class was recently expanded to include pyridinylide aminophosphine (PyAP) ligands (Chart 4.2b). At the extreme of donicity is **P5**, in which three pyridinylide amino groups are present on the phosphorus center (TEP 2041 cm^{-1}).[24] Beyond their σ-donor capacity, the PyAP ligands are of interest for their modularity, and the potential for fine-tuning of steric and electronic properties via modification of the nitrogen and carbon substituents.

If the Dielmann phosphines are indeed more strongly donating than H_2IMes, we queried whether they might afford metathesis catalysts more active than the second-generation Grubbs catalyst. Here we describe synthesis of PyAP-functionalized metathesis catalysts, catalyst screening, and criteria for ligand redesign.

Chart 4.2 Donicity of Relevant Ligands Assessed from the Tolman Electronic Parameter (TEP). (a) Leading Electron-Rich Phosphines. (b) Expanded Scale for PyAP Ligands.

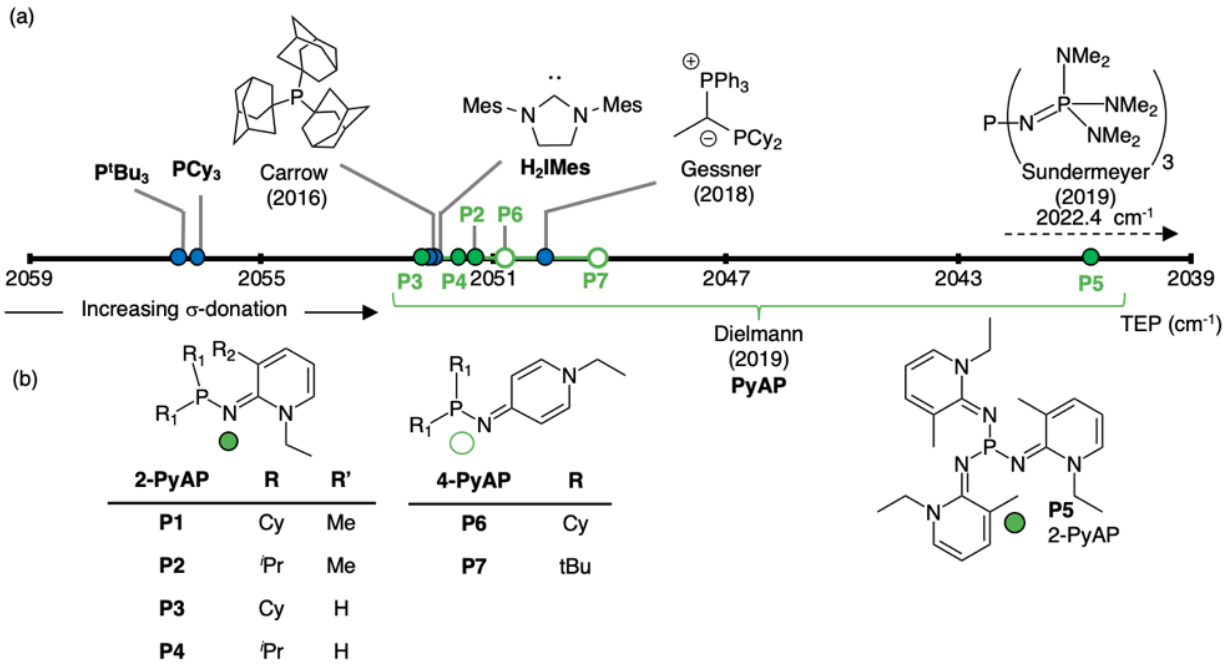

4.3 Results and Discussion

4.3.1 Synthesis

Our initial synthetic strategy targeted analogues of the fast-initiating Grela catalyst **nG**. Accordingly, we undertook ligand exchange of the first-generation Grela complex **nG-PCy$_3$** with a series of 2-PyAP ligands (Scheme 4.1). In all cases, reaction was complete within 3 h at RT, but isolated yields of the desired products were limited to a maximum of 43% by competing formation of a bis-phosphine derivative. Unexpectedly, this was the PCy$_3$ derivative **Ru-21** (see Table 4.1), rather than PyAP/PCy$_3$ or even bis-PyAP products.[10] The capacity of the PCy$_3$ ligand to compete with the more strongly donating PyAP ligands for binding to **nG-PCy$_3$** presumably reflects its greater steric accessibility.

Scheme 4.1 Reaction of PyAP Ligands with nG-PCy$_3$.

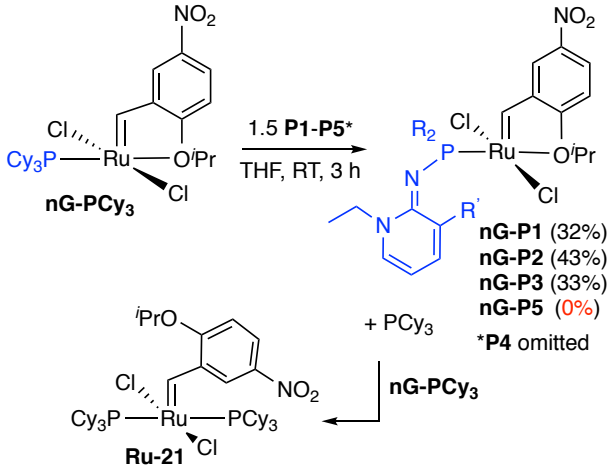

A different outcome was observed in the reaction of **nG-PCy$_3$** with **P5**, which failed to yield any of the expected **nG-P5**. An immediate colour change from brown-red to bright blue was evident, accompanied by disappearance of the NMR signals for the benzylidene proton, and emergence of multiple new $^{31}P\{^1H\}$ NMR singlets (57.5, 42.6, –15.5 ppm; ratio 1:2:4). The signal at 42.6 ppm compares well with a value of 47.3 for a closely related PyAP phosphine oxide,[25] and may thus be due to O=**P5**. As no such decomposition occurs in the absence of the NO$_2$ group (see below), we suspect that a decomposition cascade may be triggered by initial attack of the highly basic phosphine on the nitro functionality (Scheme 4.2a). Ample precedents exist for deoxygenation of

nitrobenzenes by electron-rich tertiary phosphines.[26-28] A plausible competing pathway (Scheme 4.2b), well established in the chemistry of **GII**,[29] involves nucleophilic attack of **P5** on the benzylidene carbon, in this case via the imine nitrogen. Subsequent release of a [benzyl-**P5**]Cl salt can be envisaged upon proton abstraction from a ligand, and chloride abstraction from the metal.

Scheme 4.2 Proposed Decomposition of nG-PCy$_3$ by P5.

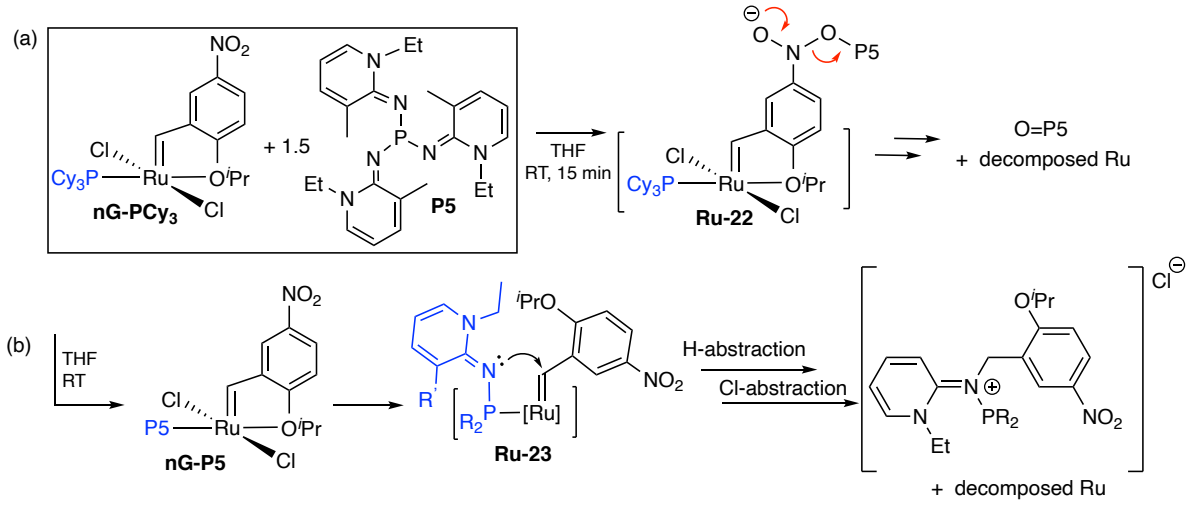

Given the synthetic challenges associated with the nitro group, we turned to the Hoveyda catalyst platform (Chart 4.1) as a potentially more tractable alternative. To preclude formation of bis-PCy$_3$ side-product **Ru-21**, we chose to employ the PPh$_3$ complex[8] **H-PPh$_3$** as precursor (Scheme 4.3), rather than its PCy$_3$-stabilized analogue **H1**. Accordingly, ligand exchange was carried out with **H-PPh$_3$** and selected 2-PyAP ligands. The latter included **P1** (which emerged as the highest-performing catalyst in catalytic studies of the low-yielding **nG** derivatives: see below), and **H5**, for which the **nG-PCy$_3$** derivative was inaccessible, as noted above. These reactions were complete within 30 min, as judged by NMR analysis, and the target complexes **H-P1** and **H-P5** were isolated in yields of 82 and 87%, respectively. This represents a dramatic improvement over the yields obtained with **nG-PCy$_3$** as precursor. The identity of the proposed structures is supported by ^{1}H and ^{31}P{^{1}H} NMR analysis (Table 4.1). Microanalytical and mass spectrometric proof of identity have not yet been obtained.

Scheme 4.3 Ligand Exchange of H-PPh$_3$ with 2-PyAP Ligands.

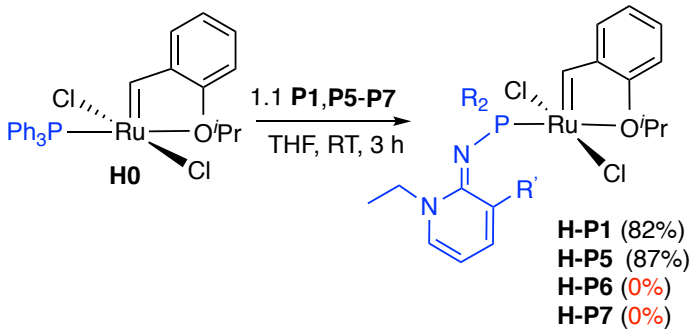

Table 4.1 Key NMR Signals and Yields for New Complexes.[a]

Complex	δ_P (ppm)	δ_H [Ru]=C*H*R (ppm)	Yield (%)
nG-P1	84.6	17.21	32
nG-P2	89.2	17.02	43
nG-P3	87.1	17.10	33
Ru-21	35.4	21.29	not isolated
H-P1 ($CDCl_3$)	89.4	17.43	82
H-P4	95.7	17.24	not isolated
H-P5	33.5	19.20	87
H-P6 (THF-d_8)	83.7	17.16	0

[a] Spectra measured in C_6D_6, unless otherwise specified.

The corresponding reaction of **H-PPh$_3$** with **P4** resulted in complete conversion to a complex presumed to be **H-P4** within 30 min at RT (Scheme 4.4a). Consistent with the proposed structure, the ^{1}H NMR spectrum revealed a new Ru=C*H*Ar singlet at 17.24 ppm, accompanied by a new $^{31}P\{^1H\}$ NMR singlet at 95.7 ppm (C_6D_6). Following reprecipitation, a second $^{31}P\{^1H\}$ NMR singlet was evident at 81.0 ppm (25% of total integration). X-ray analysis of crystals that deposited from solution over several days at RT revealed an unanticipated decomposition product, piano-stool complex **Ru-25** (Scheme 4.4b). The latter species may form via *o*-metalation at the unsubstituted *o*-site of the N-aryl ligand, as proposed for **GII** analogues bearing an N-phenyl

NHC.[30,31] Attack on the benzylidene ligand to form **Ru-24**, followed by (possibly concerted) insertion into the Ru-benzyl bond and σ-π-isomerization,[32,33] could then form piano-stool complex **Ru-25**.

Scheme 4.4 (a) Decomposition of H-P4. (b) Thermal ellipsoid plot of Ru-25 (50% probability level).

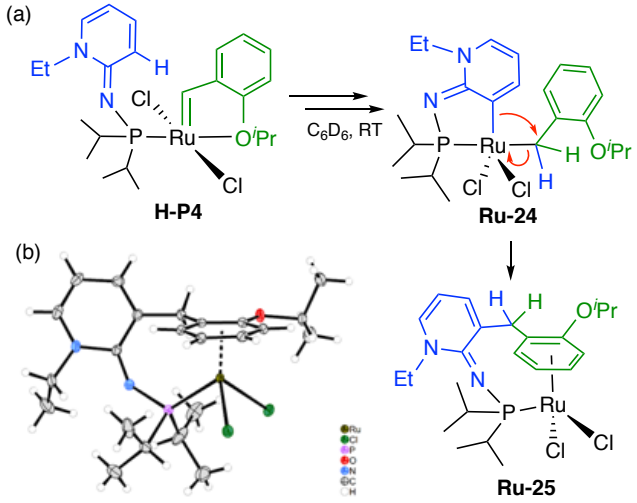

Unexpectedly, the corresponding reactions of **H-PPh$_3$** with the 4-PyAP ligands **P6** and **P7** also failed. A parallel experiment with **P6** and **HI** (Scheme 4.5), which was monitored by NMR analysis, suggested initial formation of **H-P6**, as indicated by appearance of a new [Ru]=C*H*Ar signal at 17.16 ppm (THF-d$_8$) within 15 min (ratio 1:1 vs remaining **HI**). The new signal disappeared over a further 2 h at room temperature, however, and the sole remaining benzylidene signal was that for unreacted **HI**. Cyclometallation of the sterically unprotected pyridine ligand to form **Ru-25** is again suspected, although the complexity of the spectrum precluded confirmation.

Scheme 4.5 Decomposition of HI by 4-PyAP Ligands.

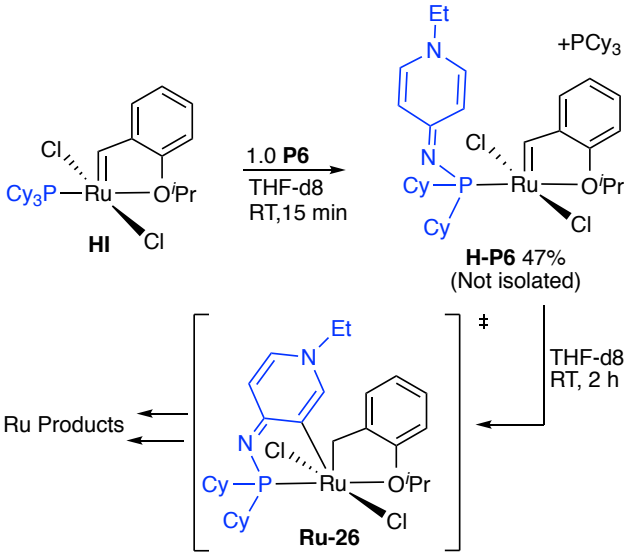

4.3.2 Catalysis

The activity of those Ru-PyAP catalysts which could be successfully isolated was assessed in ring-closing metathesis (RCM) of the benchmark substrate diethyl diallyl malonate (DDM, **2**), and compared with the reaction rates observed for **nG** and **nG-PCy$_3$**. Given the anticipated activity of the new species, reactions were carried out at a catalyst loading of 0.1 mol% at room temperature. Unexpectedly, time profiles (Figure 4.1) indicated slightly faster reaction for the first-generation complex **nG-PCy$_3$** than any of the PyAP catalysts studied. The highest-performing PyAP catalysts, **nG-P1** and **nG-P2**, delivered slightly higher yields relative to **nG-PCy$_3$** after 24 h (53% and 44%, respectively, vs. 39%), but far below that of the second-generation H$_2$IMes analogue **nG** (see inset). The low activity of the **P3 and P4** derivatives we assign to facile C–H activation at the *o*-phenyl site, as seen in the **P4** and **P6** chemistry above. Consistent with this is the improved performance of the **P1** and **P2** derivatives, in which both *o*-aryl sites are blocked. Nevertheless, these catalysts remain much less active than **nG**, suggesting that additional decomposition pathways are operative. One such pathway may involve nucleophilic attack of the PyAP nitrogen on the [Ru]=*C*HAr carbon following decoordination of the ether donor (see Scheme 4.2b above), or on the corresponding methylidene.

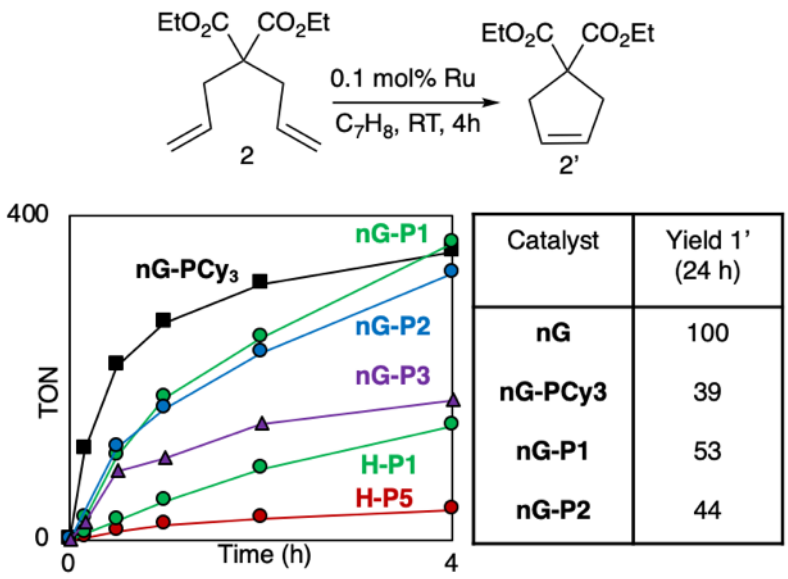

Catalyst	Yield 1' (24 h)
nG	100
nG-PCy3	39
nG-P1	53
nG-P2	44

Figure 4.1 Performance of PyAP catalysts in RCM of **2**, relative to their PCy_3 and H_2IMes analogues.

The poor performance of highly electron-rich **H-P5** is more unexpected. The **P5** ligand likewise contains a methyl-protected amino-pyridine group, and **P5** is a stronger donor than **P1** (TEP 2041, vs 2050 cm^{-1}). Slow entry into the catalytic cycle was expected from the lower lability of the styrenyl ether ligand in this Hoveyda-class catalyst, relative to its nitro-functionalized analogue. Recapture of the 2-isopropoxy styrene ligand also results in trapping of the catalyst off-cycle,[34] but nevertheless, a performance superior to **HII**,[35] which bears a less strongly donating H_2IMes ligand, would be expected.

To better understand the poor activity of **H-P5**, the catalyst was treated with styrene in an NMR-tube experiment (Scheme 4.6). Less than 5% of the cross-metathesis product **4** was observed. Moreover, the yield of 2-isopropoxystyrene **5**, which is released in the first cycle of metathesis, reaches only 56% at complete decomposition of **H-P5**. Completely absent were propenes (**6,6'**) which form via decomposition of the metallacyclobutane (MCB) intermediate.[36-38] This implies decomposition in the first cycle of metathesis. As suggested above, nucleophilic attack of the pyridinyl nitrogen on the alkylidene carbon may be responsible. Notable in **P5** is the presence of *three* pyridinyl substituents in the phosphine, which greatly increases the probability of encounter

with the [Ru]=CHR group, relative to (e.g.) **P1** and **P2**. We rule out the engagement of these potentially Bronsted basic sites in deprotonation of the MCB, another known decomposition pathway, as this would again generate propene products.[39,40]

Scheme 4.6 Products of Reaction of Ru-P5 with Styrene. (a) Generated via Metathesis. (b) Generated via MCB Decomposition During the First Cycle of Metathesis.

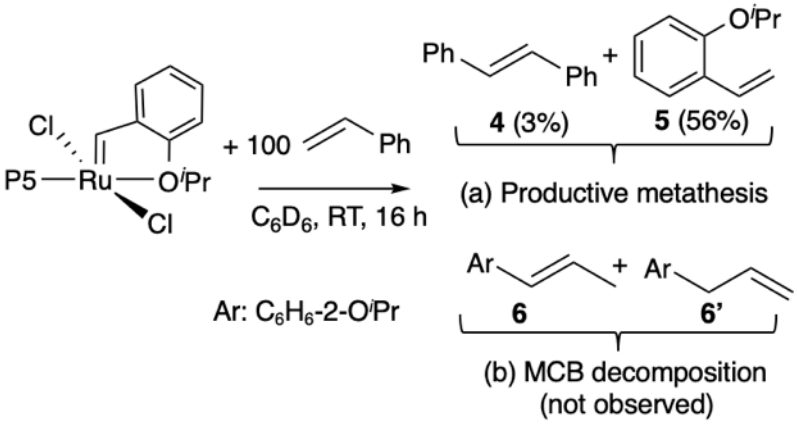

4.4 Conclusions

The foregoing describes routes to Ru-PyAP catalysts from the Ru precursors **H-PPh$_3$** and **nG-PCy$_3$**. Increased yields for the **nG-PyAP** catalysts may be achieved by utilizing **nG-PPh$_3$** as an alternative Ru precursor. Highest metathesis activity was seen for the **nG-P1** and **nG-P2** derivatives, which bear a labile, nitro-functionalized styrenyl ether, and a phosphine N-aryl group that is blocked against C-H activation (a recurring decomposition pathway for the other PyAP ligands). Nevertheless, **nG-P1** and **nG-P2** exhibited activity comparable only to the PCy$_3$-stabilized analogue **nG-PCy$_3$**, and far below that of the corresponding H_2IMes catalyst **nG**.

This study underscores the point that strong σ-donation is insufficient to achieve high metathesis activity. The higher donicity of the PyAP phosphines, which was expected to open the door to high activity, is instead undermined by facile catalyst decomposition. The importance of blocking *o*-metalation of the N-aryl group is noted above. More fundamentally, the nitrogen site in the R_2P-

N=Py unit may constitute a design flaw that enables the ligand to participate in nucleophilic attack at the [Ru]=*C*HR carbon. Replacing the N-donor atom with a carbon atom to decrease nucleophilicity could limit alkylidene abstraction, but at the cost of enhanced ligand donicity. An alternative strategy involves use of phosphines in which inductive effects, rather than π-donation, are harnessed to generate an electron-rich phosphorus center. Among these are the tri-methylpyrrolidine phosphine recently developed by the Dielmann group, which will be reported in due course.

4.5 Experimental Procedures

4.5.1 General Procedures

Reactions were carried out under N_2 in a glovebox or on a Schlenk line, unless otherwise noted. HPLC-grade solvents (C_6H_6, C_7H_8, n-hexane, tetrahydrofuran) were dried and degassed using a Glass Contour solvent purification system and stored under N_2 over 4Å molecular sieves for 16 h prior to use. NMR solvents (C_6D_6, $CDCl_3$, THF-d_8; Cambridge Isotopes) were freeze-pump-thaw degassed and stored as above. Potassium tris(1-pyrazolyl)borohydride (KTp; TCI), was used as received to quench metathesis by the reported method.[41] Metathesis catalysts **H-PPh$_3$**,[8] **HI**[8] and **nG-PCy$_3$**[10] and ligands **P1**-**P7**[24] were prepared by literature methods. Diethyl diallylmalonate (**1**, Aldrich, 98%) and styrene (Aldrich, 99%) were freeze-pump-thaw degassed[42] and stored over activated neutral alumina prior to use. Dodecane (Aldrich, anhydrous, 99%) and pentadecane (Aldrich, 99%) (GC internal standards) were freeze-pump-thaw degassed and stored under N_2 in the glovebox. Anthracene (NMR internal standard, Aldrich, 97%) was used as received. NMR spectra were recorded on Avance 300, Avance II 300 or Avance III 400 spectrometers at 23 ±2 °C. Chemical shifts are reported in ppm, and referenced to the residual proton signal of the solvent (^{1}H NMR) or 85% external H_3PO_4 (^{31}P NMR) at 0 ppm. ^{31}P{^{1}H} NMR spectra were processed with line broadening set to 10 Hz (lb = 10 Hz), to improve signal-to-noise ratios for complexes of the PyAP phosphines, which show relatively poor solubility in benzene. Chlorinated solvents could not be used, owing to rapid sample degradation. RCM experiments were analyzed using Agilent 7890A gas chromatograph (GC) equipped with auto-sampler, flame ionization detector (FID) and Agilent HP-5 polysiloxane column (30 m length, 320 μm diameter) or Shimadzu (Nexis

GC-2030) equipped with auto-samplers, flame ionization detectors (FID) and SH-RTX dimethyl polysiloxane column. Calibration curves of peak areas versus concentration were established for the starting dienes and cyclic products in the relevant concentration regimes, with ca. 1:1 (w/w) sample versus dodecane or pentadecane as internal standard.

4.5.2 Synthesis of Catalysts nG-P1, nG-P2, nG-P3 via Ligand Exchange From nG-PCy$_3$

To a stirred solution of **nG-PCy$_3$** (50.0 mg, 0.077 mmol) in 1 mL THF was added a solution of the corresponding phosphine (0.12 mmol, 1.5 equiv) in 1 mL THF. After 3 h, NMR analysis of an aliquot confirmed complete conversion of **nG-PCy$_3$**. At that point, the solvent was removed under vacuum to give a red-brown solid. The solid was dissolved in C_6H_6, filtered through Celite, then concentrated to a minimum volume. The complex was precipitated by addition of cold hexanes. The solid was filtered off and washed with hexanes (6 x 1 mL), affording **nG-P1**, **nG-P2** or **nG-P3** as brown solids.

Synthesis of RuCl$_2$(PCy$_2$(N=C$_5$H$_3$-1-NEt-3-Me)(=CHAr), nG-P1: Ar = C$_6$H$_3$-2-O^{i}Pr-5-NO$_2$. As above with the following modification; **nG-PCy$_3$** (30 mg, 0.046 mmol), was added to a solution of **P1** (17 mg 0.051 mmol, 1.1 equiv) in THF. **nG-P1** was isolated as a light brown solid. Yield: 10 mg (32%). ^{1}H NMR (300 MHz, C_6D_6) δ 17.21 (d, $^3J_{PH}$ = 4.9 Hz, 1H, [Ru]=C*H*R), 8.30 (d, $^3J_{HH}$ = 2.8 Hz, 1H, Ar sp^2-C*H*), 8.05 (dd, $^3J_{HH}$ = 9.1, $^4J_{HH}$ = 2.8 Hz, 2H, Ar sp^2-C*H*), 6.65 (d, $^3J_{HH}$ = 6.7 Hz, 1H, Ar sp^2-C*H*, **P1**), 6.33 (d, $^3J_{HH}$ = 6.7 Hz, 1H, Ar sp^2-C*H*, **P1**), 6.21 (d, $^3J_{HH}$ = 9.0 Hz, 2H, Ar sp^2-C*H*), 5.50 (t, $^3J_{HH}$ = 6.7 Hz, 1H, Ar sp^2-C*H*, **P1**), 4.54 (m, 1H, ^{i}Pr C*H*), 3.72 (q, $^3J_{HH}$ = 7.1 Hz, 2H, Et CH_2, **P1**), 3.31-1.19 (m, 22 H, overlap, P(C_6H_{11})$_2$), 2.96 (s, 3H, Me CH_3, **P1**), 1.65 (d, $^3J_{HH}$ = 6.2 Hz, 6H, ^{i}Pr CH_3), 0.95 (t, $^3J_{HH}$ = 5.8 Hz, 3H, EtCH_3, **P1**). ^{31}P{^{1}H} NMR (C_6D_6, 121.5 MHz) δ 84.6 (s). For assigned NMR spectra, see Appendix B, Figures B-18 and B-19.

Synthesis of RuCl$_2$(P^{i}Pr$_2$(N=C$_5$H$_3$-1-NEt-3-Me))(=CHAr), nG-P2: Ar = C$_6$H$_3$-2-O^{i}Pr-5-NO$_2$. Isolated as a brown solid. Yield: 21 mg (43%). ^{1}H NMR (300 MHz, C_6D_6) δ 17.02 (d, $^3J_{PH}$ = 5.1 Hz, 1H, [Ru]=C*H*R), 8.27 (d, $^3J_{HH}$ = 2.7 Hz, 1H, Ar sp^2-C*H*), 8.04 (dd, $^3J_{HH}$ = 9.1, $^4J_{HH}$ = 2.7 Hz, 1H, Ar sp^2-C*H*), 6.67 (d, $^3J_{HH}$ = 6.9 Hz, 1H, Ar sp^2-C*H* **P2**), 6.29 (d, $^3J_{HH}$ = 6.9 Hz, 1H, Ar sp^2-C*H*

P2), 6.18 (d, $^3J_{HH}$ = 9.1 Hz, 1H, Ar sp^2-C*H*), 5.50 (t, $^3J_{HH}$ = 6.7 Hz, 1H, Ar sp^2-C*H* **P2**), 4.53 (m, 1H, ^{i}Pr C*H*), 3.65 (q, $^3J_{HH}$ = 7.1 Hz, 2H, Et CH_2 **P2**), 3.26 (m, 2H, ^{i}Pr C*H* **P2**), 2.95 (s, 3H, Me CH_3 **P2**), 1.64 (d, $^3J_{HH}$ = 6.1 Hz, 6H, ^{i}Pr CH_3), 1.33 (m, 12H, ^{i}Pr CH_3 **P2**), 0.93 (t, $^3J_{HH}$ = 7.1 Hz, 3H, Et CH_3 **P2**). ^{31}P{^{1}H} NMR (C_6D_6, 121.5 MHz) δ 89.2 (s). For assigned NMR spectra, see Appendix B, Figures B-20 and B-21.

Synthesis of RuCl$_2$(PCy$_2$(N=C$_5$H$_4$-1-NEt)(=CHAr), nG-P3: Ar = C$_6$H$_3$-2-O^{i}Pr-5-NO$_2$. Isolated as a light brown solid. Yield: 18 mg (33%). ^{1}H NMR (300 MHz, C_6D_6) δ 17.10 (d, $^3J_{PH}$ = 5.4 Hz, 1H, [Ru]=C*H*R), 8.13 (d, $^3J_{HH}$ = 2.7 Hz, 1H, Ar sp^2-C*H*), 7.96 (dd, $^3J_{HH}$ = 9.1, $^4J_{HH}$ = 2.7 Hz, 2H, Ar sp^2-C*H*), 7.50 (d, $^3J_{HH}$ = 9.1 Hz, 1H, Ar sp^2-C*H*), 6.55 (t, $^3J_{HH}$ = 7.8 Hz, 1H, Ar sp^2-C*H* **P3**), 6.17 (d, $^3J_{HH}$ = 8.6 Hz, 2H, Ar sp^2-C*H* **P3**), 5.36 (t, $^3J_{HH}$ = 6.7 Hz, 1H, Ar sp^2-C*H* **P3**), 4.55 (m, 1H, ^{i}Pr C*H*), 3.64 (d, $^3J_{HH}$ = 6.4 Hz, 2H, Et CH_2 **P3**), 3.00-1.81 (m, 12 H, (C$_6H_{11}$)$_2$ **P3**), 1.69 (d, $^3J_{HH}$ = 6.1 Hz, 6H, ^{i}Pr CH_3), 1.41-1.23 (m, 10 H, (C$_6H_{11}$)$_2$ **P3**), 1.05 (t, $^3J_{HH}$ = 7.1 Hz, 3H, Et CH_3 **P3**). ^{31}P{^{1}H} NMR (C_6D_6, 121.5 MHz) δ 87.1 (s). For assigned NMR spectra, see Appendix B, Figures B-22 and B-23.

4.5.3 Synthesis of Catalysts H-P1 and H-P5 via Ligand Exchange From H-PPh$_3$.

Synthesis of RuCl$_2$(PCy$_2$(N=C$_5$H$_3$-1-NEt-3-Me))(=CHAr), H-P1: Ar = C$_6$H$_4$-2-O^{i}Pr. To a stirred solution of **H-PPh$_3$** (40 mg, 0.069 mmol) in 1 mL THF was added a solution of **P1** (25 mg, 0.076 mmol, 1.1 equiv) in 1 mL THF. After 0.5 h an aliquot was removed for NMR analysis confirming complete conversion of **H-PPh$_3$**. Once complete conversion was seen the solvent was then removed under vacuum. The solid was dissolved in C_6H_6, filtered through Celite, then concentrated to a minimum volume of C_6H_6. The complex was precipitated by addition of cold hexanes. The solid was filtered off and washed with hexanes (3 x 1mL) to afford **H-P1** as a red-brown solid. Yield: 37 mg (82%). ^{1}H NMR (300 MHz, $CDCl_3$) δ 17.43 (d, $^3J_{PH}$ = 5.0 Hz, 1H, [Ru]=C*H*R), 7.66 – 7.52 (m, 2H, Ar sp^2-C*H*), 7.27–7.12 (m, 2H, Ar sp^2-C*H*), 7.04 (d, $^3J_{HH}$ = 8.2 Hz, 2H, Ar sp^2-C*H*, **P1**), 6.08 (t, $^3J_{HH}$ = 6.8 Hz, 1H, Ar sp^2-C*H*, **P1**), 5.19 (m, 1H, ^{i}Pr CH_3), 4.19 (q, $^3J_{HH}$ = 7.3 Hz, 2H, Et CH_2, **P1**), 2.97 (s, 3H, Me CH_3, **P1**), 2.01-1.18 (m, 22 H, overlap, (C$_6H_{11}$)$_2$,

P1), 1.76 (d, $^{3}J_{HH}$ = 6.1 Hz, 6H, ^{i}Pr CH_3), 1.35 (t, $^{3}J_{HH}$ = 5.8 Hz, 3H, CH_3 of Et). $^{31}P\{^{1}H\}$ NMR ($CDCl_3$, 121.5 MHz) δ 89.4 (s). For assigned NMR spectra, see Appendix B, Figures B-14 and B-15.

$RuCl_2(P(N{=}C_5H_3\text{-}1\text{-}NEt\text{-}3\text{-}Me)_3)(=CHAr)$, H-P5: Ar = C_6H_4-2-O^{i}Pr as above with the following modifications; **H-PPh$_3$** (50 mg, 0.086 mmol), was added to a solution of **P5** (0.095 mmol, 1.1 equiv) in 1 mL THF. **H-P5** was isolated as a brick red solid, 56 mg (87% yield). ^{1}H NMR (300 MHz, C_6D_6) δ 19.20 (d, $^{3}J_{PH}$ = 4.7 Hz, 1H, [Ru]=C*H*R), 7.75 (dd, $^{3}J_{HH}$ = 7.7, $^{4}J_{HH}$= 1.7 Hz, 1H, Ar sp^2-C*H*), 7.34 (t, $^{3}J_{HH}$ = 7.8 Hz, 1H, Ar sp^2-C*H*), 6.95 (t, $^{3}J_{HH}$ = 7.4 Hz, 1H, Ar sp^2-C*H*), 6.68 (t, $^{3}J_{HH}$ = 6.8 Hz, 3H, sp^2-C*H* **P5**), 6.40 (d, $^{3}J_{HH}$ = 6.7 Hz, 3H, sp^2-C*H* **P5**), 5.51 (t, $^{3}J_{HH}$ =6.7 Hz, 3H, sp^2-C*H* **P5**), 4.66 (m, 1H, ^{i}Pr C*H*), 3.81 (q, $^{3}J_{HH}$ = 7.0 Hz, 6H, Et CH_2 **P5**), 3.05 (s, 9H, Me CH_3 **P5**), (d, $^{3}J_{HH}$ = 6.0 Hz, 6H, ^{i}Pr CH_3), 1.08 (t, $^{3}J_{HH}$ =7.1 Hz, 9H Et CH_3 **P5**). $^{31}P\{^{1}H\}$ NMR (C_6D_6, 121.5 MHz) δ 33.5 (s). For assigned NMR spectra, see Appendix B, Figures B-16 and B-17.

4.5.4 Attempted Synthesis of $RuCl_2(P(N{=}C_5H_3\text{-}1\text{-}NEt\text{-}6\text{-}Me)_3)(=CHC_6H_3\text{-}2\text{-}O^{i}Pr\text{-}5\text{-}NO_2)$, nG-P5 via Ligand Exchange from nG-PCy$_3$

To a stirred dark brown solution of **nG-PCy$_3$** (50 mg, 0.077 mmol) in 1 mL THF was added a bright red solution of **P5** (0.12 mmol, 1.5 equiv) in 1 mL THF. An immediate colour change to bright blue was observed. An aliquot was removed for NMR analysis. After 15 min 0% **nG-PCy$_3$** remained. Complete disappearance of alkylidene signals were observed. ^{1}H NMR (C_6D_6, 300 MHz; diagnostic signals only): δ 16.99 (s, 1H, [Ru]=C*H*R of **nG-PCy$_3$**). $^{31}P\{^{1}H\}$ NMR (C_6D_6, 121.5 MHz; diagnostic signals only): δ 60.6 (s, **nG-PCy$_3$**), 42.5 (s, O=**P5**). See Scheme 4.2 and Appendix B, Figures B-24 and B-25.

4.5.5 Attempted isolation of H-P4 $RuCl_2(P^{i}Pr_2(N{=}C_5H_3\text{-}1\text{-}NEt)(=CHC_6H_4\text{-}2\text{-}O^{i}Pr)$.

To a stirred solution of **H-PPh$_3$** (50 mg, 0.086 mmol) in 1 mL THF was added a solution of **P4** (23 mg, 0.095 mmol, 1.1 equiv) in 1 mL THF. After 0.5 h the solvent was then removed under vacuum.

The solid was dissolved in C_6H_6, filtered through Celite, then concentrated to a minimum volume of C_6H_6. The complex was precipitated by addition of cold hexanes. The solid was filtered off and washed with 3x 1mL hexanes resulting in a 3:1 mixture of **H-P4** and **Ru-25**. ^{1}H NMR (C_6D_6, 400 MHz; diagnostic signals for **H-P4**) δ 17.24 (s, 1H, [Ru]=C*H*R), 7.60 (d, $^3J_{HH}$ = 9.4 Hz, 1H, Ar sp^2-C*H*), 4.16 (m, 1H, ^{i}Pr C*H*), 3.79 (q, $^3J_{HH}$ = 7.7 Hz, 2H, EtCH_2 **P4**), 1.78 (d, $^3J_{HH}$ = 6.2 Hz, 6H, ^{i}Pr CH_3), 1.46 (dd, $^3J_{HH}$ = 15.0, $^4J_{HH}$ = 7.2 Hz, 12H, ^{i}Pr CH_3 **P4**), 1.01 (t, $^3J_{HH}$ = 6.5 Hz, 3H, EtCH_3 **P4**). ^{31}P{^{1}H} NMR (C_6D_6, 160 MHz) δ 95.7 (s, **H-P4**), 81.0 (s, **Ru-25**). See Scheme 4.4 and Appendix B, Figures B-26 and B-27.

4.5.6 Attempted Ligand Exchange with Phosphine P6 from HI.

Solid **HI** (10 mg, 0.015 mmol) and approximately 2 mg of anthracene were added to a J-Young tube in THF-d_8 (0.50 mL) for a final concentration of 30 mM Ru. A spectrum was taken to establish the initial ratio of **HI**: anthracene. The NMR sample was returned to the glovebox, where solid **P6** (4.8 mg, 0.015 mmol, 1 equiv) was added and the NMR tube shaken, ^{1}H NMR analysis was carried out periodically. After 15 min: 5% **Ru-26**, 14% **HI**, 47% **Ru-P6**. After 2 h no signals assigned to **H-P6** remained. ^{1}H NMR (C_6D_6, 300 MHz; diagnostic signals only): δ 20.7 (s, 1H, [Ru]=C*H*R of **Ru-26**), 17.15 (d, $^3J_{PH}$ = 4.9 Hz, 1H, [Ru]=C*H*R of **HI**), 17.06 (d, $^3J_{PH}$ =5.8 Hz, 1H, [Ru]=C*H*R of **H-P6**), 8.16 (s, 2H, ArC*H* of anthracene). See Scheme 4.4 and Appendix B, Figure B-28.

4.5.7 General Procedure for RCM of 2.

A mixture of DDM (95 µL, 0.4 mmol) and internal standard for GC analysis either dodecane (90 µL, 0.4 mmol) or pentadecane (110 µl, 0.4 mmol) was diluted in 1.8 mL C_7H_8 to give a final concentration of 200 mM DDM (**2**). A 10 µL aliquot was removed for GC-FID analysis to establish the starting ratio of **2**:IS. **nG-PCy$_3$** (52.0 µL of a stock solution of 10.0 mg **nG-PCy$_3$** in 2.00 mL C_7H_8; 0.4 µmol, 0.1 mol%) was added to the stirred solution. Aliquots were removed periodically, quenched with 100 µl KTp in THF (10 mg/mL), and analyzed by GC-FID.

4.5.8 Procedure for Self-Metathesis of Styrene (Monitored by NMR Analysis).

Solid **H-P5** (11.3 mg, 0.015 mmol) and approximately 2 mg of anthracene were added to a thick-walled J-Young NMR tube with C_6D_6 (0.70 mL). The NMR sample was taken to the spectrometer to acquire the initial ratio of **H-P5**: IS. The NMR sample was then returned to the glovebox, where styrene (294.0 μL, 1 mmol, 1 equiv) was added to give a final Ru concentration of 15 mM. The NMR tube was attached to a mechanical rotator (10 rpm) to effect mixing and ^{1}H NMR analysis was carried out periodically. ^{1}H NMR (C_6D_6, 300 MHz; diagnostic signals only): δ 19.20 (d, J = 4.7 Hz, 1H, [Ru]=C*H*R **H-P5**), 8.16 (s, 2H, ArC*H* of anthracene) 7.00 (s, 2H, =C*H*Ph of stilbene) 4.15 (m, 1H, ^{i}Pr C*H* of 2-isopropoxystyrene). See Scheme 4.6. For starting and ending spectra, see Appendix B, Figure B-29.

4.6 References

(1) Grela, K., *Olefin Metathesis-Theory and Practice*. Wiley: Hoboken, NJ, 2014.

(2) Grubbs, R. H.; Wenzel, A. G., *Handbook of Metathesis*. 2nd ed.; Wiley-VCH: Weinheim, 2015.

(3) Schwab, P.; Grubbs, R. H.; Ziller, J. W., Synthesis and Applications of $RuCl_2(=CHR')(PR_3)_2$: The Influence of the Alkylidene Moiety on Metathesis Activity. *J. Am. Chem. Soc.* **1996**, *118*, 100–110.

(4) Weskamp, T.; Kohl, F. J.; Hieringer, W.; Gleich, D.; Herrmann, W. A., Highly Active Ruthenium Catalysts for Olefin Metathesis: The Synergy of N-Heterocyclic Carbenes and Coordinatively Labile Ligands. *Angew. Chem., Int. Ed.* **1999**, *38*, 2416–2419.

(5) Scholl, M.; Trnka, T. M.; Morgan, J. P.; Grubbs, R. H., Increased Ring Closing Metathesis Activity of Ruthenium-Based Olefin Metathesis Catalysts Coordinated with Imidazolin-2-Ylidene Ligands. *Tetrahedron Lett.* **1999**, *40*, 2247–2250.

(6) Huang, J.; Stevens, E. D.; Nolan, S. P.; Petersen, J. L., Olefin Metathesis-Active Ruthenium Complexes Bearing a Nucleophilic Carbene Ligand. *J. Am. Chem. Soc.* **1999**, *121*, 2674–2678.

(7) Scholl, M.; Ding, S.; Lee, C. W.; Grubbs, R. H., Synthesis and Activity of a New Generation of Ruthenium-Based Olefin Metathesis Catalysts Coordinated with 1,3-Dimesityl-4,5-dihydroimidazol-2-ylidene Ligands. *Org. Lett.* **1999**, *1*, 953–956.

(8) Kingsbury, J. S.; Harrity, J. P. A.; Bonitatebus, P. J.; Hoveyda, A. H., A Recyclable Ru-Based Metathesis Catalyst. *J. Am. Chem. Soc.* **1999**, *121*, 791–799.

(9) Vougioukalakis, G. C.; Grubbs, R. H., Ruthenium-Based Heterocyclic Carbene-Coordinated Olefin Metathesis Catalysts. *Chem. Rev.* **2010**, *110*, 1746–1787.

(10) Michrowska, A.; Bujok, R.; Harutyunyan, S.; Sashuk, V.; Dolgonos, G.; Grela, K., Nitro-Substituted Hoveyda-Grubbs Ruthenium Carbenes: Enhancement of Catalyst Activity through Electronic Activation. *J. Am. Chem. Soc.* **2004**, *126*, 9318–9325.

(11) Marx, V. M.; Sullivan, A. H.; Melaimi, M.; Virgil, S. C.; Keitz, B. K.; Weinberger, D. S.; Bertrand, G.; Grubbs, R. H., Cyclic Alkyl Amino Carbene (CAAC) Ruthenium Complexes as Remarkably Active Catalysts for Ethenolysis. *Angew. Chem., Int. Ed.* **2015**, *54*, 1919–1923.

(12) Nascimento, D. L.; Gawin, A.; Gawin, R.; Guńka, P. A.; Zachara, J.; Skowerski, K.; Fogg, D. E., A Highly Reactive Ruthenium-Indenylidene Catalyst for Olefin Metathesis. *J. Am. Chem. Soc.* **2019**, *141*, 10626–10631.

(13) Dorta, R.; Stevens, E. D.; Scott, N. M.; Costabile, C.; Cavallo, L.; Hoff, C. D.; Nolan, S. P., Steric and Electronic Properties of N-Heterocyclic Carbenes (NHC): A Detailed Study on Their Interaction with Ni(CO)4. *J. Am. Chem. Soc.* **2005**, *127*, 2485–2495.

(14) Chen, L.; Ren, P.; Carrow, B. P., Tri(1-adamantyl)phosphine: Expanding the Boundary of Electron-Releasing Character Available to Organophosphorus Compounds. *J. Am. Chem. Soc.* **2016**, *138*, 6392−6395.

(15) Scherpf, T.; Schwarz, C.; Scharf, L. T.; Zur, J.-A.; Helbig, A.; Gessner, V. H., Ylide-Functionalized Phosphines: Strong Donor Ligands for Homogeneous Catalysis. *Angew. Chem., Int. Ed.* **2018**, *57*, 12859–12864.

(16) Weber, P.; Scherpf, T.; Rodstein, I.; Lichte, D.; Scharf, L. T.; Gooßen, L. J.; Gessner, V. H., A Highly Active Ylide-Functionalized Phosphine for Palladium-Catalyzed Aminations of Aryl Chlorides. *Angew. Chem., Int. Ed.* **2019**, *58*, 3203–3207.

(17) Ullrich, S.; Kovačević, B.; Xie, X.; Sundermeyer, J., Phosphazenyl Phosphines: The Most Electron-Rich Uncharged Phosphorus Brønsted and Lewis Bases. *Angew. Chem., Int. Ed.* **2019**, *58*, 10335–10339.

(18) Krawczyk, H.; Dzięgielewski, M.; Deredas, D.; Albrecht, A.; Albrecht, Ł., Chiral Iminophosphoranes—An Emerging Class of Superbase Organocatalysts. *Chem. - Eur. J.* **2015**, *21*, 10268–10277.

(19) Zhang, D.; Boopathi, S. K.; Hadjichristidis, N.; Gnanou, Y.; Feng, X., Metal-Free Alternating Copolymerization of CO2 with Epoxides: Fulfilling "Green" Synthesis and Activity. *J. Am. Chem. Soc.* **2016**, *138*, 11117–11120.

(20) Schwesinger, R.; Schlemper, H., Peralkylated Polyaminophosphazenes— Extremely Strong, Neutral Nitrogen Bases. *Angew. Chem., Int. Ed.* **1987**, *26*, 1167–1169.

(21) Wuensche, M. A.; Mehlmann, P.; Witteler, T.; Buss, F.; Rathmann, P.; Dielmann, F., Imidazolin-2-ylidenaminophosphines as Highly Electron-Rich Ligands for Transition-Metal Catalysts. *Angew. Chem., Int. Ed.* **2015**, *54*, 11857–11860.

(22) Mehlmann, P.; Witteler, T.; Wilm, L. F. B.; Dielmann, F., Isolation, Characterization and Reactivity of Three-Coordinate Phosphorus Dications Isoelectronic to Alanes and Silylium Cations. *Nat. Chem.* **2019**, *11*, 1139–1143.

(23) Witteler, T.; Darmandeh, H.; Mehlmann, P.; Dielmann, F., Dialkyl(1,3-diarylimidazolin-2-ylidenamino)phosphines: Strongly Electron-Donating, Buchwald-Type Phosphines. *Organometallics* **2018**, *37*, 3064–3072.

(24) Rotering, P.; Wilm, L. F. B.; Werra, J. A.; Dielmann, F., Pyridinylidenaminophosphines: Facile Access to Highly Electron-Rich Phosphines. *Chem – Eur. J.* **2020**, *26*, 406–411.

(25) Roterig, P. Synthesis and Characterization of Pyridinylylideaminophosphines. M.Sc. Thesis, University of Munster, Munster, 2019.

(26) Sundberg, R. J.; Yamazaki, T., Rearrangements and Ring Expansions During the Deoxygenation of Beta., Beta.-Disubstituted o-nitrostyrenes. *J. Org. Chem.* **1967**, *32*, 290–294.

(27) Sundberg, R. J., Deoxygenation of Nitro Groups by Trivalent Phosphorus. Indoles from o-Nitrostyrenes. *J. Org. Chem.* **1965**, *30*, 3604–3610.

(28) Cadogan, J. I. G., Reduction of Nitro- and Nitroso-Compounds by Tervalent Phosphorus Reagents. *Q. Rev., Chem. Soc.* **1968**, *22*, 222–251.

(29) Nucleophilic attack of PCy_3 on methylidene ligands in complexes $RuCl_2(L)(PCy_3)(=CH_2)$ has been crystallographically confirmed. See: (a) Lummiss, J. A. M.; McClennan, W. L.; McDonald, R.; Fogg, D. E., The First Ru(PCP) Complexes of the Electron-Rich Pincer Ligand 1,3-Bis((dicyclohexylphosphino)methyl)benzene: Structure and Mechanism in Transfer Hydrogenation Catalysis. *Organometallics* **2014**, *33*, 6738–6741. This pathway can culminate in abstraction of the methylidene moiety as $[MePCy_3]Cl$. See: (b) Hong, S. H.; Wenzel, A. G.; Salguero, T. T.; Day, M. W.; Grubbs, R. H., Decomposition of Ruthenium Olefin Metathesis Catalysts. *J. Am. Chem. Soc.* **2007**, *129*, 7961–7968. For evidence of this pathway in catalysis, see: (c) Lummiss, J. A. M.; Ireland, B. J.; Sommers, J. M.; Fogg, D. E., Amine-Mediated Degradation in Olefin Metathesis Reactions that Employ the Second-Generation Grubbs Catalysts *ChemCatChem* **2014**, *6*, 459–463. While nucleophilic attack of PCy_3 on Ru-alkylidene species is rare, Diver has demonstrated such a pathway where CO binding rendered the alkylidene carbon more electrophilic. See: Galan, B. R.; Pitak, M.; Keister, J. B.; Diver, S. T., Isocyanide-Promoted Ylidene Transfer to Phosphorus: Rearrangement in the First-Generation Grubbs Complex. *Organometallics* **2008**, *27*, 3630–3632. Attack by the highly electron-rich **P5** in the present case thus seems plausible.

(30) Hong, S. H.; Chlenov, A.; Day, M. W.; Grubbs, R. H., Double C-H Activation of an N-Heterocyclic Carbene Ligand in a Ruthenium Olefin Metathesis Catalyst. *Angew. Chem., Int. Ed.* **2007**, *46*, 5148–5151.

(31) Mathew, J.; Koga, N.; Suresh, C. H., C-H Bond Activation through s-Bond Metathesis and Agostic Interactions: Deactivation Pathway of a Grubbs Second-Generation Catalyst. *Organometallics* **2008**, *27*, 4666–4670.

(32) Snelgrove, J. L.; Conrad, J. C.; Yap, G. P. A.; Fogg, D. E., The kinetic instability of s-bound aryloxide in coordinatively unsaturated or labile complexes of ruthenium. *Inorg. Chim. Acta* **2003**, *345*, 268–278.

(33) Ireland, B. J.; McDonald, R.; Fogg, D. E., Controlling the Coordination Mode of the Arylamide Ligand. *Organometallics* **2013**, *32*, 4723–4725.

(34) Bates, J. M.; Lummiss, J. A. M.; Bailey, G. A.; Fogg, D. E., Operation of the Boomerang Mechanism in Olefin Metathesis Reactions Promoted by the Second-Generation Hoveyda Catalyst. *ACS Catal.* **2014**, *4*, 2387−2394.

(35) Goudreault, A. Y.; Walden, D. M.; Nascimento, D. L.; Botti, A. G.; Steinmann, S. N.; Michel, C.; Fogg, D. E., Hydroxide-Induced Degradation of Olefin Metathesis Catalysts: A Challenge for Metathesis in Alkaline Media. *ACS Catal.* **2020**, *10*, 3838−3843.

(36) Romero, P. E.; Piers, W. E., Mechanistic Studies on 14-Electron Ruthenacyclobutanes: Degenerate Exchange with Free Ethylene. *J. Am. Chem. Soc.* **2007**, *129*, 1698–1704.

(37) Nizovtsev, A. V.; Afanasiev, V. V.; Shutko, E. V.; Bespalova, N. B., Metathesis Catalysts Stability and Decomposition Pathway. *NATO Sci. Ser. II* **2007**, *243*, 125–135.

(38) Bailey, G. A.; Foscato, M.; Higman, C. S.; Day, C. S.; Jensen, V. R.; Fogg, D. E., Bimolecular Coupling as a Vector for Decomposition of Fast-Initiating Olefin Metathesis Catalysts. *J. Am. Chem. Soc.* **2018**, *140*, 6931–6944.

(39) Bailey, G. A.; Lummiss, J. A. M.; Foscato, M.; Occhipinti, G.; McDonald, R.; Jensen, V. R.; Fogg, D. E., Decomposition of Olefin Metathesis Catalysts by Brønsted Base: Metallacyclobutane Deprotonation as a Primary Deactivating Event. *J. Am. Chem. Soc.* **2017**, *139*, 16446–16449.

(40) Ireland, B. J.; Dobigny, B. T.; Fogg, D. E., Decomposition of a Phosphine-Free Metathesis Catalyst by Amines and Other Nitrogen Bases: Metallacyclobutane Deprotonation as a Major Deactivation Pathway. *ACS Catal.* **2015**, *5*, 4690−4698.

(41) Blacquiere, J. M.; Jurca, T.; Weiss, J.; Fogg, D. E., Time as a Dimension in High-Throughput Homogeneous Catalysis. *Adv. Synth. Catal.* **2008**, *350*, 2849–2855.

(42) Shriver, D. F.; Drezdzon, M. A., *The Manipulation of Air-Sensitive Compounds*. 2nd Ed. ed.; John Wiley & Sons: New York, 1986.

5 Conclusions and Future Work

The research presented in this thesis was aimed at increasing insight into ruthenium-catalyzed olefin metathesis by examining a specific, widely ignored catalyst decomposition pathway, and by exploring two different strategies to overcome catalyst decomposition. First, the impact of oxygen on the activity of leading and emerging, breakthrough metathesis catalysts was examined. Those findings overturn suggestions that ruthenium metathesis catalysts are oxygen-tolerant. All catalysts screened were sensitive to oxygen to varying degrees. Importantly, however, fast-initiating cyclic alkyl amino carbene (CAAC) catalysts proved more robust than their N-heterocyclic carbene (NHC) counterparts. To dissect out the impact of catalyst activity from that of catalyst robustness, the *relative* decrease in activity was assessed, by evaluating for each catalyst the percentage of activity retained under an atmosphere of oxygen, relative to that under inert atmosphere. The high performance of the CAAC catalysts emerges as due in part to their resistance to decomposition. This finding underscores their potential as robust, highly active catalysts, a point of compelling interest given the widespread belief that higher catalyst sensitivity is invariably a trade-off against high catalyst activity. A general screen of robustness in the presence of other common contaminants would be of value in confirming the utility of this promising catalyst family in metathesis processes. Research on this point is currently being carried out by Daniel do Nascimento and Christian Blanco of the Fogg group, with a focus on common contaminants in technical-grade solvents, in process chemistry, and in chemical biology.

The second part of this chapter probed the mechanism by which molecular oxygen limits metathesis yields. The **GII** platform was chosen for study, on the assumption that oxidation of the PCy_3 ligand released from the precatalyst would generate the active species common to all of these Ru metathesis catalysts (i.e. $RuCl_2(L)(=CHAr)$), while slowing the rate of decomposition to a convenient timescale. The observation of benzaldehyde in this reaction pointed toward oxidation of the alkylidene ligand via a [2+2] cycloaddition reaction similar to that in the metathesis reaction itself. This pathway accounts for 30% of decomposed **GII**. A second major pathway, which accounts for 55% of the starting **GII**, is bimolecular coupling (BMC) of two $RuCl_2(H_2IMes)(=CHPh)$ fragments, with loss of stilbene. This is important in indicating the rapidity with which BMC can occur once the stabilizing ligand is removed, at least at the 20 mM

catalyst concentrations explored. A final, minor decomposition reaction is that originally proposed, in which a Ru-Ph complex is generated following attack of O_2 at the benzylidene ligand. A point of particular interest for future work is the capacity of the decomposed ruthenium products to either induce further decomposition, or to catalyze non-metathesis reactions. This question is of substantial interest in determining whether the Ru decomposition products generated under oxidative conditions are as deleterious as those produced under inert atmosphere.

An additional avenue suggested for future work is investigation of other oxidizing agents in metathesis. A fundamental challenge for the catalytic transformation of renewable chemicals is the oxidizing environment from which these chemicals are derived. Common contaminants in such feedstocks include peroxides derived from auto-oxidation of long-chain fatty acids. A study related to that in Chapter 2, examining the impact of oxidized species on metathesis (and, more specifically, their reactivity toward the catalysts) could aid in the long-desired application of olefin metathesis to "the biorefinery": that is, transformation of biomass into value-added chemicals. Means of countering the impact of peroxides are also of considerable interest. These may potentially include identification of a radical trap that does not interfere with metathesis reactions. Of note, butylated hydroxytoluene (BHT), which offers such a radical trap, proved highly efficacious in early, unpublished work by Jay Conrad of this research group.

The rest of the thesis shifted focus from examining the impact of impurities, to strategies for their mitigation. Chapter 3 considers whether decomposition can be prevented by isolating the metathesis catalysts within a dynamic cage structure; specifically, a resorcinarene capsule that self-assembles around the catalyst in water-saturated toluene. Successful encapsulation of two cationic metathesis catalysts was established, and the catalytic activity of these assemblies was assessed relative to a control reaction with the non-encapsulated parent catalyst **HII**. A key question in these studies was the impact of the water required for capsule self-assembly on catalyst productivity, relative to **HII** in the bulk "wet" toluene. The encapsulated catalysts showed sustained activity relative to **HII**, and RCM productivity was nearly doubled for the best-performing caged catalyst. UV-vis analysis confirmed that the increase in activity is a result of reduced catalyst decomposition. Isolating the catalyst within the hydrophobic environment of the resorcinarene capsule prevented not only bimolecular decomposition, but decomposition by water. In addition,

the dynamic nature of the capsule appears to overcome the problem of rate inhibition common for catalysts immobilized in rigid pore structures, such as zeolites, metal-organic frameworks (MOFs), etc.

Identifying a strategy to overcome bimolecular decomposition is significant, given the susceptibility to this pathway exhibited by both NHC catalysts, and even more so by the important CAAC catalysts. A further avenue for future work would thus be encapsulation of a cationic CAAC catalyst, which could eliminate both intrinsic pathways for catalyst decomposition (that is, β-hydride elimination and bimolecular coupling), while simultaneously protecting the catalyst against exogenous agents.

Chapter 4 focuses on an alternative, more classical strategy: identifying potentially more robust catalysts via ligand design. Research directed at the design of highly electron-rich tertiary phosphines has expanded enormously in the last decade, and many promising new candidate ligands are thus available for incorporation into ruthenium metathesis catalysts. The specific focus was on one such ligand family, pyridinylide aminophosphines (PyAP) with the generic structure $R_2P–N=Ar$. Incorporation of PyAP within the Hoveyda-class catalyst $RuCl_2(L)(=CHC_6H_4$-*o*-$O^iPr)$, or its faster-initiating *p*-nitro Grela-class analogue, was pursued.

Exploration of synthetic routes to 2-PyAP derivatives highlighted several incompatibilities between this ligand class and structural elements present in the catalysts. First, the most basic phosphine examined was oxidized by the nitro substituent on Grela platform **nG**. This restricts the scope of the phosphines that can be incorporated, as the most highly electron-rich phosphines are also most strongly basic. Secondly, *o*-metalation of the N=Ar substituent is facile in PyAP ligands that lack *o*-aryl substituents. This triggers decomposition of the precatalyst even at room temperature. Finally, and most problematic, the N-donor in the P–N=Ar unit – that is, the unit that confers high electron density on the phosphine – appears to participate in nucleophilic attack on the [Ru]=CHR functionality that is key to metathesis activity. In consequence, despite the heightened PyAP donicity, the metathesis activity of even the highest-performing PyAP derivatives was far inferior to that of their NHC analogues.

A clear avenue for future work lies in ligand redesign to prevent these decomposition pathways. While *o*-substitution of the electron-rich pyridinyl substituents would prevent cyclometallation, the most fundamental challenge is almost certainly nucleophilic attack by the P–N=Ar nitrogen. This hypothesis should be confirmed by quantifying the suspected ammonium-phosphine by-product. By analogy to established decomposition pathways, this may be [R_2PN=(C_5H_4-1-NEt-6-Me)(CH_2Ar)]Cl (Ar = C_6H_3-2-O^{i}Pr-5-NO_2), assuming attack by nitrogen on the alkylidene ligand. Replacing the chloride ligands with bulkier pseudohalides (a theme pioneered in early work by Jay Conrad of the Fogg group) may aid the PyAP systems by blocking both nucleophilic abstraction and *o*-metalation. Finally, a more drastic redesign strategy would abandon π-donor-substituted phosphines, instead turning to ligands in which inductive effects generate a highly electron-rich phosphine. A potential candidate includes tri-methylpyrrolidine phosphine, which was recently developed by the Dielmann group. Preliminary work on the synthesis and screening of **Ru-27**, carried out in collaboration with Janina Werra of the Dielmann group, indicated that **Ru-27** is considerably more active and less prone to decomposition than the Ru-PyAP catalysts.

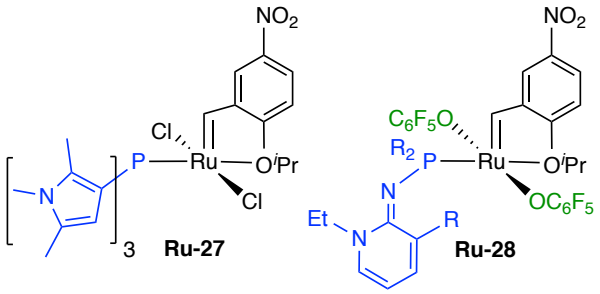

Figure 5.1 Potential second-generation PyAP ligands for metathesis catalysis.

APPENDICES

In each of Appendices A-F, data are presented in the order of discussion in the body of the thesis.

A. Tabulated Data for Figures, Histograms, etc.

Table A-1 Data for Control Reactions at Catalyst Loadings that Reveal the Impact of O_2.[a]

Substrate	Catalyst	Loading (mol%)	Yield			Average Yield
			Trial A (N_2; vial)	Trial B (N_2; vial)	Trial C (Ar; Schlenk)	
1	**GII**	0.01	15	14	11	13±2
1	**HII**	0.01	37	42	43	41±4
1	**nG**	0.01	50	51	56	52±4
1	**UC**	0.01	45	48	52	48±3
1	**nG^C**	0.01	66	72	69	69±3
1	**Ru2^C**	0.01	93	91 (Ar; Schlenk)	92	92±1
2	**nG^C**	0.001	71	69	73	71±2
2	**Ru2^C**	0.001	71	68	74	71±3
2	**GII**	0.0025	20	17	20	19±2
2	**HII**	0.0025	77	78	78	78±1
2	**nG**	0.0025	91	96	95	94±3
2	**UC**	0.0025	91	90	87	89±2
2	**M2**	0.25	58	–	55	57±2
2	**HC**	5	19	–	21	20±1

[a]See Fig. 2.1 in Chapter 2.

Table A-2 RCM and mRCM Data at Catalyst Loadings that Reveal the Impact of O_2.[a]

Substrate	Catalyst	Loading (mol%)	Yield			Average Yield
			Trial A (8% O_2 in Ar; Schlenk)	Trial B (8% O_2 in Ar; Schlenk)	Trial C (8% O_2 in Ar; Schlenk)	
1	**GII**	0.01	6	5	8	6±1
1	**HII**	0.01	20	22	20	21±1
1	**nG**	0.01	23	18	19	21±3
1	**UC**	0.01	5	6	6	6±1
1	**nG^C**	0.01	43	44	41	43±2
1	**Ru2^C**	0.01	73	69	67	70±3
2	**nG^C**	0.001	53	49	49	50±3
2	**Ru2^C**	0.001	54	55	56	55±1
2	**GII**	0.0025	11	10	7	9±2
2	**HII**	0.0025	24	30	28	27±3
2	**nG**	0.0025	52	47	47	49±2
2	**UC**	0.0025	4	1	5	3±2
2	**M2**	0.25	30	–	29	30±1
2	**HC**	5	8	–	10	9±1

[a] See Fig. 2.1 in Chapter 2.

Table A-3 Data for RCM of 2 at Excessive or Insufficient Catalyst Loadings.[a]

Atmosphere	Catalyst	Loading (mol%)	Trial A	Trial B	Average
N_2	**GII**	0.05	63	65	64±1
N_2	**HII**	0.05	100	100	100±0
N_2	**nG**	0.05	100	100	100±0
N_2	**UC**	0.05	100	100	100±0
N_2	**nG^C**	0.05	100	100	100±0
N_2	**Ru2^C**	0.05	100	100	100±0
O_2	**GII**	0.05	45	48	47±2
O_2	**HII**	0.05	96	95	96±1
O_2	**nG**	0.05	100	100	100±0
O_2	**UC**	0.05	29	28	29±1
O_2	**nG^C**	0.05	100	100	100±0
O_2	**Ru2^C**	0.05	100	100	100±0
N_2	**nG^C**	0.0025	100	100	100±0
N_2	**Ru2^C**	0.0025	100	100	100±0
O_2	**nG^C**	0.0025	75	77	77±2
O_2	**Ru2^C**	0.0025	90	83	87±4
N_2	**GII**	0.001	14	13	14±1
N_2	**HII**	0.001	14	14	14±0
N_2	**nG**	0.001	19	21	20±1
N_2	**UC**	0.001	9	9	9±0

[a]See Fig. 2.2 in Chapter 2.

Table A-4 Tabulated Data for Figure 2.2, with Supplementary Values.

Substrate	Catalyst	(mol%)	TON (Control)	% Drop in Yield[a]	% O_2-Resistance[b]
2	**HC**	5.0	4	55	45
2	**M2**	0.25	228	47	53
2	**GII**	0.0025	7600	53	47
2	**HII**	0.0025	31200	65	35
2	**nG**	0.0025	37600	48	52
2	**UC**	0.0025	35600	97	3
2	**nG^C**	0.001	71000	30	70
2	**Ru2^C**	0.001	71000	23	77

[a] % Drop = $\frac{N_2 \text{ Yield} - O_2 \text{ Yield}}{N_2 \text{ Yield}} \times 100$ [b] % O_2-resistance = 100 – (% Drop)

Table A-5 Catalytic Data for Experiments Performed in Air.

Substrate	Atmosphere	Catalyst	Loading (mol%)	Yield Trial A	Yield Trial B	Yield Average
1	Air	**GII**	0.01	0	0	0±0
1	Air	**HII**	0.01	0	0	0±0
1	Air	**nG**	0.01	0	0	0±0
1	Air	**UC**	0.01	0	0	0±0
1	Air	**nGC**	0.01	6	3	5±3
1	Air	**Ru2C**	0.01	4	11	8±4
2	Air	**GII**	0.0025	7	7	7±0
2	Air	**HII**	0.0025	5	5	5±0
2	Air	**nG**	0.0025	8	8	8±0
2	Air	**UC**	0.0025	0	0	0±0
2	Air	**nGC**	0.0025	8	9	9±1
2	Air	**Ru2C**	0.0025	25	22	24±2

Table A-6 Calculated T_1 Relaxation Times for ^{31}P Nuclei of Phosphorus Compounds.[a]

Compound	T1 Relaxation time (s)
dppb	1.5
PCy_3	6
$O{=}PCy_3$	2.2
GII	1.3

[a]T1 relaxation time determined by an inversion recovery pulse sequence, varying d7 time to give a null signal: T1=d7null/ln(2).

Table A-7 Reported TEP Values for Strongly Donating Phosphine and Carbene Ligands.

Ligand	TEP (cm^{-1}) **$Ni(CO)_3L$**	Conditions measured
$P(tBu)_3$[1,2]	2056.1	Solid[b]
PCy_3[1,2]	2056.4	Solid[b]
H2IMes[3]	2052	CH_2Cl_2
PAd_3[3]	2052.1	Solid[b]
$PCy_2(C(PPh_3)Me$[1,2]	2050.1	Solid[b]
DmaP$_3$P[4]	2022.4	Solid
P2[5]	2049.6	Solid
P3[5]	2052.2	CH_2Cl_2
P4[5]	2051.6	Solid
P5[5]	2040.7	CH_2Cl_2
P6[5]	2050.8	CH_2Cl_2
P7[5]	2049.2	CH_2Cl_2

[a]See Chart 4.2. [b]Calculated from linear correlation between ν(CO) of Rh(acac)(CO)(L) and $Ni(CO)_3(L)$ analogues.

B. NMR Spectra

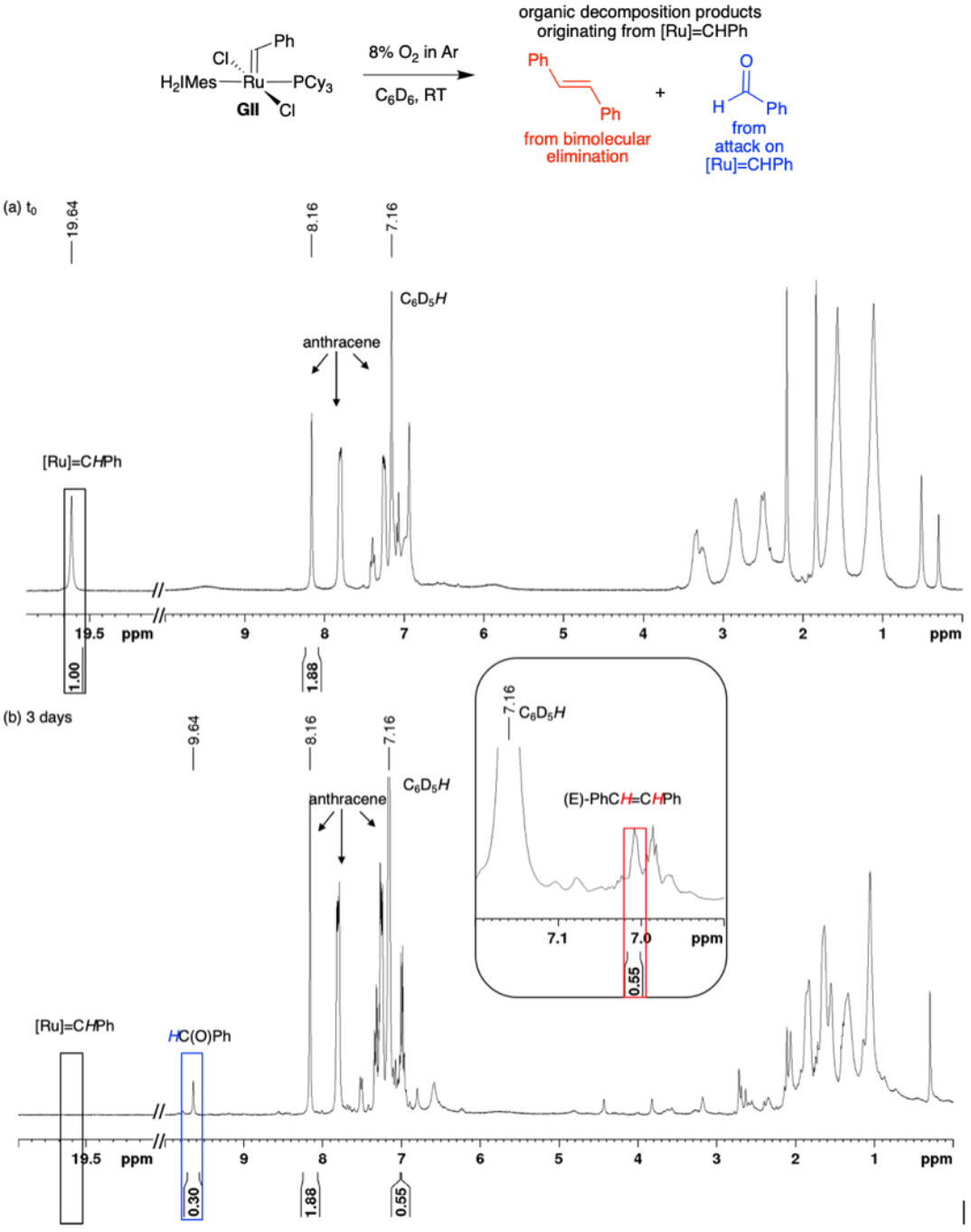

Figure B-1 ^{1}H NMR spectra (300 MHz) showing decomposition of **GII** by O_2 in C_6D_6, with anthracene as internal standard. (a) Initial spectrum, showing **GII**: anthracene integration ratio. (b) After 3 d at RT. Inset: stilbene and dppb CH_2 signals. For the corresponding experiment without dppb, to permit accurate stilbene quantitation, see Figure B-3.

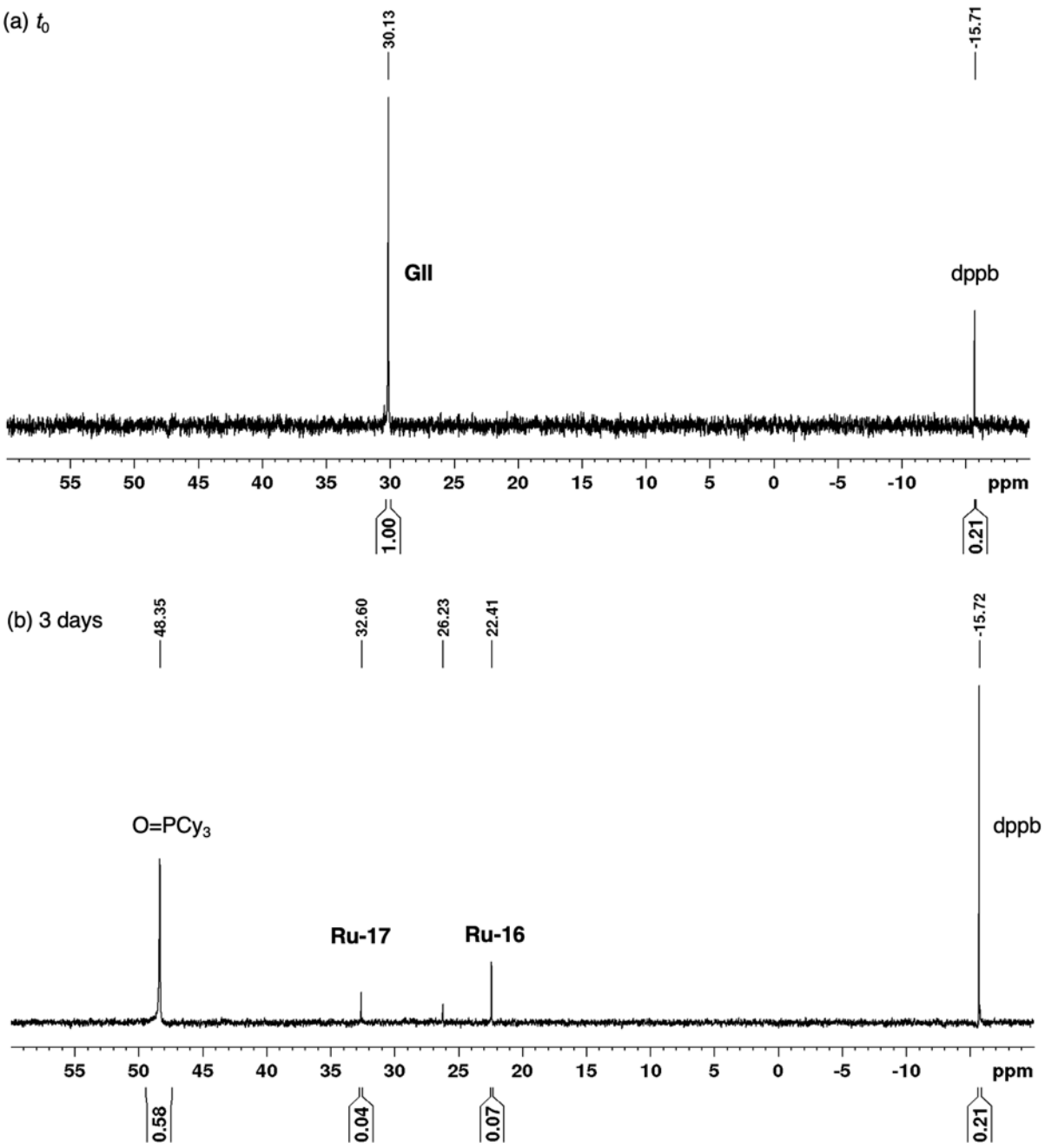

Figure B-2 Representative $^{31}P\{^{1}H\}$ NMR spectra showing decomposition of **GII** with 8% O_2 (C_6D_6, 121 MHz). (a) Initial spectrum, showing **GII**:dppb integration ratio. (b) After 3 days at RT: vertical intensity is increased to show the signals for the minor Ru products **Ru-16** and **Ru-17**.

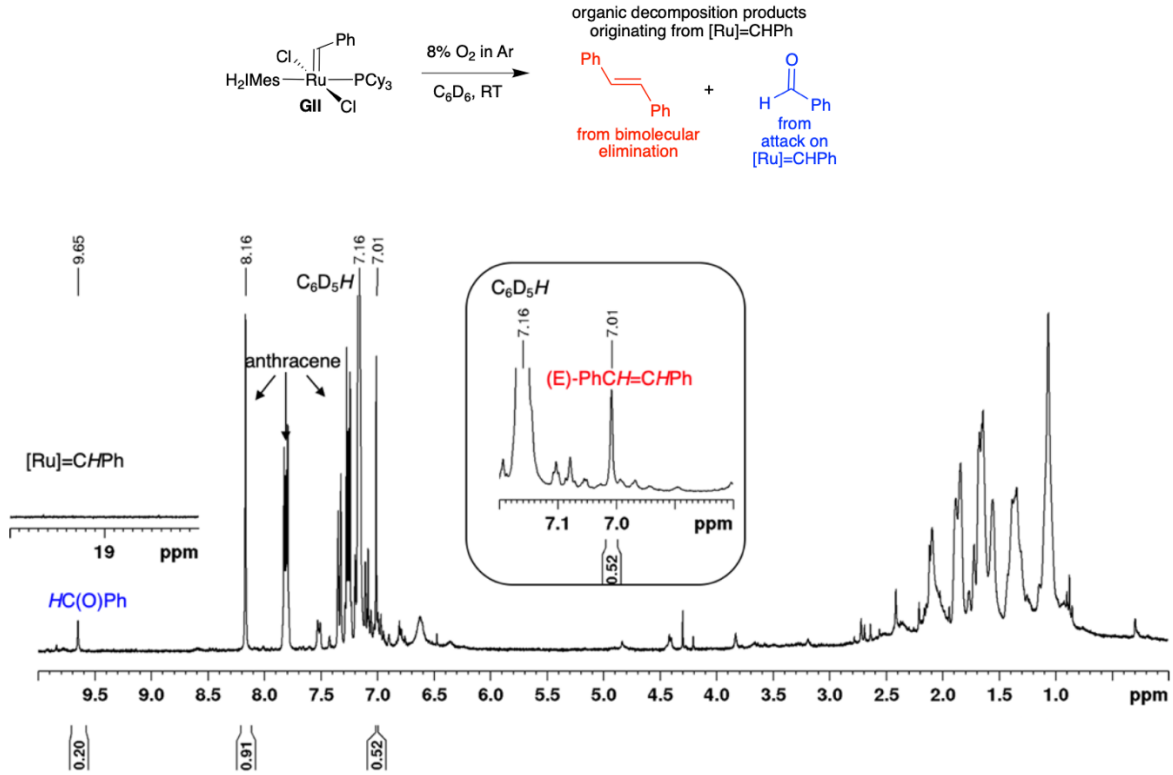

Figure B-3 ^{1}H NMR spectrum showing complete decomposition of **GII** with 8% O_2 (C_6D_6, 300 MHz). Experiment carried out without dppb to enable quantitation of stilbene (cf. Figure B-1, with dppb present).

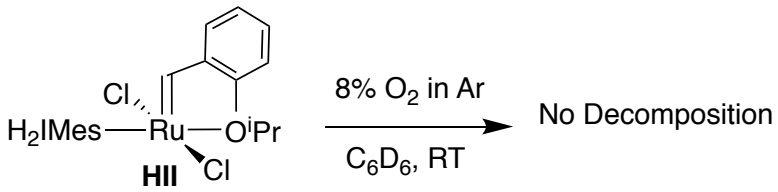

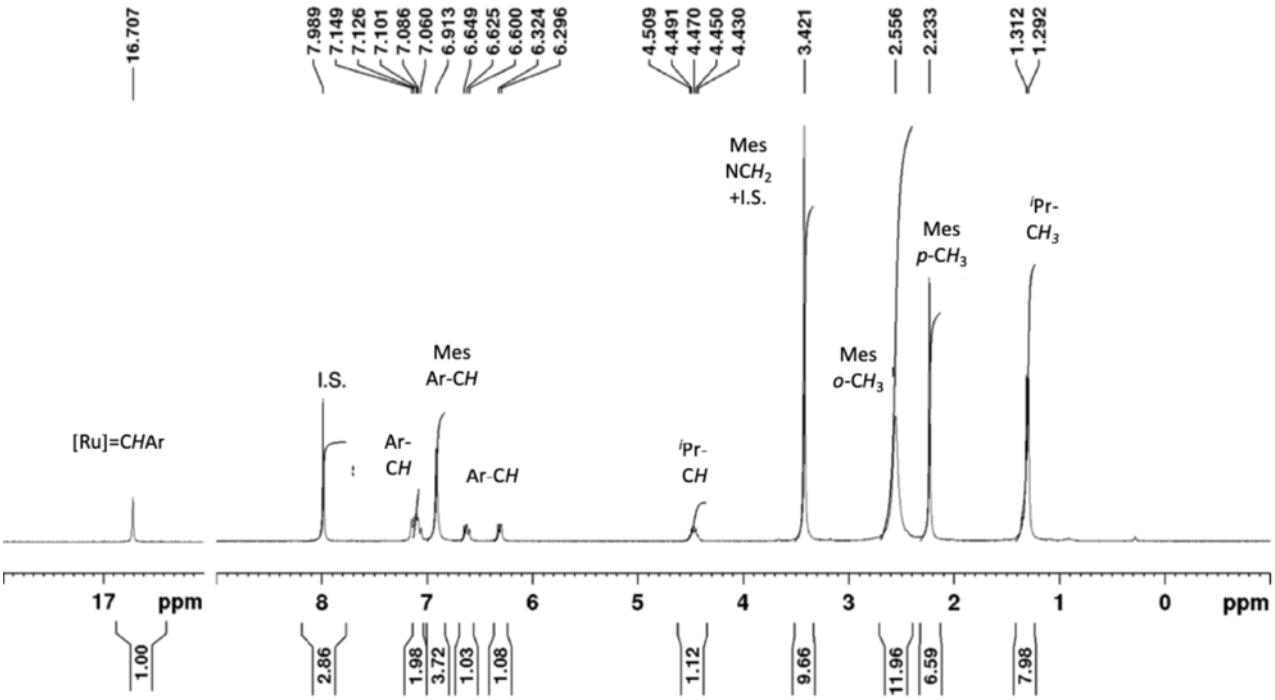

Figure B-4 ^{1}H NMR spectrum (C_6D_6, 300 MHz) showing zero decomposition of **HII** relative to DMT as internal standard (I.S.) on exposure to 8% O_2 for 14 d at RT.

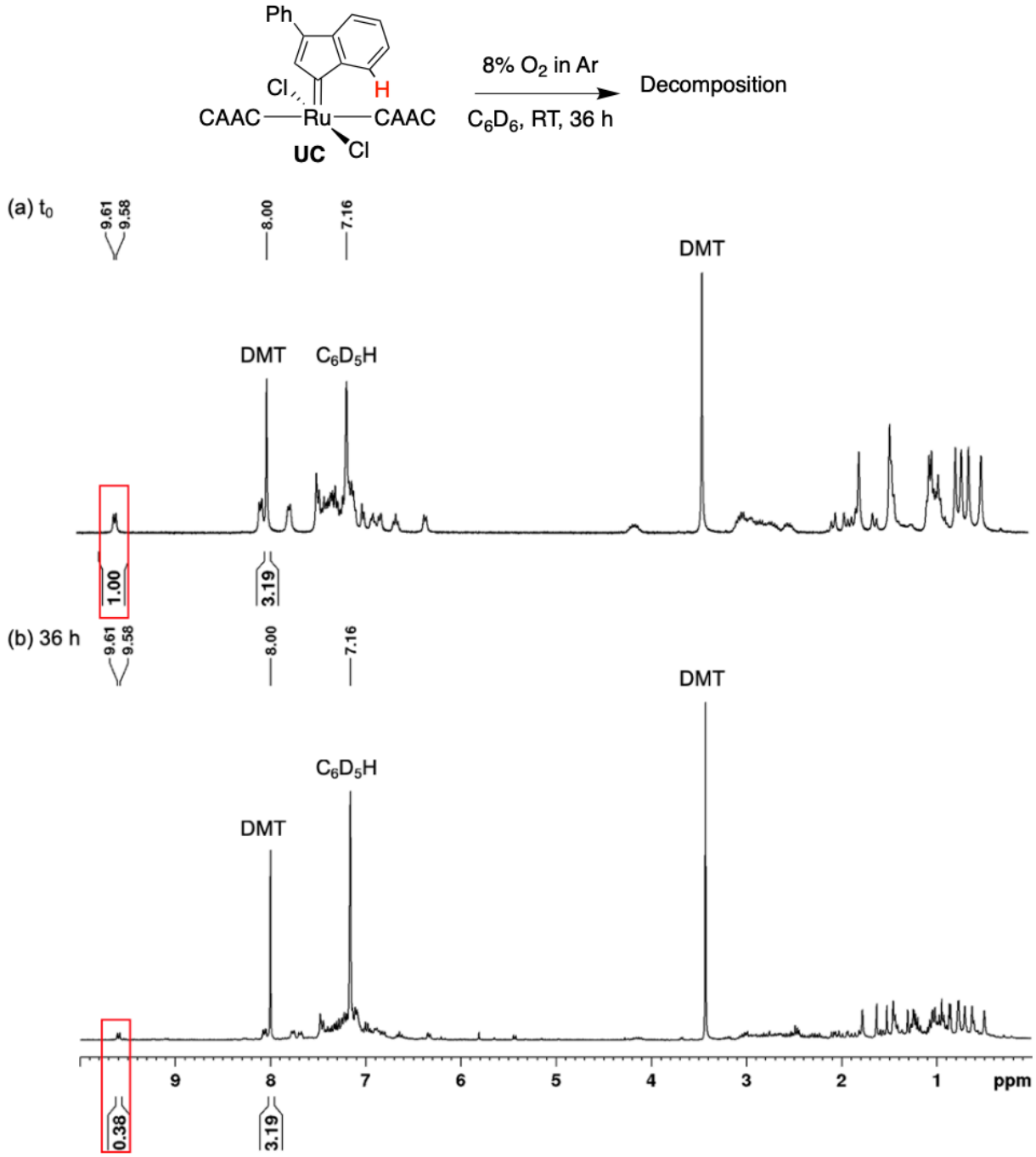

Figure B-5 ^{1}H NMR spectra showing decomposition of **UC** by 8% O_2 relative to DMT as internal standard (C_6D_6, 300 MHz). (a) Initial spectrum, showing **UC**:DMT integration ratio. (b) After 36 h at RT.

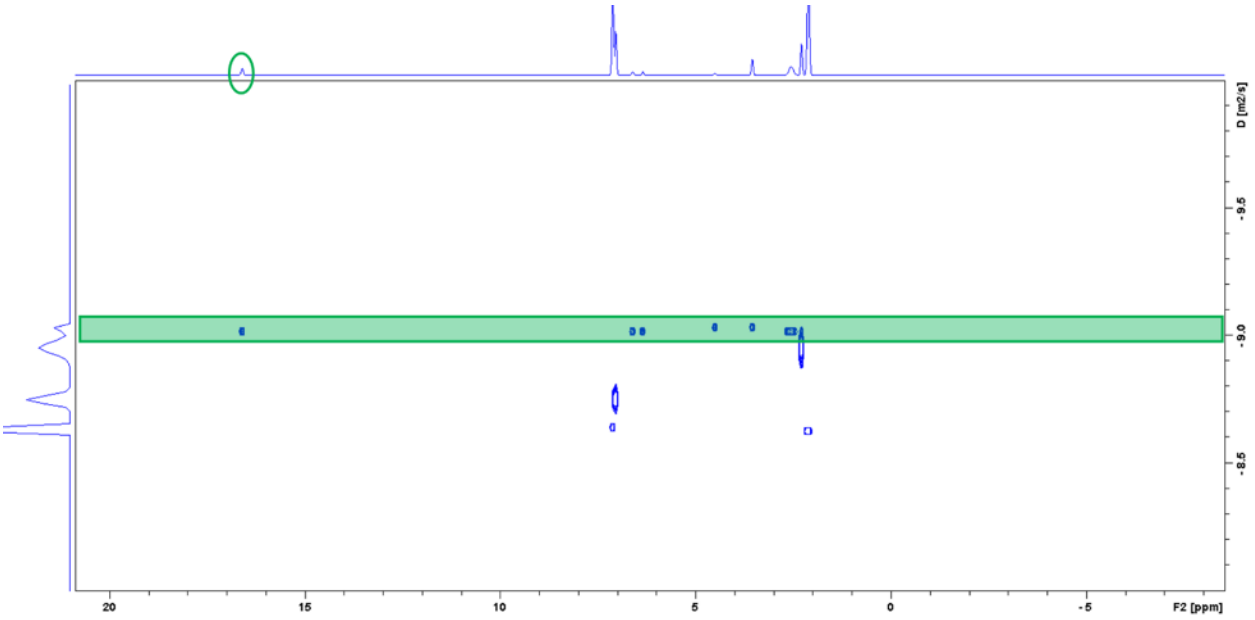

Figure B-6 DOSY-NMR spectrum of **HII** (1.0 mM in $CDCl_3$; 300 MHz), showing its low diffusion constant (log_D= –9.08). Highlighted in green are the signals due to the catalyst, most notably the singlet due to the [Ru]=C*H*Ar proton at 16.6 ppm.

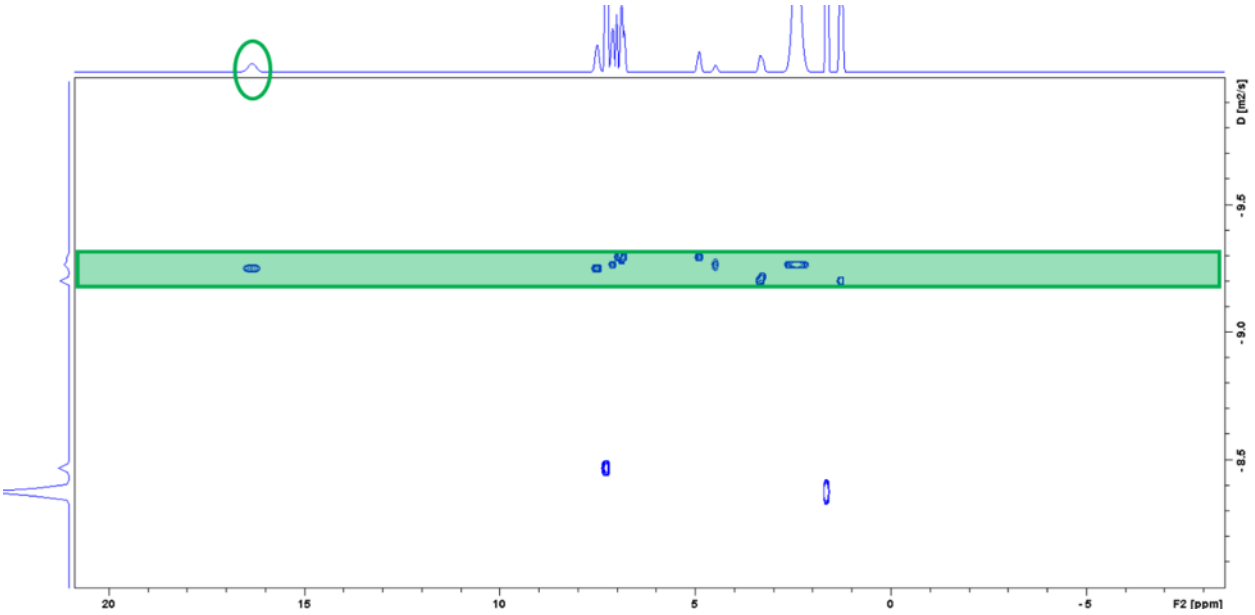

Figure B-7 DOSY-NMR spectrum of **SC** (1.0 mM in $CDCl_3$; 300 MHz), showing its low diffusion constant (log_D= –9.22). Highlighted in green are the signals due to the catalyst, most notably the singlet due to the [Ru]=C*H*Ar proton at 16.5 ppm.

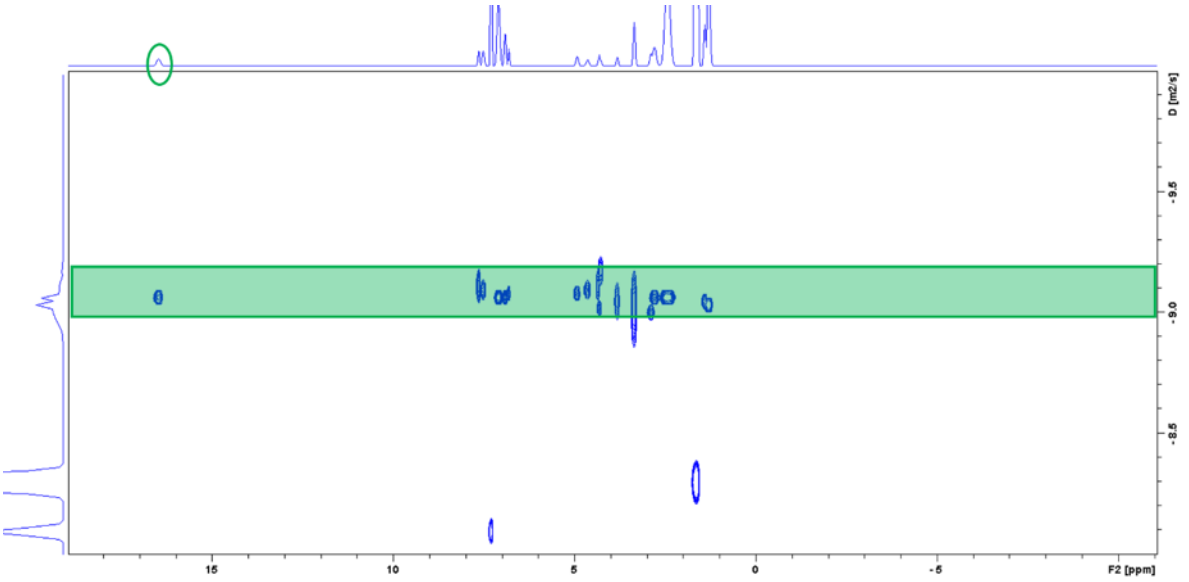

Figure B-8 DOSY-NMR spectrum of **AM** (1.0 mM in $CDCl_3$; 300 MHz) showing its low diffusion constant (log_D= –9.10). Highlighted in green are the signals due to the catalyst, most notably the singlet due to the [Ru]=C*H*Ar proton at 16.9 ppm.

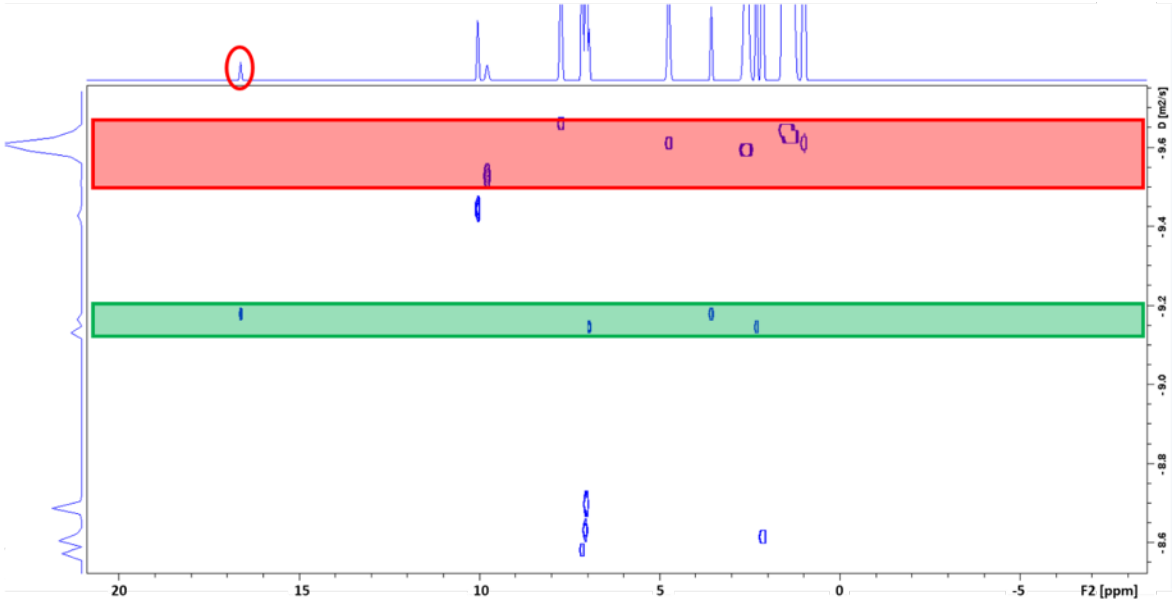

Figure B-9 DOSY-NMR spectrum of **HII** (1.0 mM) and the resorcin[4]arene capsule (monomer concentration 7.5 mM in H_2O-saturated C_7D_8; 300 MHz), showing the difference in diffusion constant for **HII** and the capsule, confirming that **HII** is not encapsulated. Highlighted in green are the signals due to **HII**, including the [Ru]=C*H*Ar singlet at 16.6 ppm (log_D= –9.20). Highlighted in red are the signals for the hexameric capsule (log_D= –9.57).

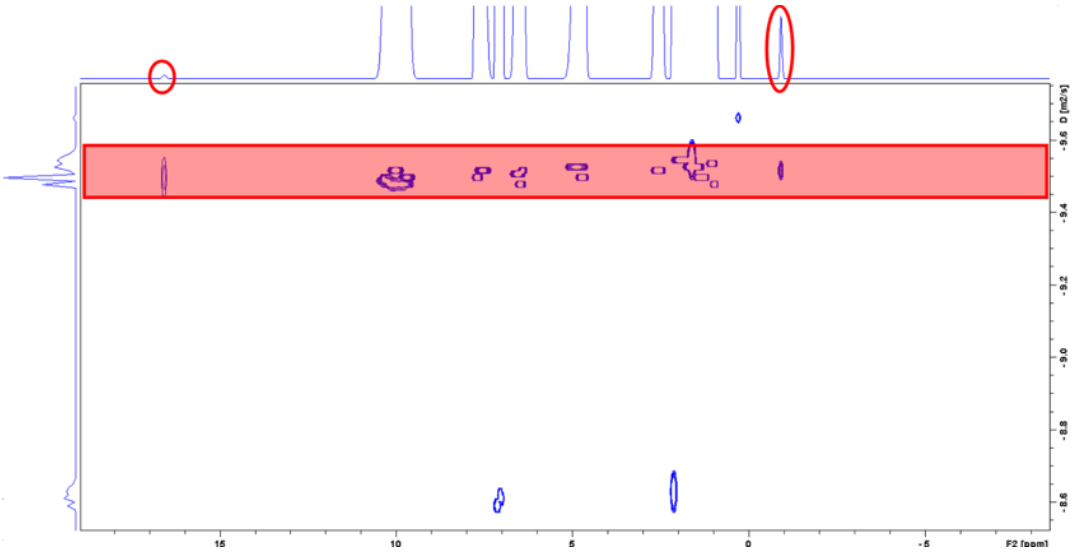

Figure B-10 DOSY-NMR spectrum of **SC** (1.0 mM) and the resorcin[4]arene capsule (monomer concentration 7.5 mM) in H_2O-saturated C_7D_8 (300 MHz), showing the same diffusion constant for **SC** and the hexameric capsule (highlighted in red; $\log_D$= –9.52). Circled are signals for the [Ru]=C*H*Ar proton at 16.5 ppm and the shifted ammonium protons at –0.9 ppm.

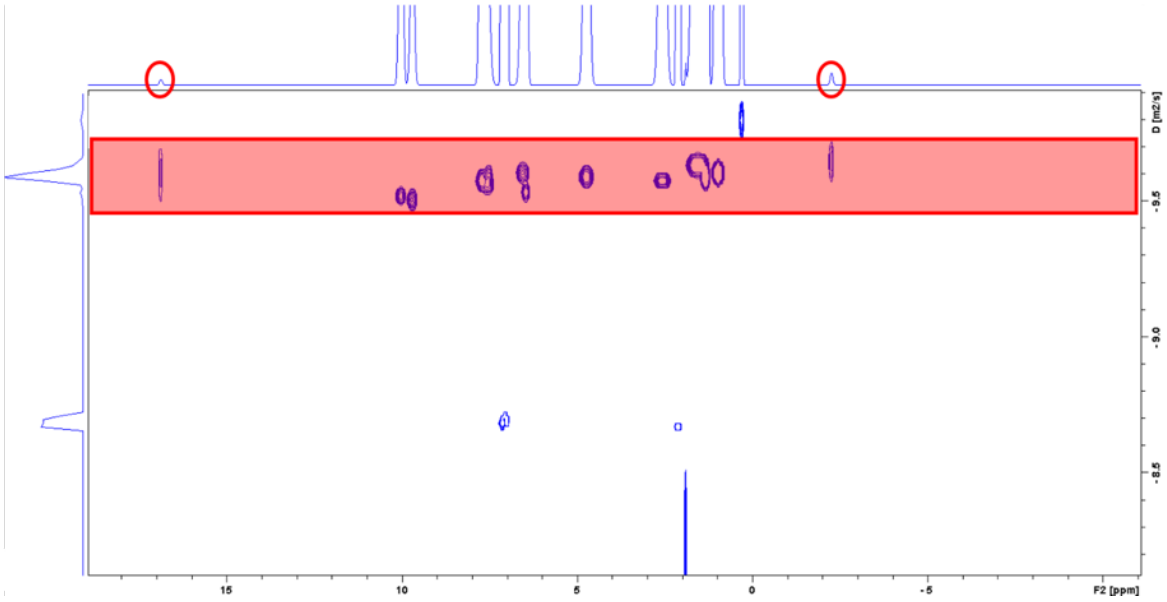

Figure B-11 DOSY-NMR spectrum of **AM** (1.0 mM) and the resorcin[4]arene capsule (monomer concentration 7.5 mM in H_2O-saturated C_7D_8; 300 MHz), showing the same diffusion constant for **AM** and the hexameric capsule (highlighted in red, $\log_D$= –9.60). Circled are singlets for the [Ru]=C*H*Ar proton at 16.9 ppm and the shifted ammonium protons at –2.3 ppm.

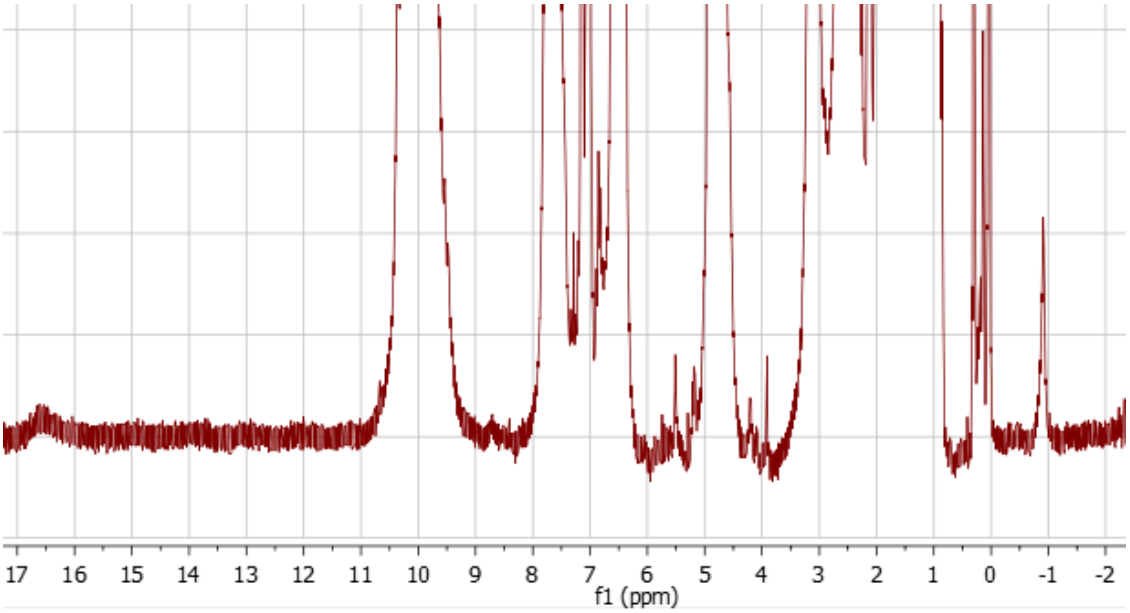

Figure B-12 Representative ^{1}H NMR spectrum (300 MHz, C_7D_8) of **SC** encapsulated in the resorcin[4]arene cage, showing the broadened signal for the [Ru]=C*H*Ar proton at 16.5 ppm, and the methylammonium signal at –0.9 ppm.

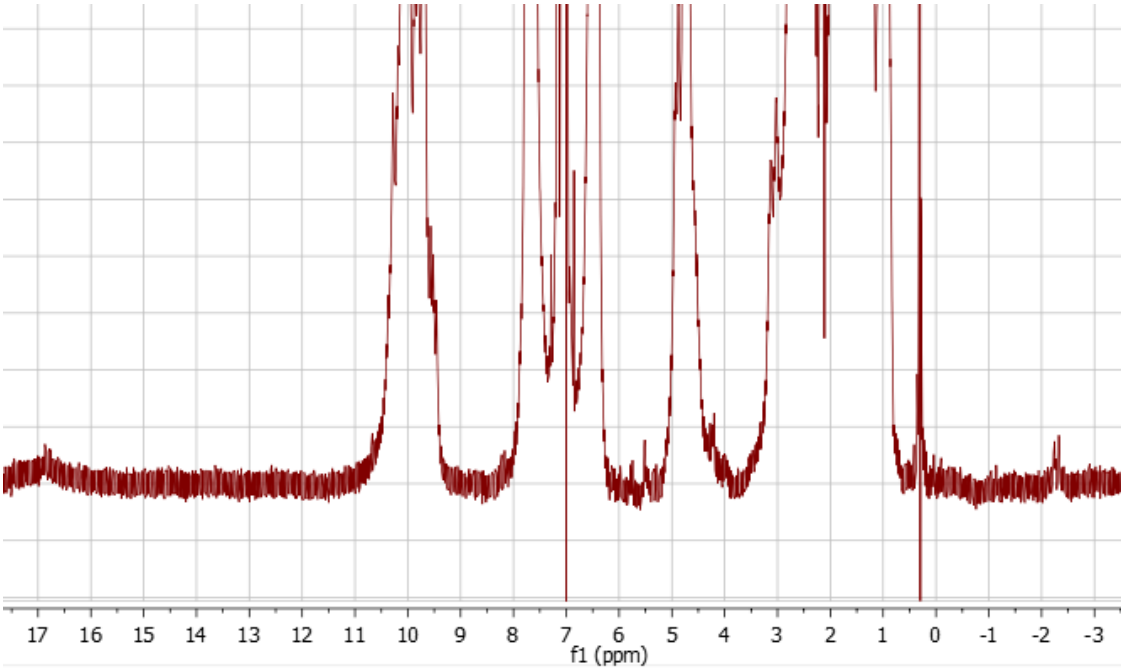

Figure B-13 Representative ^{1}H NMR spectrum (300 MHz, C_7D_8) of **AM** encapsulated in the resorcin[4]arene cage, showing the broadened signal for the [Ru]=C*H*Ar proton at 16.9 ppm, and the ethylammonium signal at –2.3 ppm.

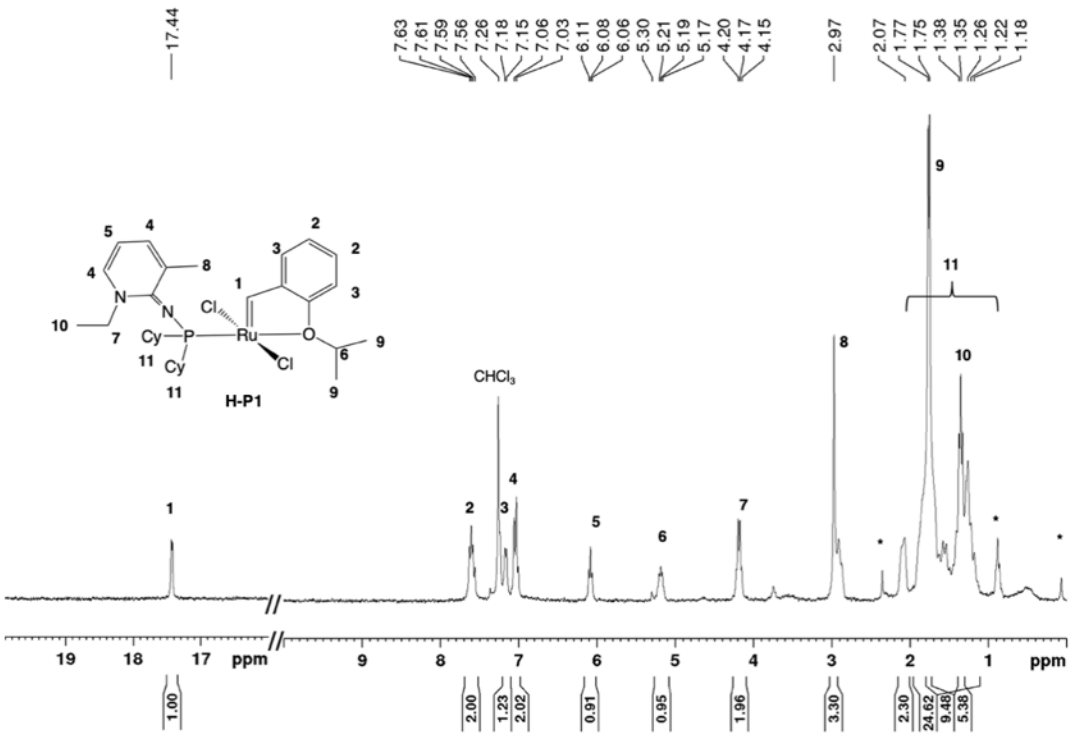

Figure B-14 ^{1}H NMR spectrum ($CDCl_3$, 300 MHz) of $RuCl_2(PCy_2(N{=}C_5H_3\text{-}1\text{-}NEt\text{-}6\text{-}Me)(=CHC_6H_4\text{-}2\text{-}O^{i}Pr)$, **H-P1**.

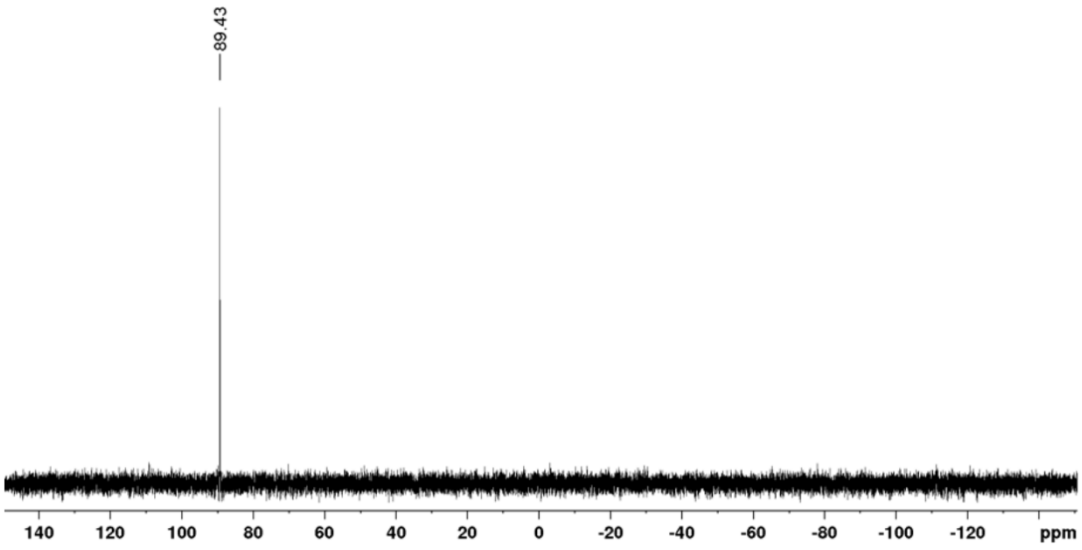

Figure B-15 $^{31}P\{^{1}H\}$ NMR spectrum (C_6D_6, 121 MHz) of $RuCl_2(PCy_2(N{=}C_5H_3\text{-}1\text{-}NEt\text{-}6\text{-}Me))(=CHC_6H_4\text{-}2\text{-}O^{i}Pr)$, **H-P1**.

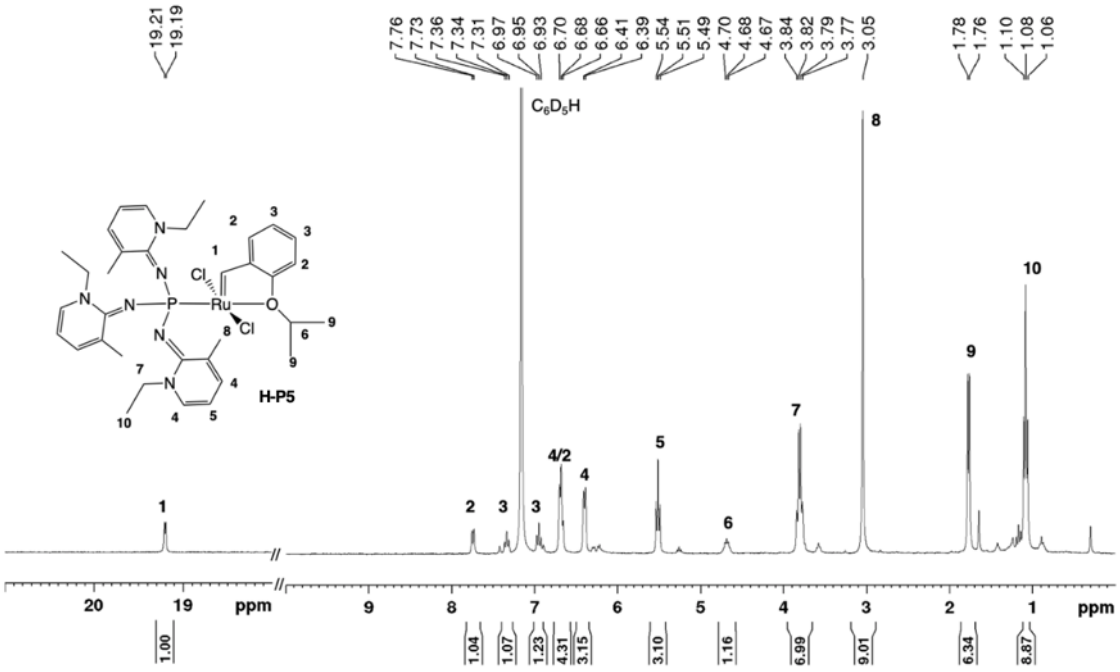

Figure B-16 ^{1}H NMR spectrum (C_6D_6, 300 MHz) of $RuCl_2(P(N{=}C_5H_3\text{-}1\text{-}NEt\text{-}6\text{-}Me)_3)(=CHC_6H_4\text{-}2\text{-}O^{i}Pr)$, **H-P5**.

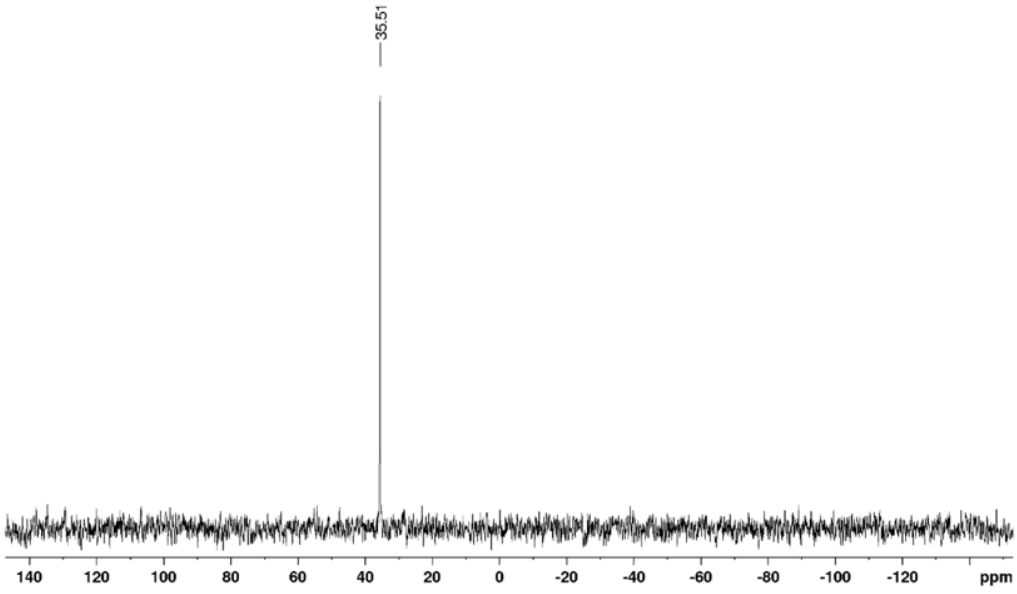

Figure B-17 $^{31}P\{^{1}H\}$ NMR spectrum (C_6D_6, 121 MHz) of $RuCl_2(P(N{=}C_5H_3\text{-}1\text{-}NEt\text{-}6\text{-}Me)_3)(=CHC_6H_4\text{-}2\text{-}O^{i}Pr)$, **H-P5**.

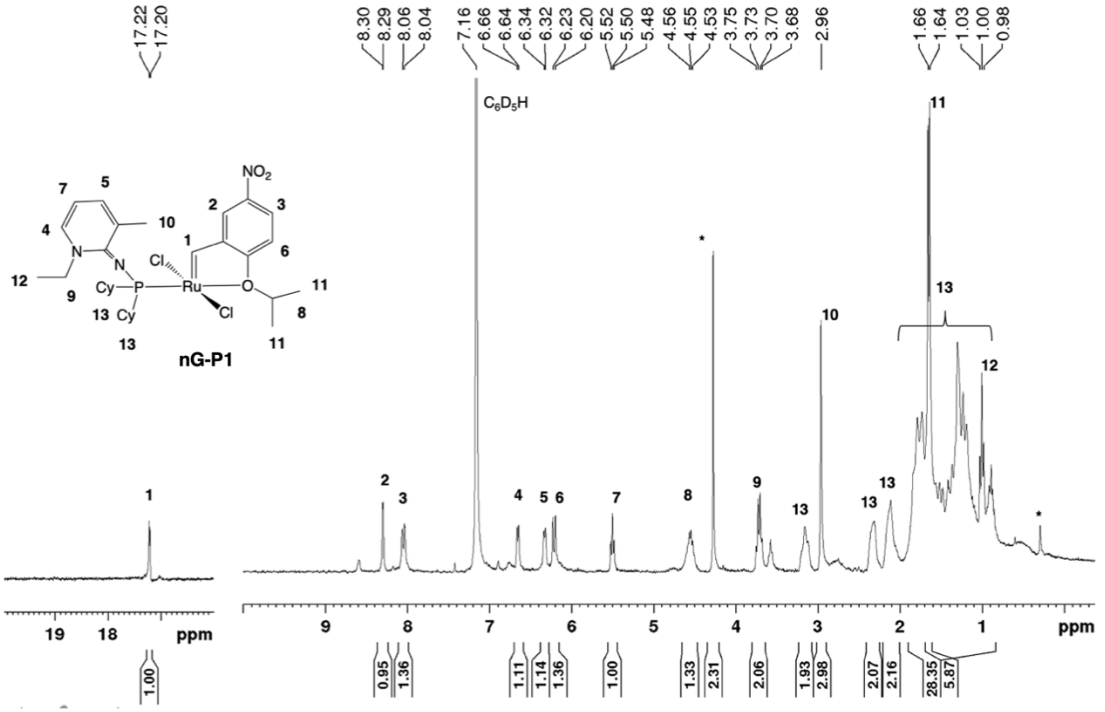

Figure B-18 ^{1}H NMR spectrum (C_6D_6, 300 MHz) of $RuCl_2(PCy_2(N{=}C_5H_3\text{-}1\text{-}NEt\text{-}6\text{-}Me))(=CHC_6H_3\text{-}2\text{-}O^{i}Pr\text{-}5\text{-}NO_2)$, **nG-P1**.

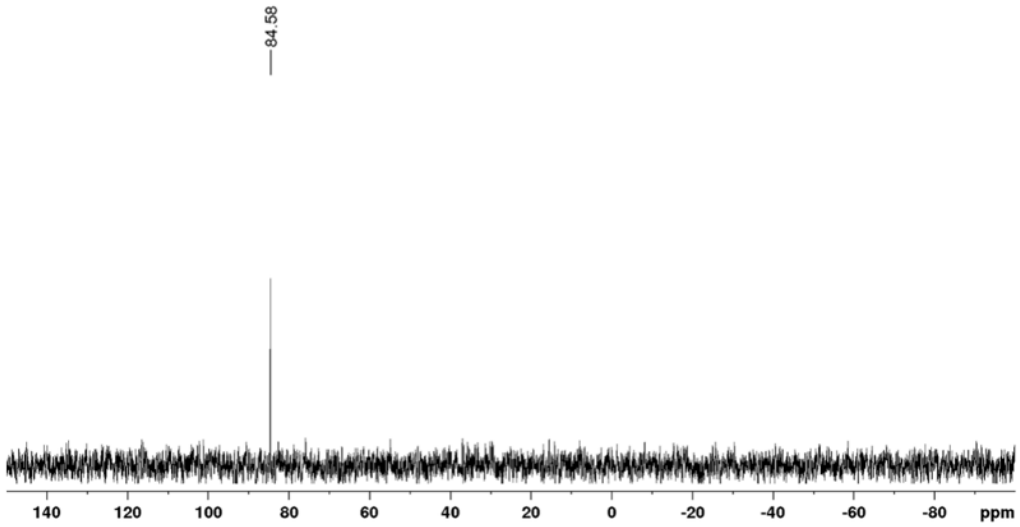

Figure B-19 $^{31}P\{^{1}H\}$ NMR spectrum (C_6D_6, 121 MHz) of $RuCl_2(PCy_2(N{=}C_5H_3\text{-}1\text{-}NEt\text{-}6\text{-}Me))(=CHC_6H_3\text{-}2\text{-}O^{i}Pr\text{-}5\text{-}NO_2)$, **nG-P1**.

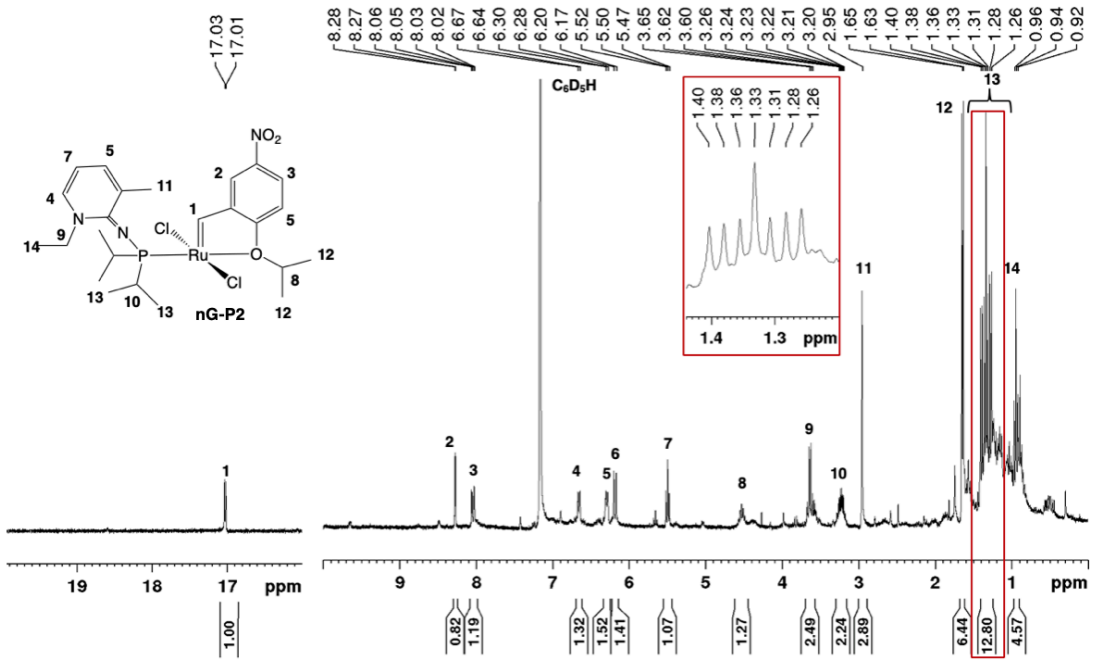

Figure B-20 ^{1}H NMR spectrum (C_6D_6, 300 MHz) of $RuCl_2(P^iPr_2(N{=}C_5H_3\text{-}1\text{-}NEt\text{-}6\text{-}Me))(=CHC_6H_3\text{-}2\text{-}O^iPr\text{-}5\text{-}NO_2)$, **nG-P2.**

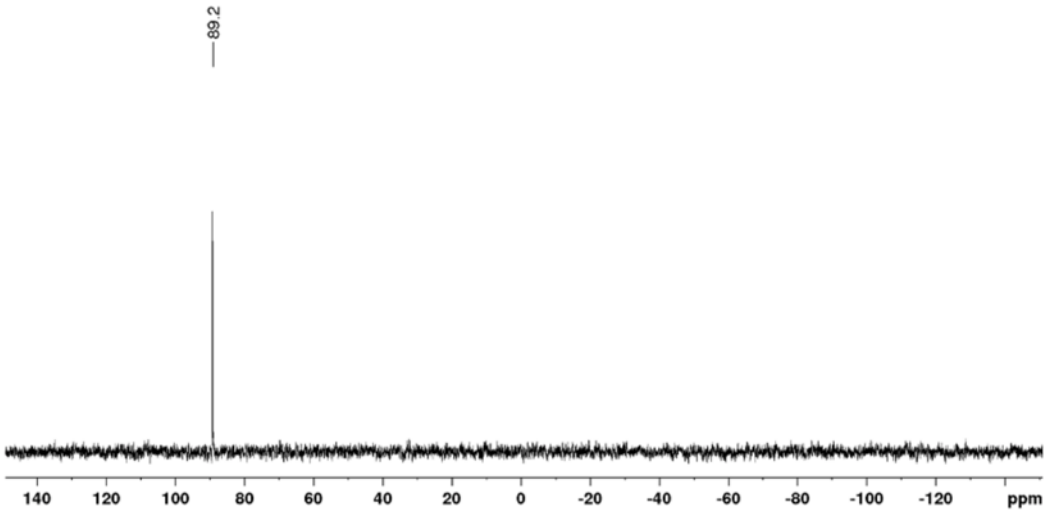

Figure B-21 $^{31}P\{^{1}H\}$ NMR spectrum (C_6D_6, 121 MHz) of $RuCl_2(P^iPr_2(N{=}C_5H_3\text{-}1\text{-}NEt\text{-}6\text{-}Me))(=CHC_6H_3\text{-}2\text{-}O^iPr\text{-}5\text{-}NO_2)$, **nG-P2**.

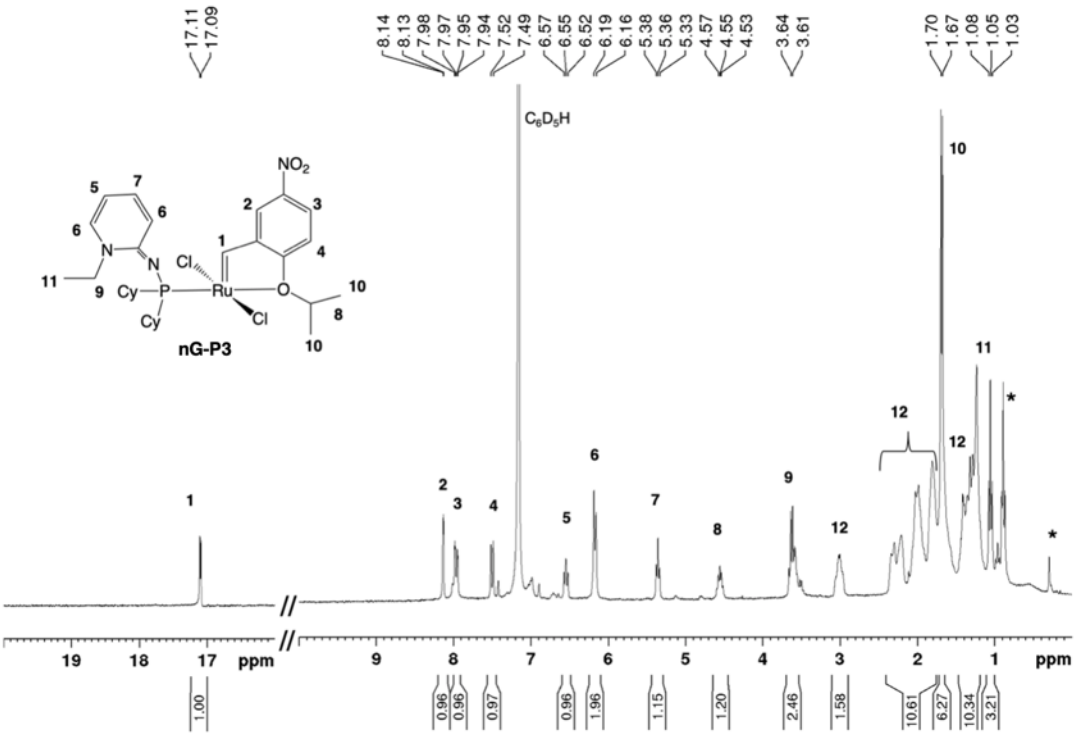

Figure B-22 ^{1}H NMR spectrum (C_6D_6, 300 MHz) of $RuCl_2(PCy_2(N{=}C_5H_4\text{-}1\text{-}NEt)(=CHC_6H_3\text{-}2\text{-}O^{i}Pr\text{-}5\text{-}NO_2)$, **nG-P3.**

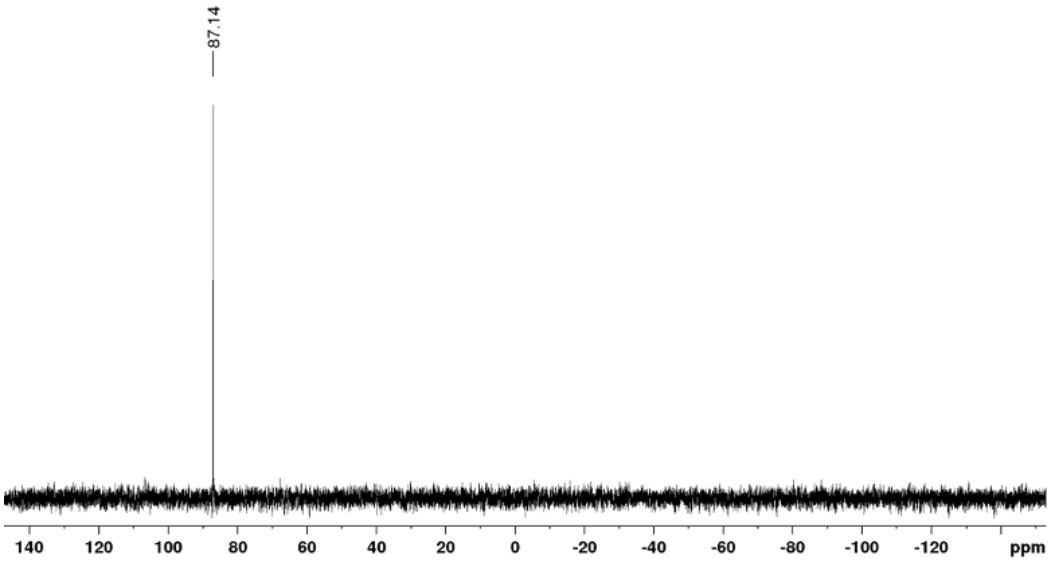

Figure B-23 $^{31}P\{^{1}H\}$ NMR spectrum (C_6D_6, 121 MHz) of $RuCl_2(PCy_2(N{=}C_5H_4\text{-}1\text{-}NEt))(=CHC_6H_3\text{-}2\text{-}O^{i}Pr\text{-}5\text{-}NO_2)$, **nG-P3**.

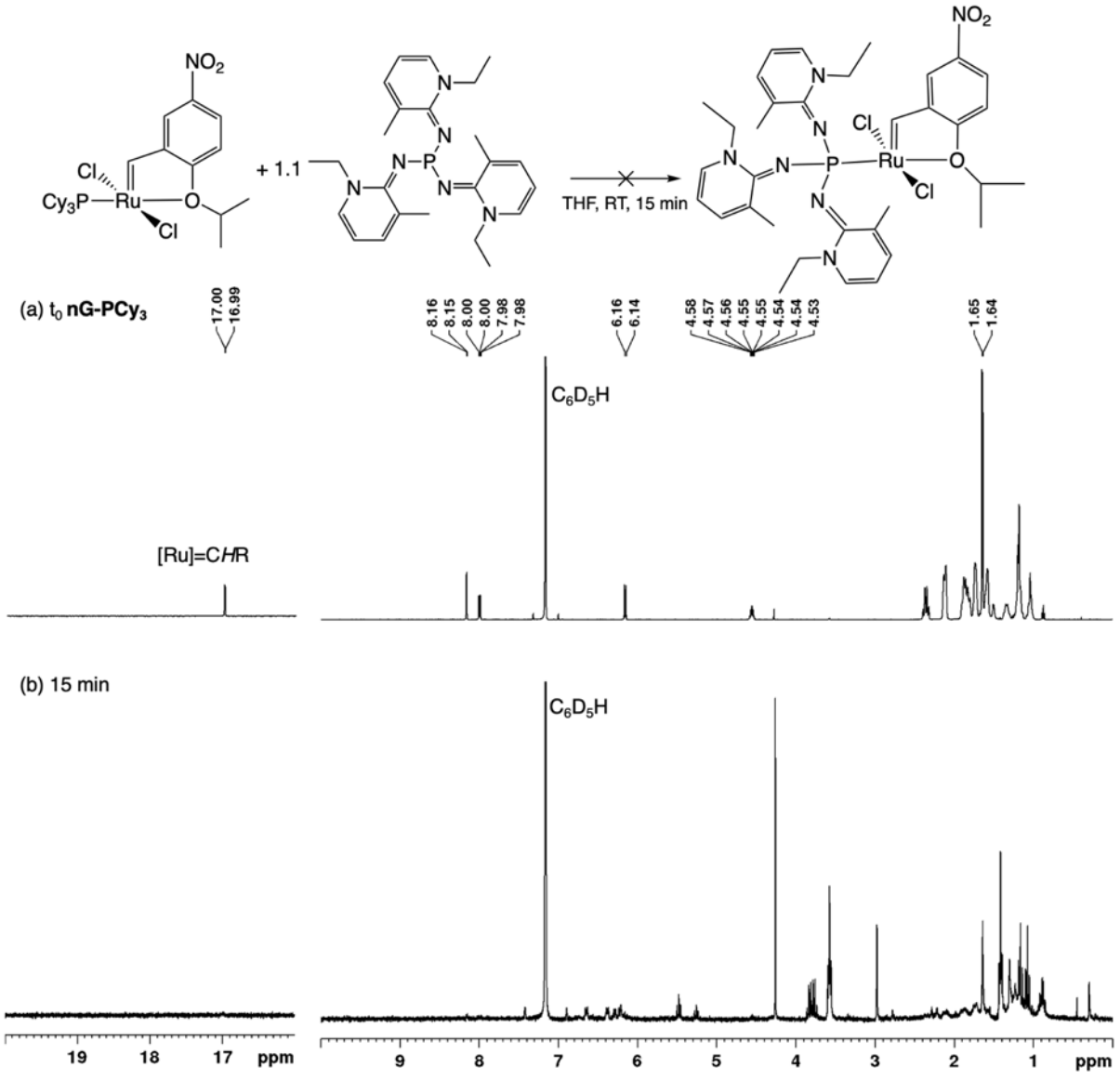

Figure B-24 ^{1}H NMR spectra (C_6D_6, 300 MHz) showing incompatibility of the highly basic phosphine **P5** with nitro-substituted catalyst **nG-PCy$_3$**. (a) Initial spectrum of **nG-PCy$_3$**, prior to adding **P5**. (b) Spectrum 15 min after adding **P5.**

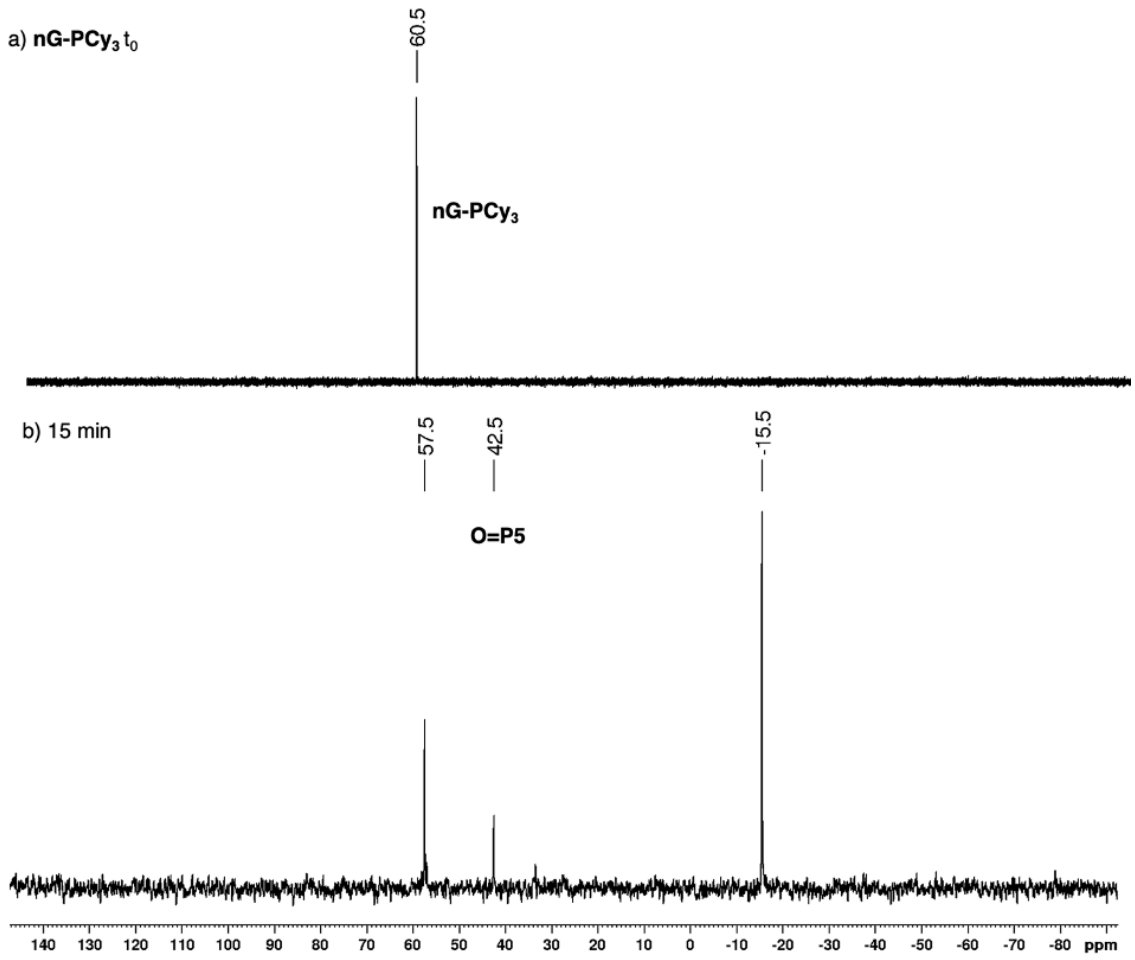

Figure B-25 $^{31}P\{^{1}H\}$ NMR spectra (C_6D_6, 121.5 MHz) showing incompatibility of the highly basic phosphine **P5** with nitro-substituted **nG-PCy3.** (a) Initial spectrum of **nG-PCy3.** (b) Spectrum 15 min after adding **P5**.

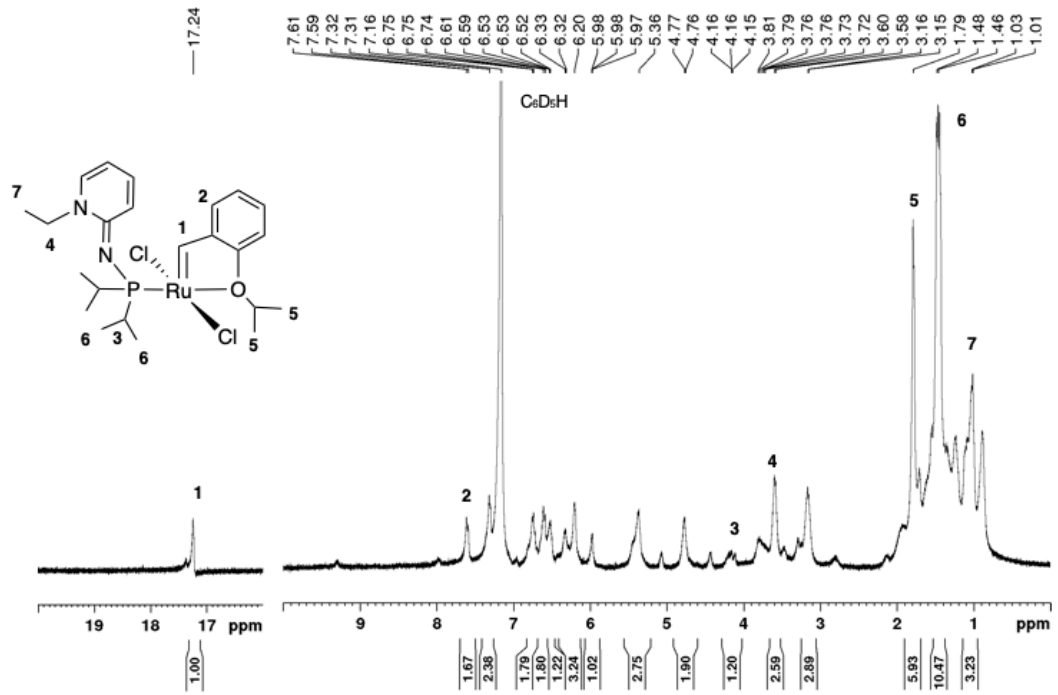

Figure B-26 ^{1}H NMR spectrum (C_6D_6, 400 MHz) showing attempted isolation of **H-P4**, resulting in a mixture of **H-P4** and **Ru-25**. Identifiable signals for **H-P4** (major product) are labelled.

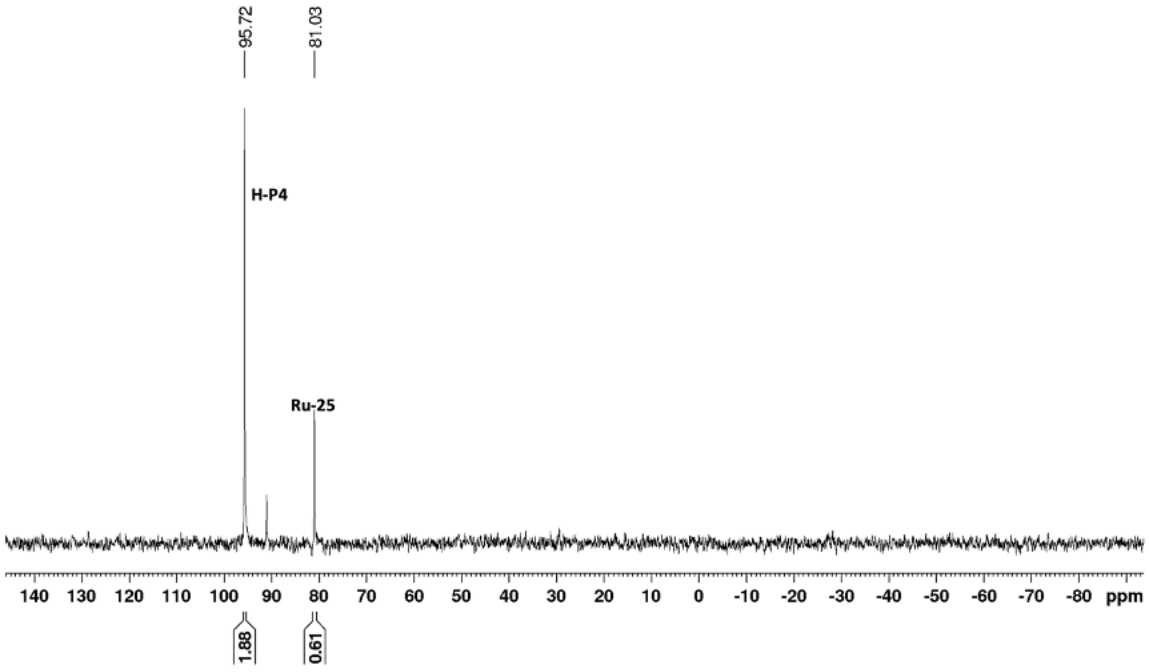

Figure B-27 ^{31}P{^{1}H} NMR spectrum (C_6D_6, 160 MHz) after attempted isolation of **H-P4**, showing a mixture of **H-P4** and **Ru-25**.

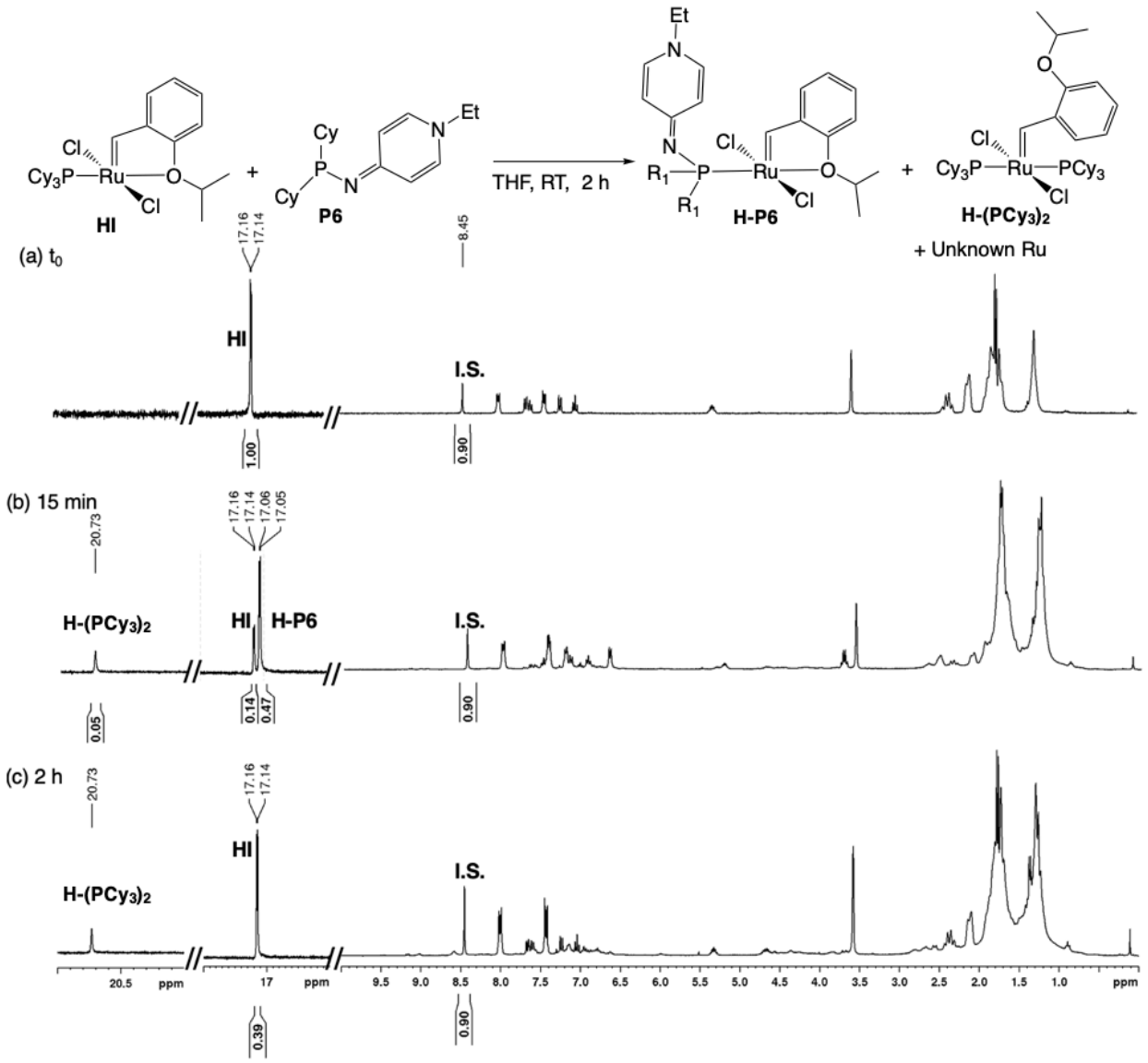

Figure B-28 ^{1}H NMR spectrum (C_6D_6, 300 MHz) showing decomposition of **HI** upon addition of phosphine **P6**. (a) Initial spectrum, showing **HI**:anthracene integration ratio. (b) 15 min after the addition of **P6**, showing 47% conversion to **H-P6.** (c) 2 h after the addition of **P6**, showing complete decomposition of **H-P6.**

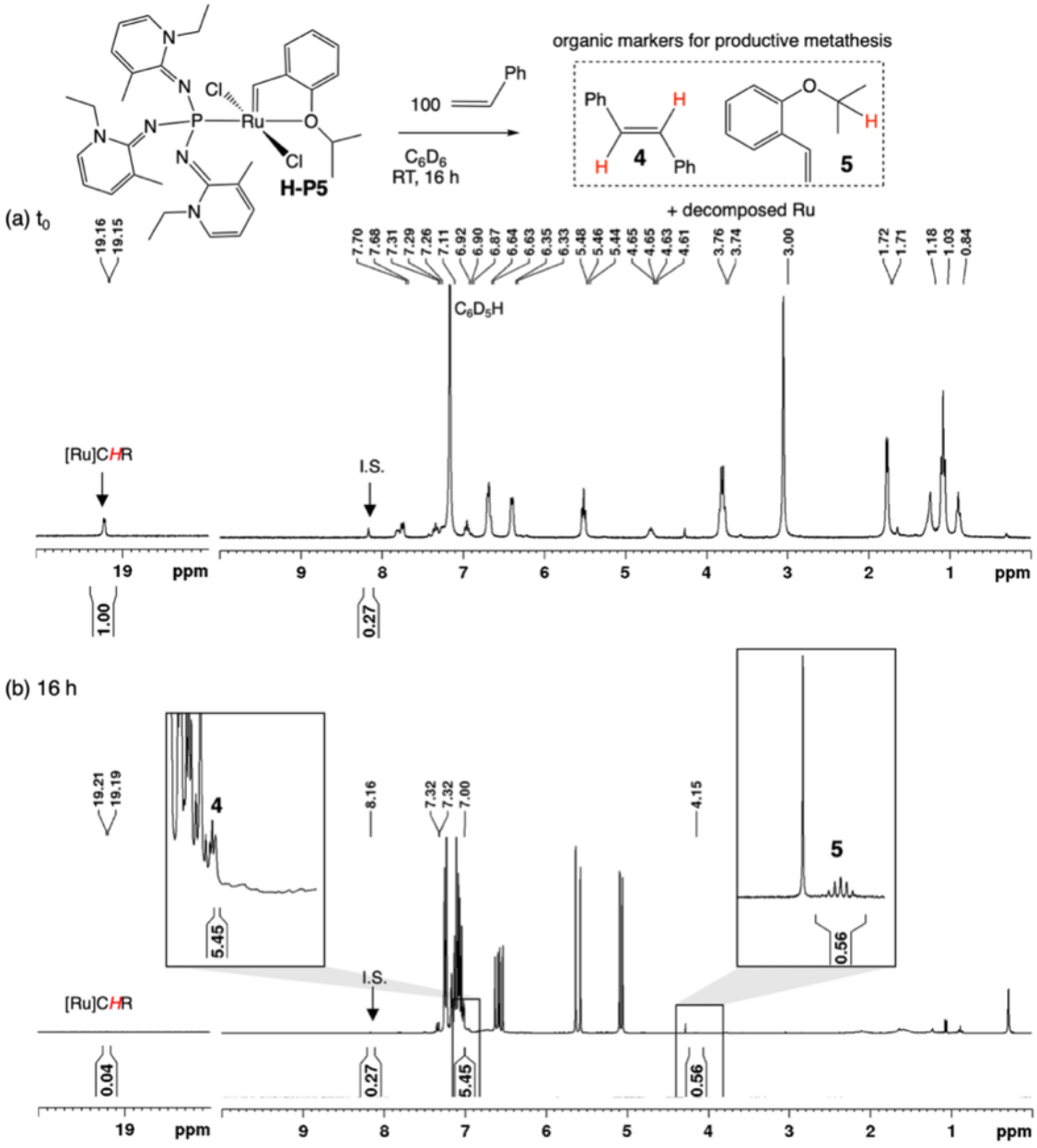

Figure B-29 ^{1}H NMR spectrum (C_6D_6, 300 MHz) for the self-metathesis of styrene with **H-P5.** (a) Initial spectrum, showing the **H-P5**:anthracene integration ratio. (b) 16 h after the addition of styrene.

C. UV-Vis Spectra

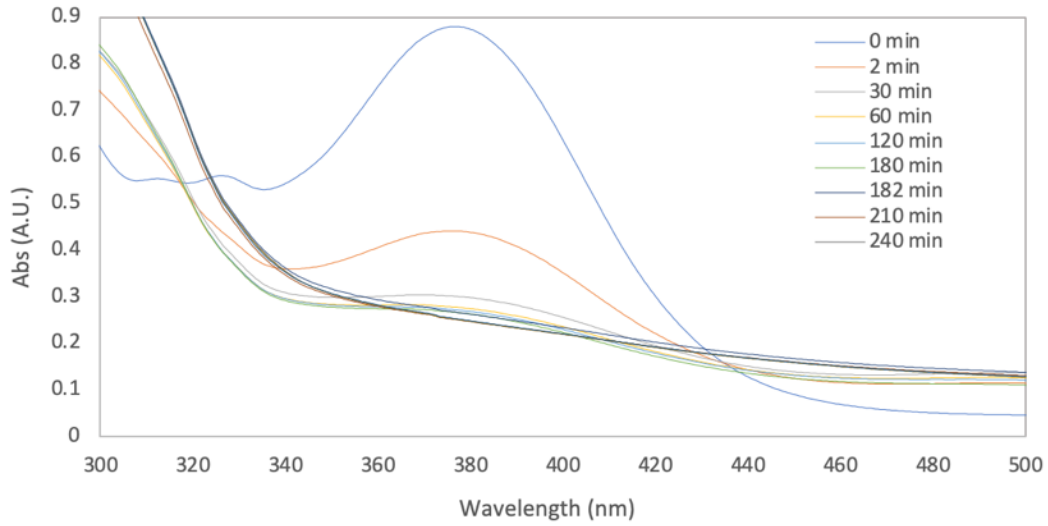

Figure C-1 Degradation of **HII** (2.0 mM in H_2O-saturated toluene) during RCM of **1** (200 mM) at RT. An equal amount of **1** was added at 180 min, diluting [**HII**] to 1.0 mM and maintaining [**1**]=200 mM.

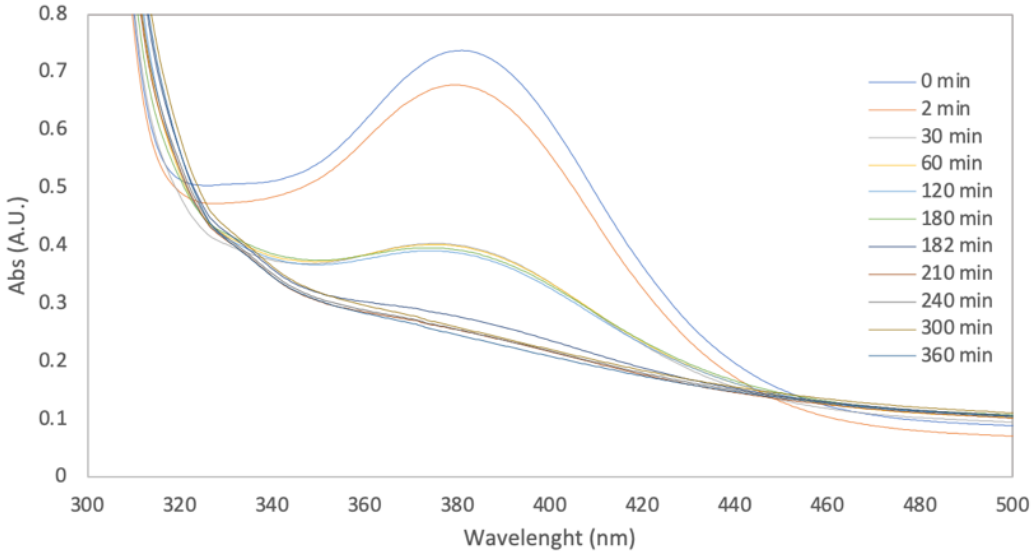

Figure C-2 Degradation of **SC**@resorcin[4]arene (2.0 mM **SC**; 15.0 mM resorcin[4]arene in H_2O-saturated toluene) during RCM of **3** (200 mM) at RT. An equal amount of **3** was added at 180 min, diluting [**SC**] to 1.0 mM and the [resorcin[4]arene] to 7.5 mM, but maintaining [**3**]=200 mM.

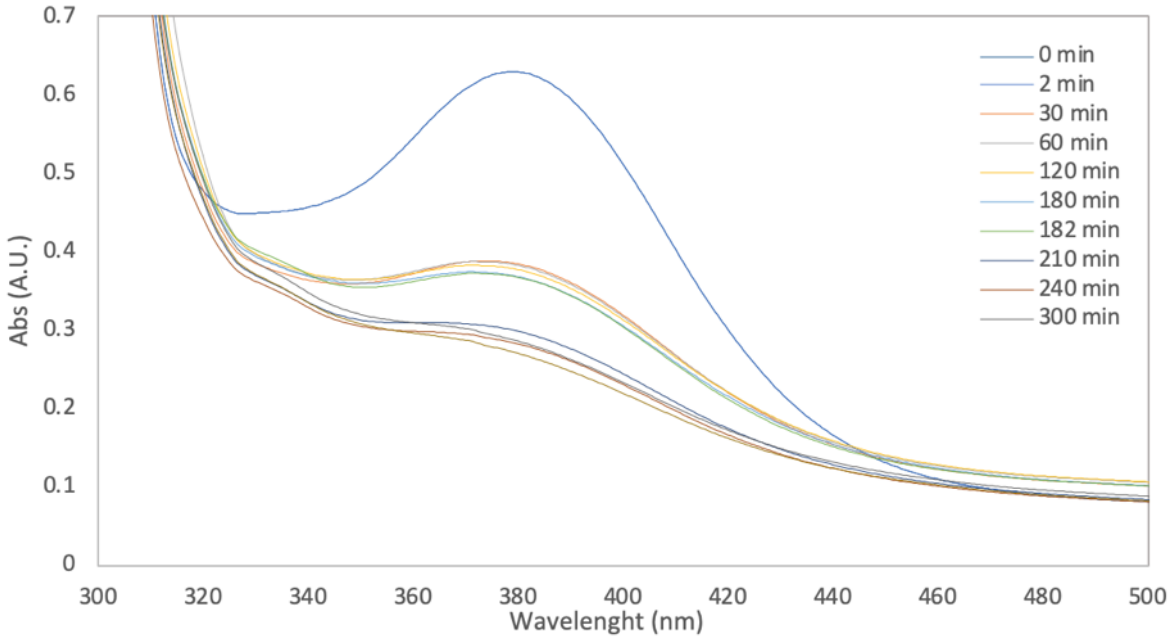

Figure C-3 Degradation of **AM**@resorcin[4]arene (2.0 mM **AM**; 15.0 mM resorcin[4]arene in H_2O-saturated toluene) during RCM of **3** (200 mM) at RT. An equal amount of **3** was added at 180 min, diluting [**AM**] to 1.0 mM and the [resorcin[4]arene] to 7.5 mM, but maintaining [**3**]=200 mM.

D. Molecular Dynamics Simulations

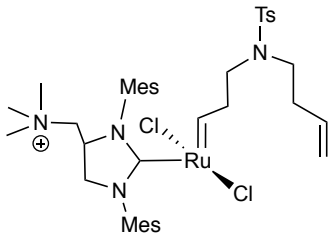

Figure D-1 Depiction of the anticipated alkylidene intermediate **SC'** generated by metathesis of **SC** and diene **3**.

A diffusion rate of 0.26 x 10^{-5} cm^2/s was calculated from the molecular dynamics simulations, which corresponds to a diffusion constant of $\log_D = -9.57$. The interior of the capsule was enlarged by the cationic guest to approximately 1,930 $Å^3$, as determined by the Connolly roll method.[6]

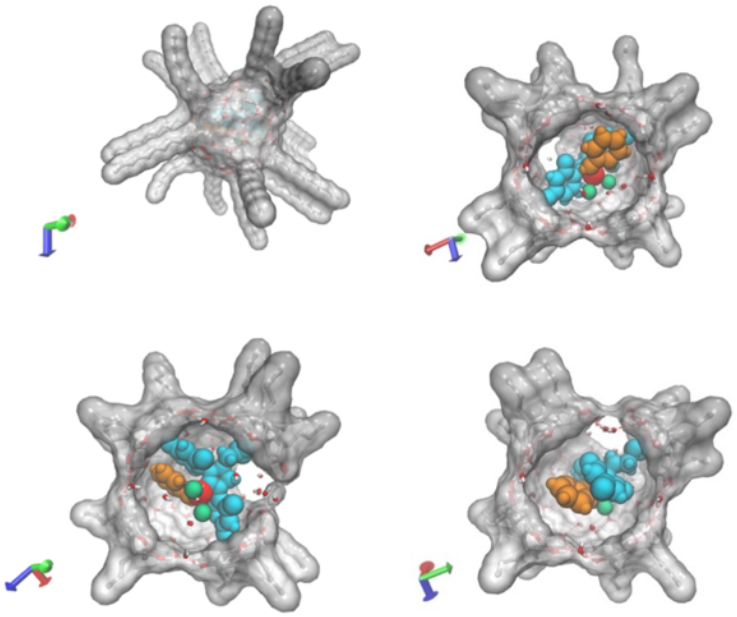

Figure D-2 Illustrations of the van der Waals volume of **SC'**@resorcin[4]arene obtained from molecular dynamics simulations: Top left: Model of the **SC'**@resorcin[4]arene catalyst. Solvent molecules and carbon-bound hydrogen atoms omitted for clarity. Other images are orthogonal projections showing the encapsulated molecule and the unoccupied space, with occluding capsule monomers and alkyl side-chains omitted for clarity.

E. Crystallographic Data

Single crystals were obtained from a saturated benzene solution of **H-P5**. Single-crystal X-ray diffraction data were collected on a Bruker APEX-II CCD diffractometer. The crystal was kept at 100 K during data collection. Using Olex2,[7] the structure was solved with the ShelXT[8] structure solution program using Intrinsic Phasing and refined with the ShelXL[9] refinement package using Least Squares minimization.

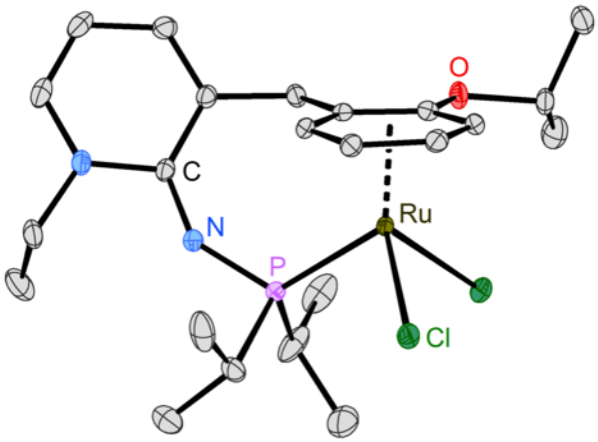

Figure E-1 Molecular view of **Ru-25** in the solid state, with thermal ellipsoid plot at the 50% probability level. Hydrogen atoms are omitted for clarity.

Table E-1 Crystal Data and Structure Refinement for Ru-25.

Crystal data and structure refinement for P21c_a.			
Identification code	P21c_a	ρ_{calc}g/cm^3	1.397
Empirical formula	$C_{35}H_{47}Cl_2N_2OPRu$	μ/mm^{-1}	0.696
Formula weight	714.68	F(000)	1488.0
Temperature/K	100	Crystal size/mm^3	0.311 × 0.043 × 0.037
Crystal system	monoclinic	Radiation	MoKα (λ = 0.71073)
Space group	$P2_1/c$	2Θ range for data collection/°	3.444 to 55.788
a/Å	12.2784(3)	Index ranges	$-16 \leq h \leq 16$, $-17 \leq k \leq 17$, $-28 \leq l \leq 28$
b/Å	13.4340(4)	Reflections collected	51178
c/Å	21.3853(6)	Independent reflections	8094 [R_{int} = 0.0597, R_{sigma} = 0.0370]
α/°	90	Data/restraints/parameters	8094/6/397
β/°	105.6140(10)	Goodness-of-fit on F^2	1.042
γ/°	90	Final R indexes [I>=2σ (I)]	R_1 = 0.0289, wR_2 = 0.0682
Volume/Å^3	3397.29(16)	Final R indexes [all data]	R_1 = 0.0346, wR_2 = 0.0715
Z	4	Largest diff. peak/hole / e Å^{-3}	0.63/-0.47

F. References

(1) Scherpf, T.; Schwarz, C.; Scharf, L. T.; Zur, J.-A.; Helbig, A.; Gessner, V. H., Ylide-Functionalized Phosphines: Strong Donor Ligands for Homogeneous Catalysis. *Angew. Chem., Int. Ed.* **2018**, *57*, 12859–12864.

(2) Weber, P.; Scherpf, T.; Rodstein, I.; Lichte, D.; Scharf, L. T.; Gooßen, L. J.; Gessner, V. H., A Highly Active Ylide-Functionalized Phosphine for Palladium-Catalyzed Aminations of Aryl Chlorides. *Angew. Chem., Int. Ed.* **2019**, *58*, 3203–3207.

(3) Chen, L.; Ren, P.; Carrow, B. P., Tri(1-adamantyl)phosphine: Expanding the Boundary of Electron-Releasing Character Available to Organophosphorus Compounds. *J. Am. Chem. Soc.* **2016**, *138*, 6392−6395.

(4) Ullrich, S.; Kovačević, B.; Xie, X.; Sundermeyer, J., Phosphazenyl Phosphines: The Most Electron-Rich Uncharged Phosphorus Brønsted and Lewis Bases. *Angew. Chem., Int. Ed.* **2019**, *58*, 10335–10339.

(5) Rotering, P.; Wilm, L. F. B.; Werra, J. A.; Dielmann, F., Pyridinylidenaminophosphines: Facile Access to Highly Electron-Rich Phosphines. *Chem – Eur. J.* **2020**, *26*, 406–411.

(6) Connolly, M. L., The Molecular Surface Package. *J. Mol. Graphics* **1993**, *11*, 139–141.

(7) Dolomanov, O. V.; Bourhis, L. J.; Gildea, R. J.; Howard, J. A. K.; Puschmann, H., OLEX2: A Complete Structure Solution, Refinement and Analysis Program. *J. Appl. Crystallogr.* **2009**, *42*, 339–341.

(8) Sheldrick, G. M., SHELXT - Integrated Space-Group and Crystal-Structure Determination. *Acta Crystallogr., Sect. A* **2015**, *71*, 3-8.

(9) Sheldrick, G. M., Crystal Structure Refinement with SHELXL. *Acta Crystallogr.; Sect. C* **2015**, *71*, 3–8.